STUDIES OF LIQUID MERCURY AND LIQUID MERCURY-GALLIUM SYSTEMS BY X-RAY DIFFRACTION

Thesis by

Roger William Caputi

In Partial Fulfillment of the Requirements

For the Degree of

Doctor of Philosophy

California Institute of Technology

Pasadena, California

1965

(Submitted November 3, 1964)

Acknowledgments

I wish to thank Sergio E. Rodriguez, a fellow graduate student, who collaborated fully on the design and development of the experimental equipment, and who developed the computer program for the final data reduction.

I also wish to thank Professor C. J. Pings for his encouragement, guidance, and support which made this thesis possible.

I am also indebted to the California Institute of Technology for its generosity in both scholarship and monetary support, and to the Office of Naval Research and the Air Force Office of Scientific Research for financial research support.

And I wish to thank my wife, Sue, for the encouragement and help which made this thesis possible.

Abstract

The purpose of this study was to determine the radial distribution of pure mercury and mercury-gallium mixtures by x-ray diffraction. Work was also done to resolve the problem of whether microdroplets of the solute metal existed in the solvent metal of the mercury-gallium system or whether the mercury-gallium mixtures were true solutions.

The experimental system used a reflection geometry from a horizontal free surface of the liquid metals. A silver x-ray tube was used in conjunction with a scintillation detector and pulse height analyzer. Data points were taken over an S range of approximately 1.6 $Å^{-1}$ to 17.4 $Å^{-1}$.

Three samples were run at 0°, 30°, and 50° C. The compositions of the three samples were pure mercury, 0.9658 mole fraction of mercury, and 0.0197 mole fraction of mercury.

The peak positions of the final radial distribution functions for all samples showed no significant change over the temperature range used. The average positions of the first and second peaks of the mercury curves were 3.01 Å and 5.80Å respectively. The coordination numbers for mercury as determined by the symmetrical curve method were 7.5, 7.3, and 7.0 atoms for the 0°, 30°, and 50° C runs respectively.

The final results indicated that both samples of mercury-gallium were true solutions.

Table of Contents

Title	Page
Introduction	1
Theory	4
Experimental	12
Data Analysis	38
Results and Conclusions	56
References	75
Appendix I	80
Appendix II	82
Appendix III	84
Appendix IV	140
Appendix V	150
Propositions	178

List of Figures

	Title	Page
Figure 3-1.	Geometry of experimental system.	13
Figure 3-2.	LiF crystal spectral analysis of silver radiation.	16
Figure 3-3a.	Pulse amplitude distribution of Ag K_α from a gallium surface.	17
Figure 3-3b.	Pulse amplitude distribution of Ag K_α from a mercury surface.	17
Figure 3-4.	Detailed plan of sample cell and supporting jackets.	21
Figure 3-5.	Exploded isometric view of sample cell and supporting jackets.	22
Figure 3-6.	Side view of mounted sample assembly.	27
Figure 3-7.	Overhead view of mounted sample assembly.	28
Figure 4-1.	Analytical approximations to i (S) curves for all runs.	52
Figure 4-2.	Analytical approximation plus experimental data points of a single i (S) curve.	53
Figure 4-3.	Graphical representation of the direct inversion for all runs.	54
Figure 5-1.	$4\pi r^2 \Sigma \bar{\rho}_i(r)$ versus r for all runs.	65
Figure 5-2.	g (r) versus r for pure mercury at three temperatures.	69
Figure 5-3.	g (r) versus r for high mercury-low gallium at three temperatures.	70
Figure 5-4.	g (r) versus r for high gallium-low mercury at three temperatures.	71
Figure 5-5.	g (r) versus r for four samples at 0° C.	72
Figure 5-6.	g (r) versus r for four samples at 30° C.	73
Figure 5-7.	g (r) versus r for four samples at 50° C.	74

Introduction

Because of the increased interest in developing a more quantitative and more general atomic or molecular model for liquids, a corresponding increase of interest in experimentally determining liquid structure at the atomic level has quite naturally developed. Of the number of techniques used, the method of x-ray diffraction has proved to be one of the most powerful.

The earliest experiments were carried out on liquids which were both simple in structure and simple in handling techniques. For these reasons mercury was one of the first substances to be studied. One of the first analyses of mercury was carried out by Debye and Menke (1) in 1930. Since that time over ten papers have been published on the structure of mercury. Ironically an appreciable number of the studies of this "most studied" element show marked discrepancies.

Greater interest in metallurgy and alloys has given a further boost to structure studies of liquid metals and their alloys. It is interesting to note that a major portion of the more recent liquid alloy studies reported in a review article by Furukawa (2) were carried out by the Soviet Union.

The liquid systems of pure mercury and mercury-gallium alloys described in this thesis were picked for several reasons. Because of the previously mentioned disagreements over the structure of liquid mercury, it was decided to determine experimentally the structure of mercury using the same equipment used on the alloys. In this way any comparison with the alloy results would not be confused by unknown differences in experimental equipment or data reduction techniques. The

mercury-gallium alloy system is of interest because of the low mutual solubilities of the two elements and the subsequent question stated by Spicer and Bartholomay (3) of whether true solutions of the two metals were formed or that the solute metal atoms accumulated in the form of microdroplets dispersed in the solvent metal. Work has been done on the binary system of mercury-indium by Kim, Standley, Kruh, and Clayton (4). Because of the unlimited solubility of the system, it was possible to cover the entire range of concentrations from pure mercury to pure indium. The final results of their investigation indicated that the mercury-indium system was a true solution.

Three samples were studied for the experimental work of this thesis. These were pure mercury and two mercury-gallium alloy systems. One system had a high mercury, low gallium concentration; the other system had a high gallium, low mercury concentration. For the actual mole fraction values of these two systems see Appendix I.

Each of the three samples were studied by means of x-ray diffraction at three controlled temperatures (0°, 30°, and 50° C) to give a total of nine experimental runs.

In order to simplify terminology and nomenclature when referring to the samples or experimental runs, the following terms are used. High gallium is used to denote the sample having a high gallium, low mercury concentration, and high mercury is used to denote the sample having a high mercury, low gallium concentration. A six character code, such as MM30A3, is used for each experimental sub-run. The first two characters signify sample composition, i.e. MM for pure

mercury, MG for high mercury, GM for high gallium, and GG for pure gallium. The third and fourth characters or digits are the nominal run temperature in degrees centigrade. The fifth character indicates the experimental run, and the final digit indicates the sub-run. Therefore the example given above designates the third sub-run of the first main run for pure mercury at 30° C. When a complete experimental run is used directly or when the use of a sub-run designation is not applicable, the sub-run designation is dropped.

Theory

The theoretical basis and possibility of x-ray diffraction in liquids were first pointed out by Debye (5). His basic equation for the scattering of x-rays by a non-crystalline array of atoms as a function of angle is given by

$$I_{coh} = \sum_m \sum_n f_m f_n \frac{\sin Sr_{mn}}{Sr_{mn}} \qquad (2\text{-}1)$$

where I_{coh} = coherent intensity of scattered x-rays in electron units

f_m, f_n = atomic scattering factor for the m^{th} and n^{th} atoms

$S = \frac{4\pi \sin \theta}{\lambda}$

r_{mn} = magnitude of the vector separating the m^{th} and n^{th} atoms

2θ = angle between the incident and scattered beam

λ = wavelength of incident x-rays.

The double summation is carried out over all atom pairs in the sample. It is also assumed that all orientations in space of r_{mn} are equally probable.

The following mathematical development for a single element monatomic liquid will be quite brief and will serve only to give an outline of the actual derivation. The reason for this condensation is that there are many completed and detailed derivations presently available. A few of these are by Debye (5), Zernike and Prins (6), Warren and Gingrich (7), Warren (8), Randall (9), James(10) and Paalman and Pings (11). Using equation (2-1) and recognizing that in the limit as r_{mn} goes to zero $\frac{\sin Sr_{mn}}{Sr_{mn}}$ goes to one,

$$I_{coh} = N f^2 + \sum_{m \neq n} \sum f^2 \frac{\sin S r_{mn}}{S r_{mn}} \qquad (2\text{-}2)$$

By assuming that the atomic distribution around the reference atom can be regarded as a continuous function, equation (2-2) can be written

$$\frac{I_{coh}}{N f^2} - 1 = \int_0^\infty 4\pi r^2 \rho(r) \frac{\sin Sr}{Sr} \, dr \qquad (2\text{-}3)$$

where $4\pi r^2 \rho(r) \, dr$ is the number of atoms found between r and r+d r away from any given atom, and N is the total number of atoms in the sample.

Since the integral of equation (2-3) does not converge, a new integral is written

$$\frac{I_{coh}}{N f^2} - 1 = \int_0^\infty 4\pi r^2 [\rho(r) - \rho_0] \frac{\sin Sr}{Sr} \, dr \qquad (2\text{-}4)$$

The premise that equation (2-4) does converge is based on the fact that $\rho(r)$ approaches ρ_0 quite closely for r values of just a few atomic diameters. The approximation that the left side of the equation does not change with the added integral on the right is described and justified in Warren and Gingrich (7) and in James (10). The term ρ_0 is just the average atomic density of the sample.

Finally equation (2-4) can be transformed by means of a Fourier inversion to

$$4\pi r (\rho(r) - \rho_0) = \frac{2}{\pi} \int_0^\infty Si(S) \sin Sr \, dS \qquad (2\text{-}5)$$

where $i(S) = \frac{I_{coh}}{Nf^2} - 1$

The limits of 0 to ∞ in the previous equation obviously cannot be met. The lower limit is set by how close to the main beam scattered radiation can be measured. The upper limit is $\frac{4\pi \sin\theta}{\lambda}$, and for θ equals 90° the maximum is $\frac{4\pi}{\lambda}$. For all practical cases this limit is quite small compared to infinity; at best it is of the order of 20 Å^{-1}. Fortunately the integral convergence is sufficiently rapid that the relatively low upper limit can replace the infinite limit quite well. For a detailed discussion about the errors arising from this "truncation" at low S see Waser and Schomaker (12) or Klug and Alexander (13).

A plot of $\rho(r)$, as determined from equation (2-5), versus r is one way of presenting the radial distribution function.

In the case of a two element monatomic liquid, the derivation originally carried out by Warren, Krutter, and Morningstar (14) is used. Although their development was specifically for polyatomic liquids, or glasses, it can be applied to the two element monatomic liquid with no difficulty in spite of the direct statement of Furumoto (15) to the contrary.

Starting with equation (2-1) and splitting out the self-scattering terms results in

$$I_{coh} = \sum N_m f_m^2 + \sum_{m \neq n} \sum f_m f_n \frac{\sin Sr_{mn}}{Sr_{mn}} \qquad (2\text{-}6)$$

where N_m = number of atoms of m.

By again assuming a continuous function for the atomic density around the

reference atom, equation (2-6) can be rewritten

$$I_{coh}=\sum N_m f_m^2+\int_0^\infty \sum f_m \sum f_n \rho_{mn}(r)\, 4\pi r^2 \frac{\sin Sr}{Sr}\, dr \quad (2\text{-}7)$$

Since f_m and f_n are different functions of S, it is mathematically impossible to determine the function $\sum \rho_{mn}(r)$ by a Fourier inversion. In order to eliminate this difficulty Warren et al. (14) introduced the approximation that the atomic scattering factor f_m could be replaced by f_e, the scattering factor for a single electron, multiplied by a constant K_m an effective atomic number. This approximation assumes that all f_m's have the same angular dependence so that they all differ only by the constant K_m. In actual practice this uniform angular dependency is not true. If the two elements differ in atomic number by only one or two units, the approximation is quite good, but it becomes more "approximate" as the difference in atomic number increases.

If this approximation is substituted in equation (2-7), there is obtained

$$I_{coh}=\sum N_m f_m^2+ f_e^2 \int_0^\infty \sum K_m \sum K_n \rho_{mn}(r)\, 4\pi r^2 \frac{\sin Sr}{Sr}\, dr \quad (2\text{-}8)$$

By introducing the average atomic density ρ_o as was done in equation (2-4), there results

$$I_{coh}=\sum N_m f_m^2+ f_e^2 \int_0^\infty \sum K_m \sum K_n \left(\rho_{mn}(r)-\rho_o\right) 4\pi r^2 \frac{\sin Sr}{Sr}\, dr \quad (2\text{-}9)$$

Now by means of a Fourier inversion the final equation can be written

$$4\pi r\left[\Sigma K_m \Sigma K_n \rho_{mn}(r) - \Sigma K_m \Sigma K_n \rho_o\right] = \frac{2}{\pi}\int_0^\infty Si(S)\sin Sr\, dS \qquad (2\text{-}10)$$

where $$i(S) = \frac{I_{coh} - \Sigma N_m f_m^2}{f_e^2}$$

$$f_e^2 = \left[\frac{\Sigma f_m}{\Sigma Z_m}\right]^2$$

Z_m = atomic number.

It is interesting to note that while all of the derivations of the monatomic single element liquid equations carried out in the references mentioned above lead to the identical result, a major part of the references using the same approximation (i. e. Warren et al. (14)) and essentially the same derivation came up with a variety of final equations for polyatomic liquids. Equation (2-10) is the form derived by Mackenzie (16).

Listed below are the final equations of several authors.

$$4\pi r\left[\Sigma K_m \rho_m'(r) - \Sigma K_m \rho_o'\right] = \frac{2}{\pi}\int_0^\infty Si(S)\sin Sr\, dS \qquad (2\text{-}11)$$

where $4\pi r^2 \rho_m'(r)\, dr$ = effective number of electrons between r and r+d r

ρ_o' = average electronic density

$I(S) = i(S)$ of equation (2-10).

$$4\pi r\left[\Sigma X_m \Sigma K_m K_n \rho_{mn}(r) - \Sigma X_m \Sigma Z_m Z_n X_n \rho_o\right] = \frac{2}{\pi}\int_0^\infty Si(S)\sin Sr\, dS \qquad (2\text{-}12)$$

where X_m = mole fraction of m

Z_m = actual atomic number of m

$$i(S) = \frac{I_{coh} - \Sigma X_m f_m^2}{f_e^2}$$

$$4\pi r\left[\Sigma K_m \Sigma K_n \rho_{mn}(r) - (\Sigma K_m)^2 \rho_o\right] = \frac{2}{\pi}\Sigma(K_m^2)\int_0^\infty Si(S)\sin Sr\, dS \quad (2\text{-}13)$$

where $$i(S) = \frac{I_{coh}}{\Sigma N_m f_m^2} - 1$$

Equation (2-11) is the final form in the derivations of Warren et al. (14), Klug and Alexander (17), Peiser, Rooksby, and Wilson (18), and Zarzycki (19). Equation (2-12) is the final form of Kruh (20), and equation (2-13) is the final form of Furukawa (2).

There are a couple of interesting points of difference between the four equations, other than the minor ones of atomic versus electronic densities and mole fraction versus atomic summation.

In equations (2-10), (2-11), and (2-12) the expression for i (S) contains the term f_e^2 as defined under equation (2-10). In equation (2-13) f_e^2, as derived from the expression for i (S), has the value $\Sigma f_m^2 / \Sigma K_m^2$. This result for f_e^2, although not an unreasonable one, is not the one obtained if the derivation of Warren et al. (14) is followed as Furukawa (2) claimed it was.

The second point of interest is the coefficient of ρ_o of equation (2-12). The terms $Z_m Z_n$ following the second summation symbol were qualitatively justified in a physical sense by Kruh (20), but in the mathematical derivations

of all four equations the effective atomic numbers K_m and K_n should be used.

Although these and other minor discrepancies exist among the four equations, there is no clear means of choosing which equation is truly the most correct or best. To the extent that all of the equations are based upon an approximation (i. e. $f_m = f_e K_m$) whose validity and accuracy will vary greatly depending upon the actual system, neither of the two variations mentioned above can necessarily be ruled out as "incorrect".

In the case of the present study, equation (2-10) was used with two modifications. The first and relatively minor change was to divide by $N_m + N_n$ to convert to mole fractions as in equation (2-12). The second and more important modification was to redefine f_e in the form

$$f_e = \frac{\sum f_m}{\sum K_m}$$

Carrying out the two operations mentioned above and dividing by $(\sum X_m f_m)^2$, the final equation can be written as

$$4\pi r \left[\frac{\sum X_m \sum K_m K_n \rho_{mn}(r)}{(\sum X_m K_m)^2} - \rho_o \right] = \frac{2}{\pi} \int_0^\infty Si(S) \sin Sr \, dS \quad (2\text{-}14)$$

where

$$i(S) = \frac{I_{coh} - \sum X_m f_m^2}{(\sum X_m f_m)^2}$$

One of the several advantages gained by this modification is that the direct output of the inversion is in terms of the atomic rather than the electronic distribution.

In order to simplify the nomenclature of equation (2-14), the different

values of $\rho_{mn}(r)$ and their appropriate coefficients have been replaced by $\bar{\rho}_i$ so that equation (2-14) can be written in the form

$$4\pi r \left[\Sigma \bar{\rho}_i(r) - \rho_o \right] = \frac{2}{\pi} \int_0^\infty Si\,(S) \sin Sr \, d\,S \qquad (2\text{-}15)$$

Experimental

In all experimental systems that have been used or are in use now for x-ray diffraction work on liquids, one of two basic geometries is employed.

The transmission method is generally used on low density, low atomic number liquids such as argon, nitrogen, or oxygen. The liquid sample is normally positioned so that it is cylindrically symmetrical with respect to the goniometer axis. A detailed description of a system for cryogenic liquids using transmission geometry is described by Honeywell, Knobler, Smith, and Pings (21).

The second method is that of reflection. This method is normally used on highly absorbing liquids such as mercury or gallium. For this system the surface of the liquid is either a free horizontal surface or defined by a thin flat plate. In either case the surface is placed on and parallel to the axis of the goniometer. It was this second geometry and the use of a free horizontal surface that was employed by the author.

When the reflection method is used on metals such as mercury or gallium, the scattering phenomenon can be considered a surface effect on a macroscopic scale. Because of the high absorption of radiation of both metals the effective x-ray penetration into the liquid is of the order of 0.001". On the atomic scale this distance is of the order of 100,000 atomic diameters so that essentially all scattered radiation is coming from a bulk liquid environment. The overall geometry of x-ray beam, sample cell, and detector is shown in Figure 3-1.

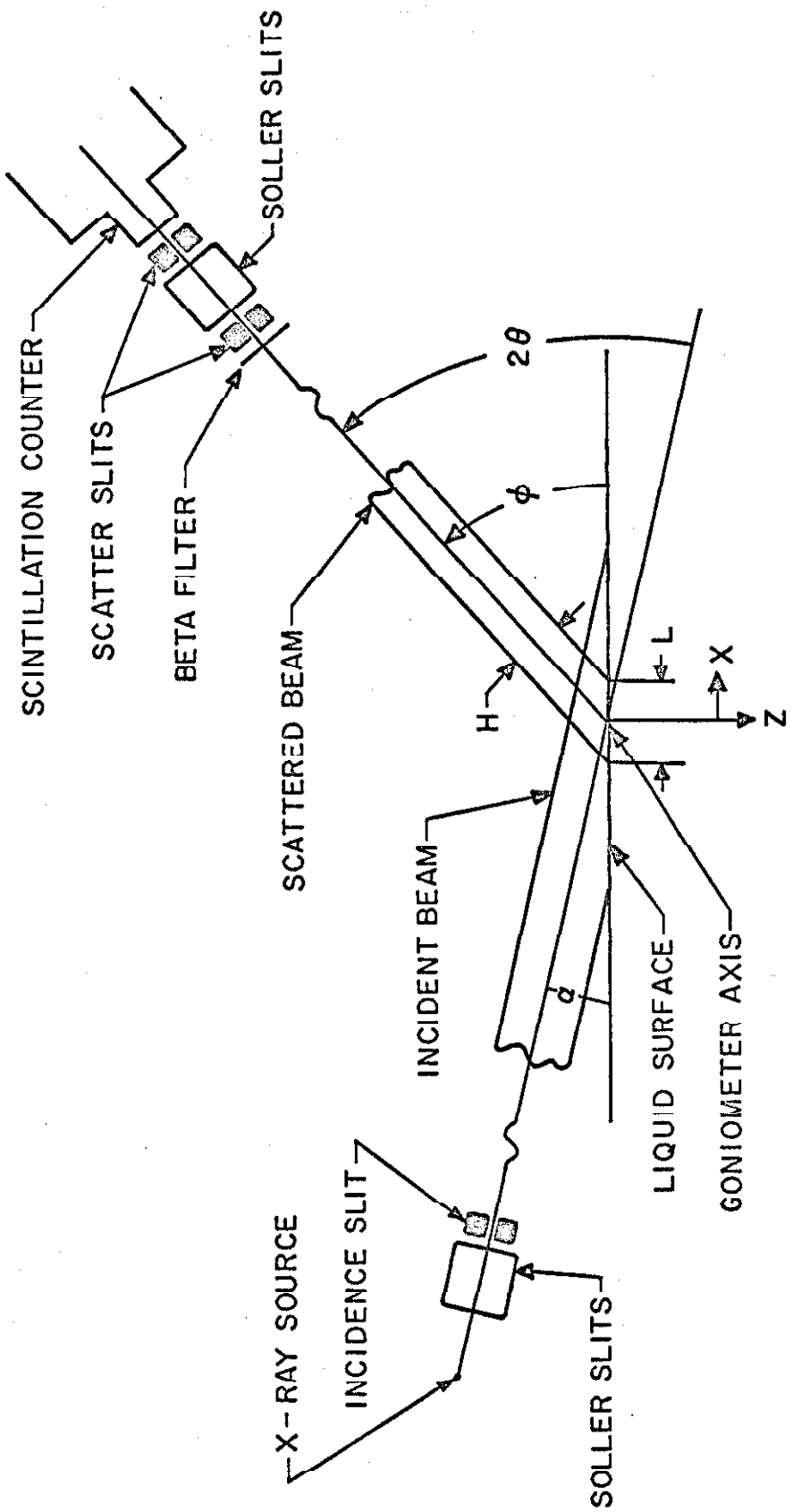

Figure 3-1. Geometry of experimental system.

The basic goniometer used was the Norelco Wide Range Goniometer. The x-ray generator (tube, transformer, etc.) was Norelco's water cooled diffraction unit which had a stated filament current stability of ± 0.1% and a voltage stability of ± 0.25% (22). The quoted voltage stability was for a 25 hour period and included drift. No rigorous long term testing was carried out to check whether the above quoted figures were accurate. Several periodic short term checks were made and within the accuracy used throughout the experimental series there were no measurable changes or drifts in actual beam intensity. The x-ray tube used in all experimental runs contained a silver target. The standard running conditions of the tube were 12 ma at 40 KV. It is interesting to note that the maximum running conditions recommended by Norelco were 6 ma at 40 KV. In this laboratory two Norelco silver tubes were run at a minimum of 12 ma at 40 KV. The first tube was used for approximately 1100 hours and the second tube for approximately 830 hours under these "overload" conditions with no apparent deterioration of the tube. This overcurrent condition was quite necessary in order to increase beam intensity and thereby reduce the experimental running time to something compatible with time limits on long term temperature stability and control, and with laboratory commitments on the control equipment for other experiments. Even with the increased beam intensity it took almost 80 hours for a single temperature run. It was necessary to use silver K_α radiation rather than molybdenum K_α radiation so that the fluorescence radiation of mercury, which is sufficiently lower in energy than the silver line,

could be eliminated by means of the pulse height analyzer. This necessity was unfortunate since the molybdenum tube could be run at a maximum of 20 ma at 50 KV.

A spectral analysis of the silver radiation was carried out using a single crystal LiF analyzer and is shown in Figure 3-2. Once the silver K_α line was established, a pulse amplitude distribution was run in order to determine the general shape and position of the line with respect to the voltage base of the linear amplifier and pulse height analyzer. Using the silver K_α line scattered from the LiF crystal it was established that the line peaked at 54 volts and had the general shape of a Gaussian curve. Once the peak position was determined, two pulse amplitude distributions were taken, one from a gallium surface and one from a mercury surface. The results of these runs are shown in Figures 3-3a and 3-3b respectively. On the basis of these results the window setting on the pulse height analyzer for the high gallium system was 35 - 85 volts and for the high mercury and pure mercury systems it was 45 - 85 volts.

The complete detection system used in the calibration series mentioned above and for the actual sample runs is described below. The detector "chain" starting at the scintillator consisted of a NaI(Tl) scintillation crystal optically coupled to a photomultiplier tube, a preamplifier, a stabilized high-voltage supply, a high-gain linear amplifier, a single channel pulse height analyzer, a scaler-timer unit, and a digital printer.

The detector unit, which was assembled in the laboratory, used a Harshaw type HG detector crystal (0.500" diameter x 0.100" NaI(Tl) single crystal),

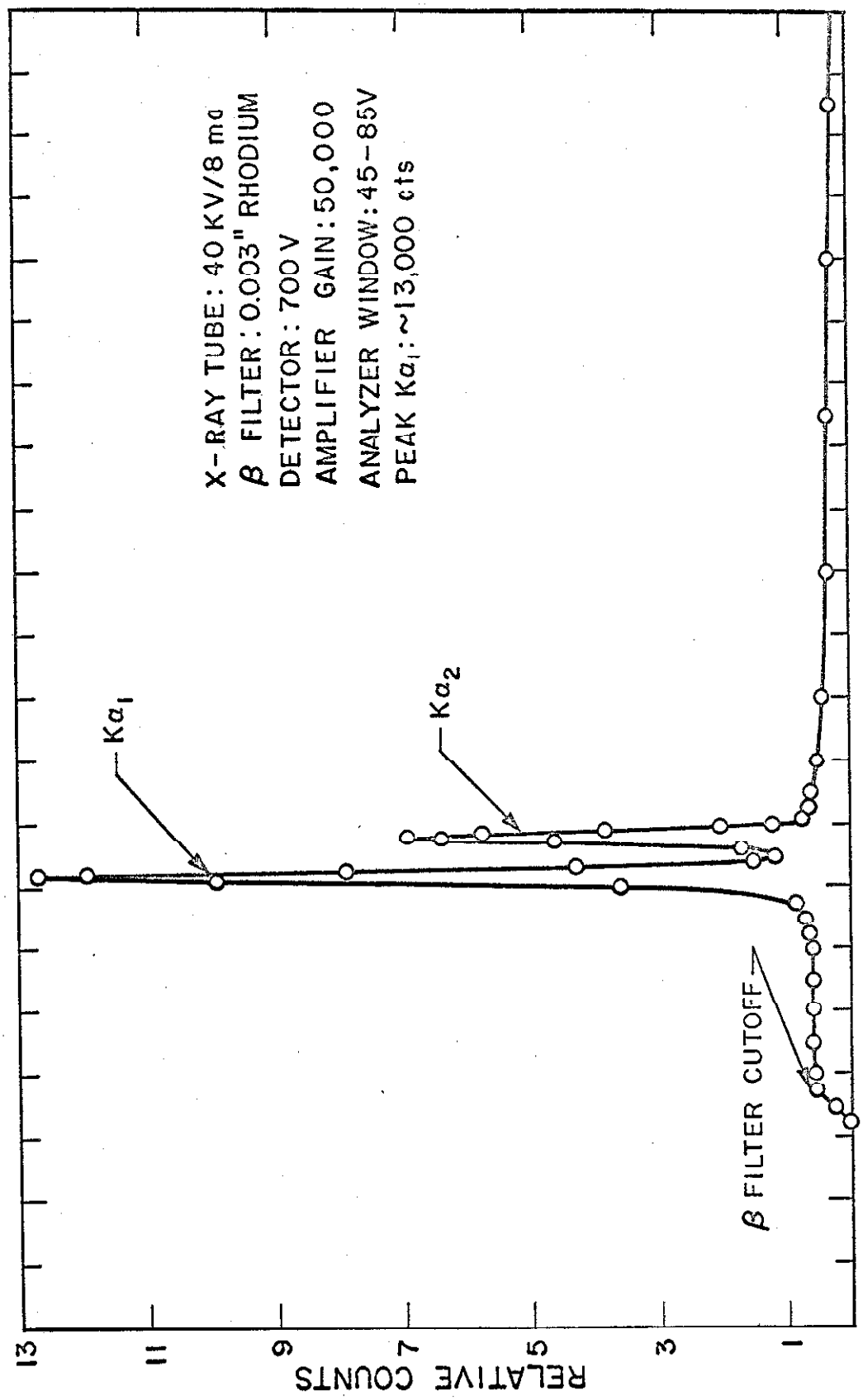

Figure 3-2. LiF crystal spectral analysis of silver radiation.

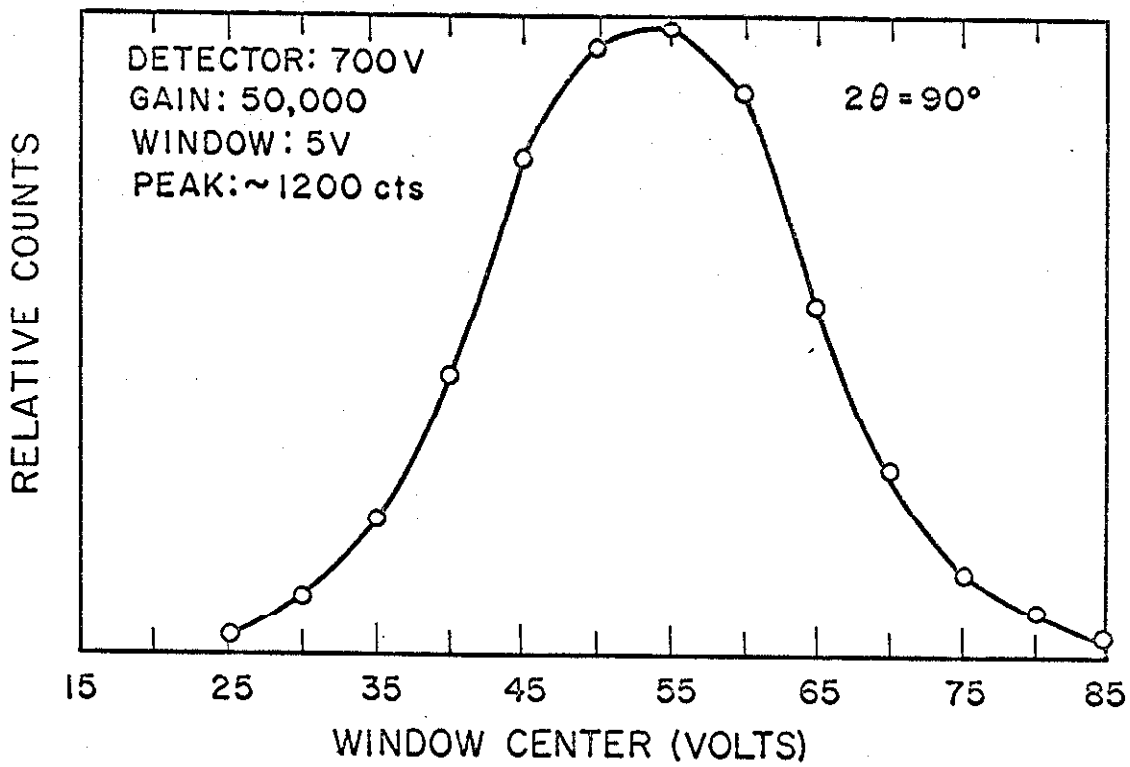

Figure 3-3a. Pulse amplitude distribution of Ag K_α from a gallium surface.

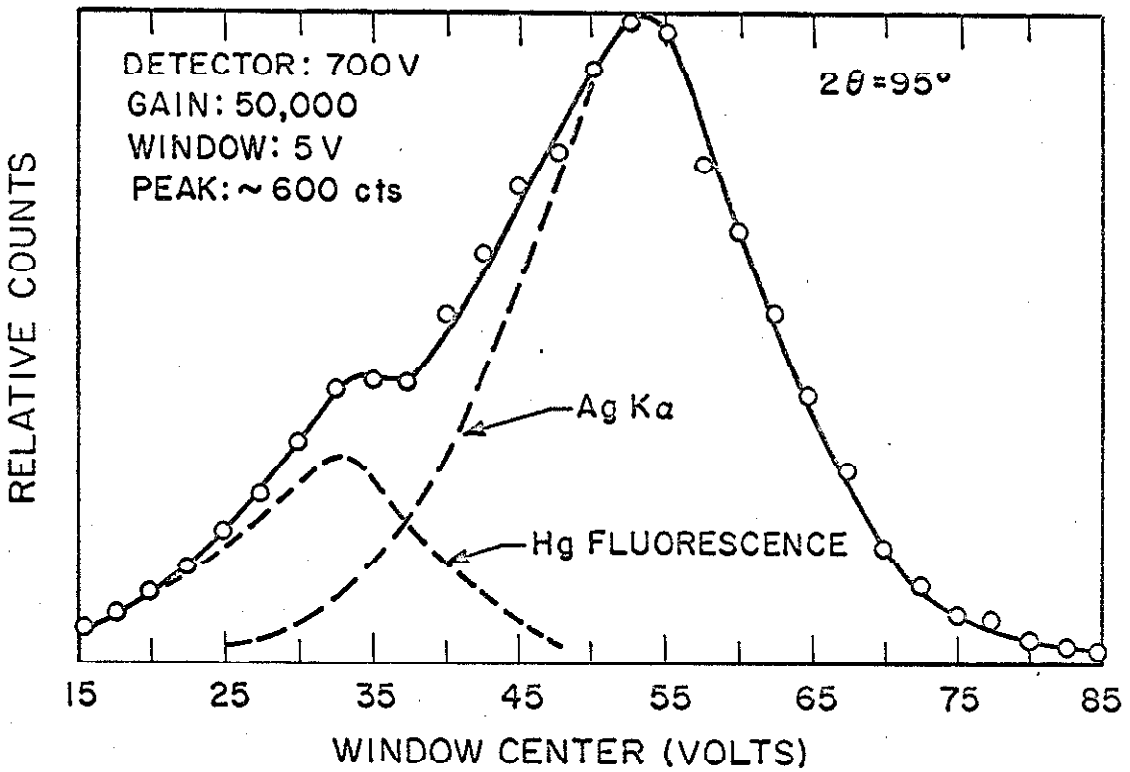

Figure 3-3b. Pulse amplitude distribution of Ag K_α from a mercury surface.

a Dumont 6291 photomultiplier tube, a high voltage cascade base, and a preamplifier.

Once the photomultiplier tube and crystal were optically coupled, the entire unit was light shielded with black electrical tape, radiation shielded with 1/8" of lead sheet, magnetically shielded with a standard mu-metal sheath, and finally, electrostatically shielded with heavy copper foil. Both the radiation and electrostatic shields were extended to cover all but a narrow entrance slit over the center of the detector crystal.

The cascade base was wired according to drawing B2-1845, reference (22). It was found that for long term stability and low noise performance a mica-filled, low-loss bakelite tube socket and 1% deposited film resistors were necessary. Before final assembly the tube base and socket, including the resistance cascade, were washed with reagent grade methanol, dried, assembled, and sealed with electrical tape to minimize contamination from dust and fumes in the laboratory. The final resistance cascade constructed was given a coating of anti-corona insulating lacquer immediately after the methanol wash to further minimize the chance of contamination. It was found that the general area of tube base, tube socket, and high-voltage and signal connectors were quite a sensitive noise source, and the greater the care used in protecting these parts from contamination, the lower the noise level.

The preamplifier was built according to drawing 2943 of Franklin Electronics Inc. In the strict sense the device was not a preamplifier but an

impedence matching unit between the high impedence output of the photomultiplier and the relatively lower input impedence of the linear amplifier.

The remaining systems used in the detector "chain" were Nuclear-Chicago units of their 8000 Series. These units were stabilized high-voltage supply (8200), linear amplifier (8150), pulse height analyzer (8300), timer (8600), scaler (8250), and digital printer (Hewlett-Packard 560A). The overall electronic specifications are given in the 8000 Series Instruction Manuals of Nuclear-Chicago. A short series of semi-quantitative checks were made on the high-voltage supply, linear amplifier, and pulse height analyzer for performance and reliability. In general the variability of all three units was significantly greater than the stated limits, but far below any measurable variation with respect to the actual count data and its uncertainty.

The standard running conditions for the system were 700 volts on the photomultiplier tube, a gain of 50,000 x from the linear amplifier, and 35-85 volts or 45-85 volts for the pulse height analyzer, depending upon the sample studied. Under these conditions the silver K_α line was centered at 54 volts, and the 35-85 volt and 45-85 volt windows admitted approximately 97% and 82% of the silver K_α line respectively.

One particular problem, which was of major importance and required an appreciable amount of time, was that of obtaining a low and stable background count. Since the maximum count rate for a large number of data points was of the order of 1 ct/sec, it was necessary to reduce background, primarily electrical noise, to as low a level as possible in order to obtain a meaningful count in a

reasonable time interval. A major part of the background noise was eliminated by means of the previously mentioned construction techniques for the detector itself. Further noise reductions were made by the use of line-regulating and filtering transformers. In spite of the claims of the manufacturer (Nuclear-Chicago), spurious counts due to line transients were picked up. This problem was particularly bad in this laboratory where other electronic equipment was being used concurrently. It was finally necessary to shield, clean, or protect by grounding or bridging capacitors several switches and relays used in the automatic counting devices to eliminate spurious counts. By means of these precautions, stable backgrounds of 0.040 cts/sec and 0.025 cts/sec were obtained for the 35-85 volt and 45-85 volt windows respectively. Since these background levels were quite satisfactory for a 1 ct/sec data point, no further noise reduction was attempted. The study of low level background noise is a time consuming operation and practically cannot be carried out to perfection. Since noise count rates are subject to the usual statistical uncertainties, and since the count rates are quite low initially, it becomes impractical to collect sufficient data to critically assess the effects of any particular alteration.

The basic sample cell and its attendant support and temperature control assembly are shown in detail in Figures 3-4 and 3-5.

The choice of construction materials of the complete unit was based on several requirements. These were thermal and physical stability over the temperature range of interest, machinability, non-reactive and non-wetting towards gallium and mercury, physically light so that support other than the

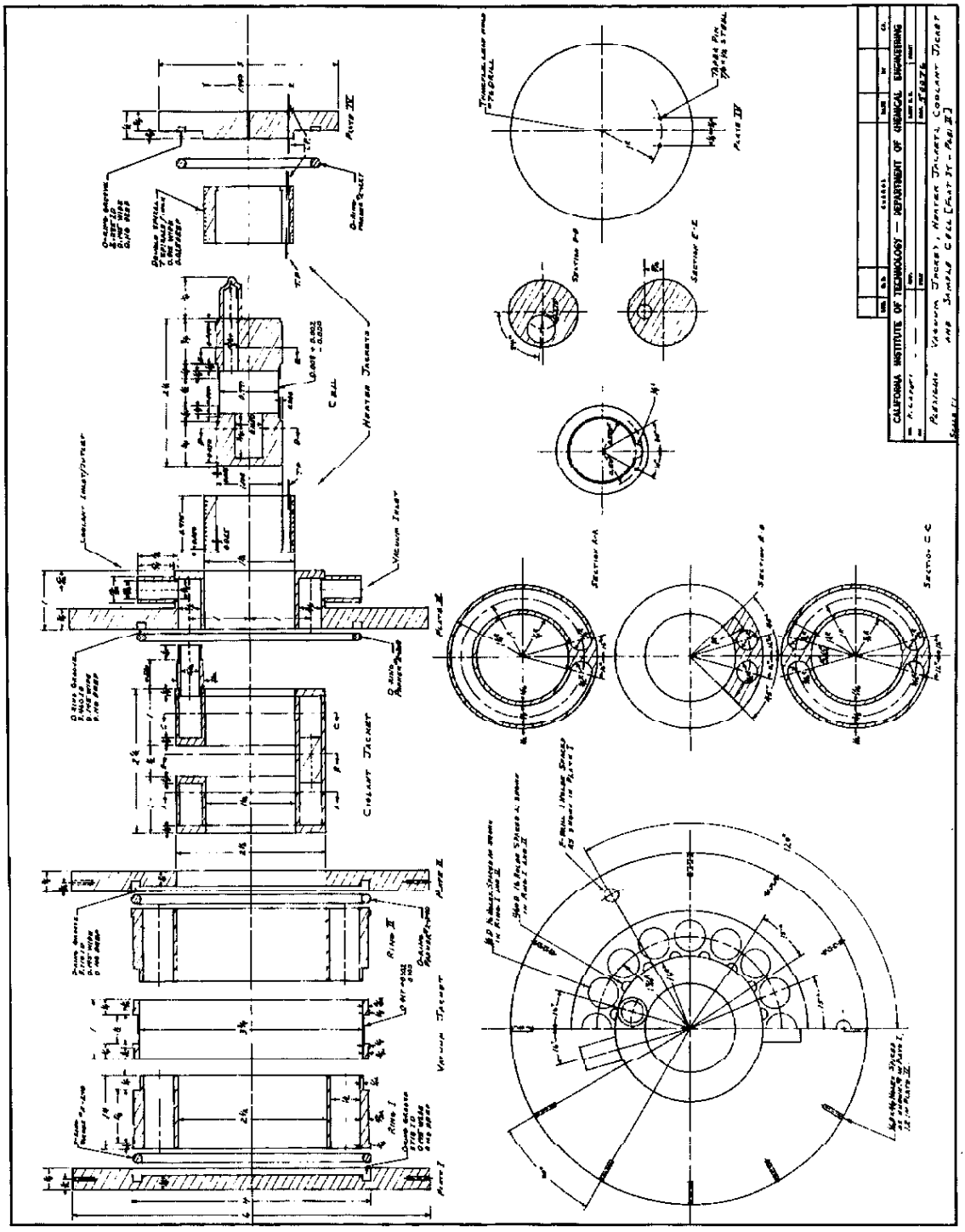

Figure 3-4. Detailed plan of sample cell and supporting jackets.

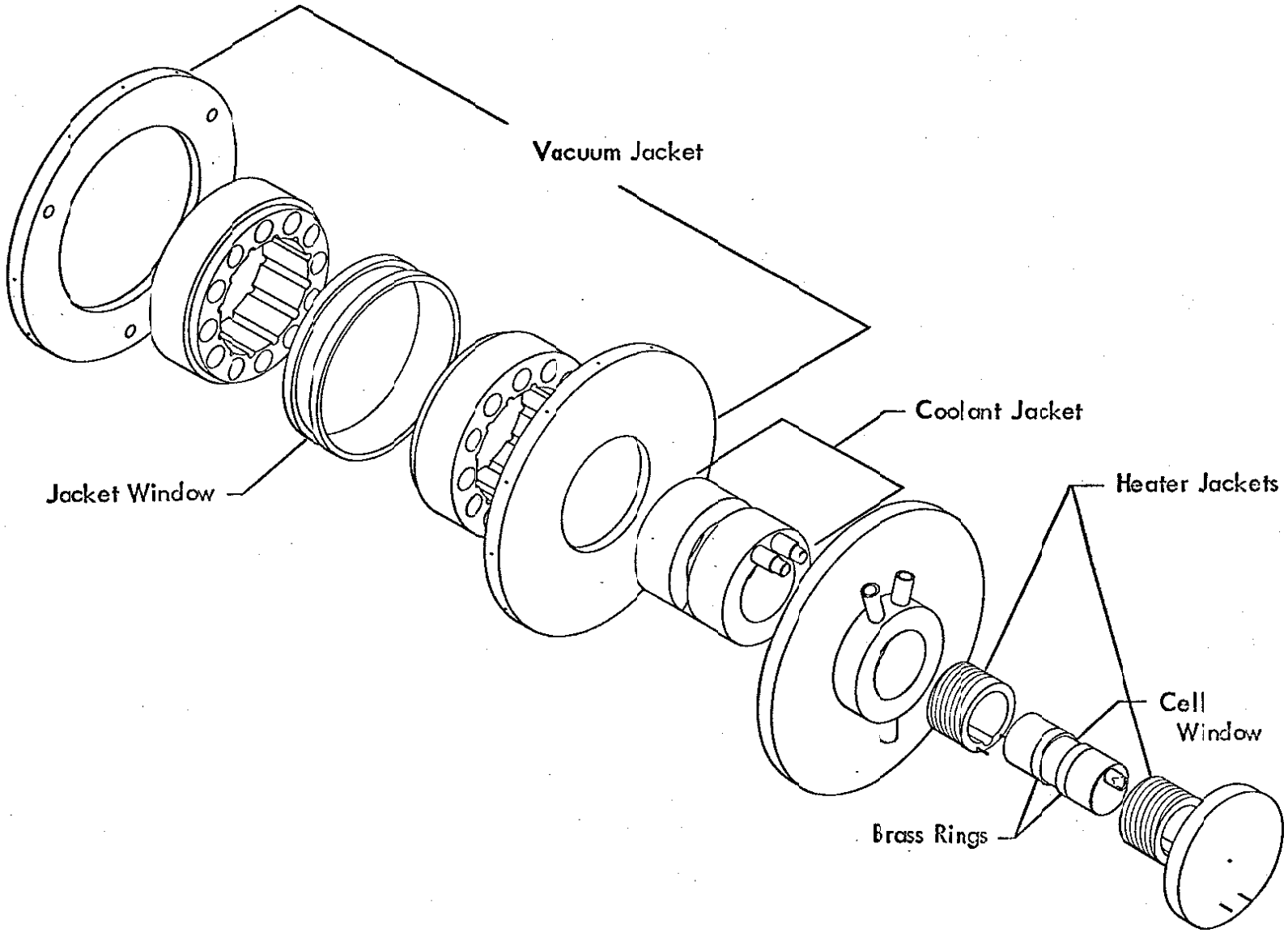

Figure 3-5. Exploded isometric view of sample cell and supporting jackets.

center shaft of the goniometer was unnecessary, transparency, and low absorption cross section for x-rays. These last two criteria are strictly necessary only for the windows of the sample cell and vacuum jacket. In actual practice Lucite (T. M. DuPont) or Plexiglas (T. M. Rohm and Haas), a methyl methacrylate plastic, was found to meet all of the above mentioned requirements quite well.

The basic criteria of the physical design of the complete unit were rapid assembly and disassembly for sample replacement, minimum and simple adjustment for sample alignment, accurate and uniform temperature control, and ease of construction. With varying degrees of success all of these goals were met. In a number of instances the optimums of two or more requirements were mutually exclusive, and compromises had to be made. The six months of almost continuous use showed the design to be quite successful.

The sample cell was patterned after the cell reported by Rodriguez and Pings (23) and designed to provide liquid level control, protect the sample from atmospheric reaction or contamination, minimize incident and scattered beam absorption, and permit visual inspection. Level control was accomplished by rotating the cell, and the subsequent filling or emptying of the offset well with the sample liquid lowered or raised the liquid level in the main well. With the offset and main wells approximately half full, a cell rotation of 1° would change the level in the main well ~0.002". Sample protection was obtained by loading the cell under vacuum, maintaining the vacuum, and heat sealing the loading tube. Beam absorption was minimized by using Plexiglas (T. M. Rohm and Haas), a material of low absorption cross section, and machining a thin window on

the cell. An 0.008" plastic window will pass ~99% of the silver K_{α} line. Visual inspection was assured by polishing the machined cell to transparency.

The heater jackets were built to slip fit over either end of the cell and seat against alignment shoulders at the ends of the cell. The double spiral of both heater jackets was wound with Chromel A heater wire (#36 wire, 25.3 ohms/ft). The two jackets were connected in series to give a total resistance of 258 ohms.

The coolant jacket was built to fit snugly over the heater jacket and cell assembly to form a single unit. It was necessary to build a coolant jacket with asymmetric gas flow in order to provide a viewing slot for the x-ray beams.

The outer vacuum jacket was composed of several pieces for ease of construction and sample mounting. Plate I was designed to bolt to a hub and shaft which could be fitted into the goniometer center sleeve. Rings I and II were connected with a machined and polished vacuum window by means of a slip fit. Both rings were bored out and fluted so as to reduce thermal conduction and to facilitate evacuation. Before assembly the window shoulders of Rings I and II were well greased with silicone grease to provice both lubrication in mounting the window and a vacuum seal. Then with the use of Plate II the entire vacuum jacket was mounted onto Plate I and positively centered by means of the recess in Plate I. The jacket was held together as a unit with spring clips connecting circumferences of Plates I and II. At this point Plate III was connected to the coolant jacket and cell assembly by silicone grease seals. This complete unit was then inserted into the vacuum jacket, Plate IV seated, and the entire

device evacuated to ~1 μ Hg. Vacuum seals between the plates and rings were obtained by the use of O-rings. Vacuum seals at the window, coolant jacket connections, and thermocouple lead hole in Plate IV were obtained by silicone grease seals. The heater connectors were taper pins imbedded in Plate IV with indium packing for vacuum tightness and electrical continuity.

The purpose of the vacuum was threefold. It maintained the entire structure as a rigid unit, it provided thermal insulation from the laboratory, and it minimized the possibility of air diffusion through the thin cell window. A slight modification of this system had to be introduced for the high temperature runs of the pure mercury and high mercury samples. Because of mercury condensation on the inside of the cell window, it was necessary to build a second outer window containing a resistance heater and to run the vacuum jacket at a pressure of one atmosphere of air. By the use of this captive volume of hot air, it was possible to greatly reduce the temperature gradient between the sample and cell window, and thus eliminate the condensation problem. Under the original vacuum conditions the mercury film build-up on the cell window for a pure mercury sample at 50° C was sufficiently rapid to reduce the scattered beam intensity to 90% of its initial value in about one hour.

The entire device, both modified and unmodified, described above weighed only a few pounds, excluding the metal hub and shaft, and had the added advantage that it and the hub and shaft could be completely removed as a unit from the goniometer, such as for alignment checks, without disturbing thermocouple, heater, or vacuum connections. For a general view of the

complete system mounted on the goniometer see Figures 3-6 and 3-7.

The procedure used for the preparation and analysis of the two mercury-gallium mixtures was essentially the same as that of Spicer and Bartholomay (3).

The stock metals used for the samples were Ballard's triply distilled mercury and Alcoa's 99.9999% gallium. Both mixtures were prepared with an excess quantity of the minor component and stored under an acidic solution of gallium chloride (pH=1, 1.4×10^{-2} molar in gallium chloride). This cover solution destroyed any oxide film on the metals. The presence of these films would greatly reduce the effective metal to metal contact and subsequent intersolubility effects. Both samples were kept at 42° C for 25 days. During this time the samples were shaken regularly. The samples were then thoroughly washed with distilled water, dried, and placed in a vacuum desiccator at 22° C.

Two aliquots were taken from the interior of each sample by means of a plastic needle and syringe and analysed. The four test samples were weighed and stored under 12 N HCl to dissolve the gallium contained in the amalgam. The HCl was renewed periodically as long as there was any evolution of hydrogen gas. The test samples were then thoroughly washed with distilled water, dried with an acetone wash, and weighed. Using the initial and final weights of the four samples, the mole fractions of the two components of the original samples were calculated. Since the analysis of the high mercury-low gallium mixture was quite satisfactory, a known amount of pure mercury was added to dilute the gallium slightly. This was done to eliminate the possibility of pure gallium coming out of solution as the temperature was decreased and forming a floating

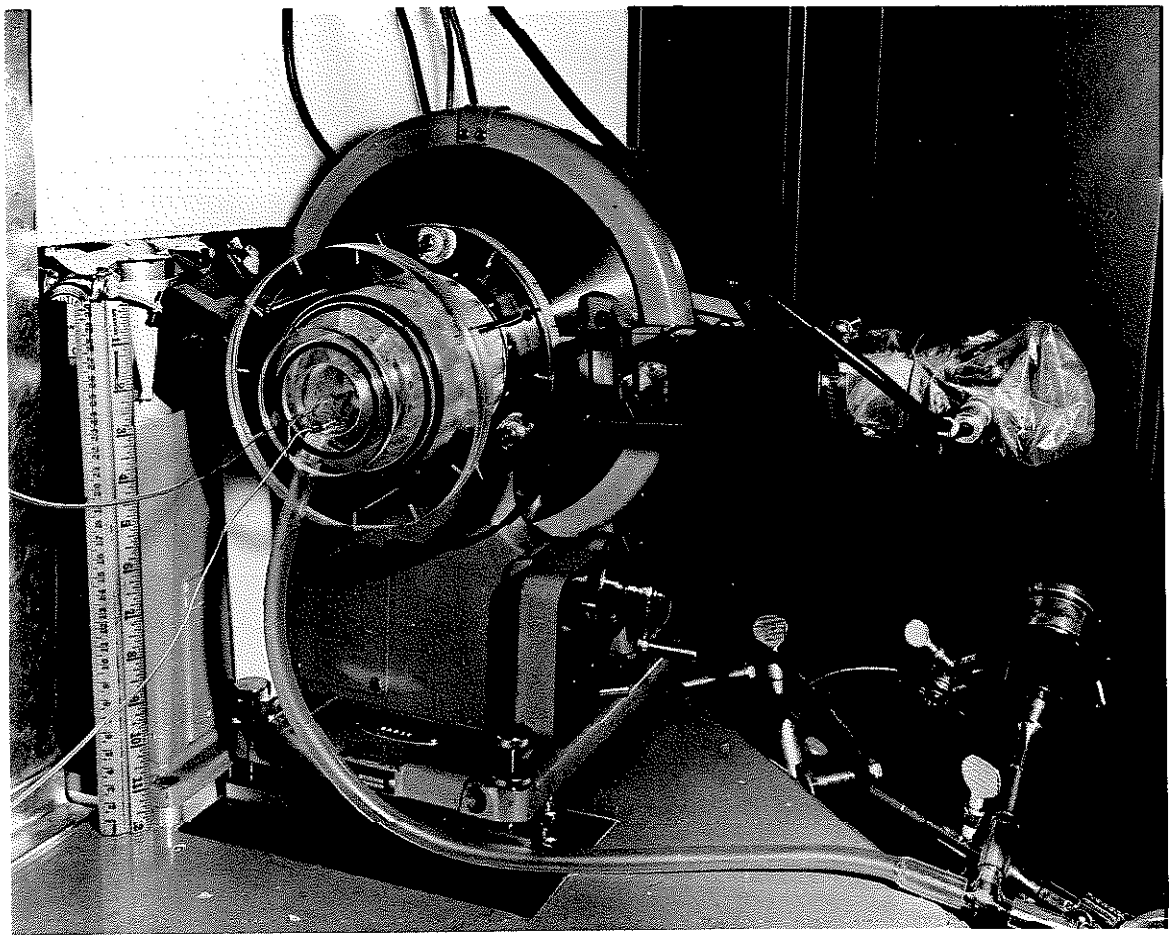

Figure 3-6. Side view of mounted sample assembly.

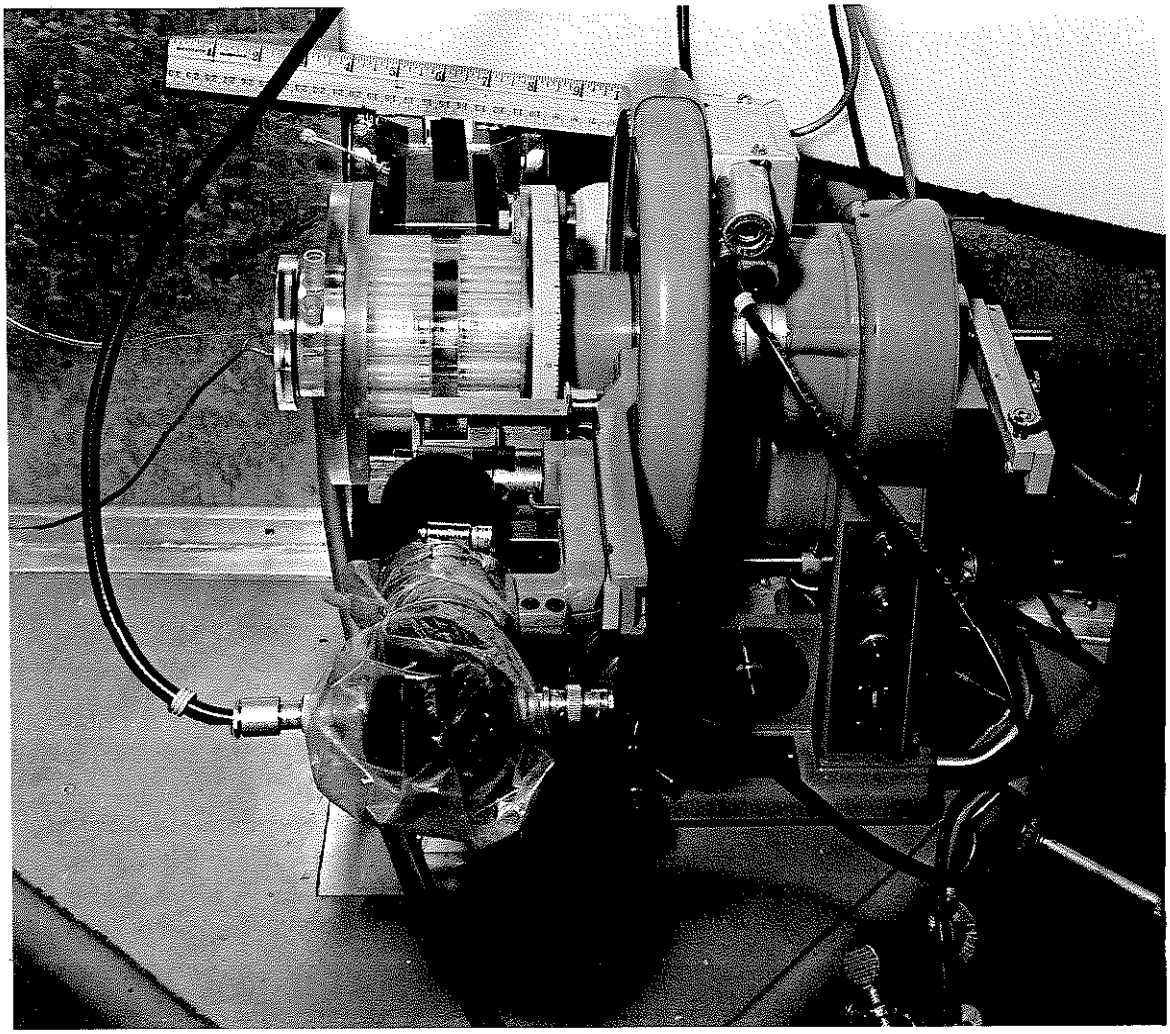

Figure 3-7. Overhead view of mounted sample assembly.

film on the solution surface.

The calculated values for the various mole fractions of the two samples are given in Table 3-1.

Table 3-1

Composition of Sample Mixtures

	Sample	
	MG	GM
Mole Fraction of Mercury (1st. aliquot)	0.9632	0.0197
Mole Fraction of Gallium (1st. aliquot)	0.0368	0.9803
Mole Fraction of Mercury (2nd. aliquot)	0.9625	0.0197
Mole Fraction of Gallium (2nd. aliquot)	0.0375	0.9803
Average Mole Fraction of Mercury	0.9628	0.0197
Average Mole Fraction of Gallium	0.0372	0.9803
Average Mole Fraction of Mercury (after dilution)	0.9658	------
Average Mole Fraction of Gallium (after dilution)	0.0342	------

Before loading any samples, all cells were thoroughly cleaned with detergent washes, completely rinsed with distilled water, dried, and then stored for a minimum of a week in a vacuum desiccator. This last step proved to be quite important in minimizing wetting of the cell walls by the gallium solutions.

It also minimized contamination of the samples. Briggs (24) found essentially the same result for that of glass. It has been proposed by Boyer (25) that the wetting of surfaces is caused by reaction of the gallium with adsorbed air or oxygen and the formation of an adhering film by means of this metallic oxide layer.

Immediately prior to the actual loading, the cell was removed from the desiccator and connected to a miniature three way plastic stopcock. This stopcock was in turn connected to a vacuum line and graduated syringe. As soon as the cell was in place, it was evacuated and kept under vacuum for at least two hours. An excess of the sample to be loaded was then poured into the syringe, taking care to retain all floating oxide films in the original sample container. The basic idea in loading the syringe, and subsequently the cell, was to remove the main bulk of the sample from beneath the oxide surface and minimize sample contamination in the cell. When the cell was loaded by opening the stopcock and draining the syringe, a second flotation separation occurred. After the correct volume of sample was added, the cell was again pumped on with vigorous shaking for at least an hour to remove any gas that had been trapped in the sample. Finally, the filling tube of the evacuated cell was collapsed and heat sealed to give a permanent vacuum seal.

The basic temperature control system was composed of an insulating vacuum jacket, a coolant jacket which used a cold gas coolant, heater jackets which used electrical resistance heating, and a copper-constantan thermocouple and attendant equipment for temperature measurement and control.

When the coolant jacket, as previously shown in Figures 3-4 and 3-5, was actively used, an insulated tube was connected from a sealed Dewar bottle of liquid nitrogen to the inlet tube of the coolant jacket. A resistance heater immersed in the liquid nitrogen was then used to boil the liquid nitrogen and produce a stream of cold gas which was fed through the coolant jacket. As a test of both the cooling ability of the gas and the temperature stability of the entire sample assembly, an experimental run was carried out where the temperature of the sample was maintained at about -60° C for several hours. Examination later showed that this low temperature had no effect on the outer jackets or the inner sample cell. This temperature was by no means an ultimate lower limit for the device and was more an arbitrary and convenient choice to determine if the system had any marked thermal weaknesses at low temperatures. The upper temperature limit was approximately 60° C and was determined by the softening point of the plastic.

Normally the coolant jacket was only used actively if the temperature of the experimental run was below room temperature. In this case the boiling rate of the liquid nitrogen was adjusted to lower the sample temperature about 5° C below the desired temperature. Using this value as a base, the heater jackets were used to raise and control the temperature of the sample to the desired one. In the case of runs above room temperature only the heater jackets were used.

The power for the heater jackets was derived from a magnetic amplifier controlled and driven by a Leeds and Northrup Series 60 C.A.T. Control Unit.

The control unit was in turn fed by a Leeds and Northrup recorder and D.C. amplifier. The signal input to the D.C. amplifier was the voltage difference between the measuring thermocouple and a reference voltage. The reference voltage was chosen according to the copper-constantan temperature-E.M.F. tables of reference (26) for the temperature of interest.

A series of calibrating runs for a range of temperatures were made to determine the temperature gradients to be expected over the surface of the sample and from the surface of the sample to the measuring thermocouple attached to the lower half of the cell window. This thermocouple was copper-constantan (#40 B.S. gauge) soldered to a sheet copper oval (0.75" x 0.30" x 0.003") which was sealed to the cell window by a film of silicone grease.

The maximum surface temperature gradient over that part of the surface viewed by the detector was 0.01° C.

A second series of calibrating runs were carried out in order to determine the absolute temperature of the surface as measured by the window thermocouple. This thermocouple was calibrated at the ice point and boiling point of water. A platinum resistance thermometer was calibrated at the ice point and in turn used to check the stability of the reference ice bath used in the above mentioned thermocouple calibration. The ice bath used distilled water ice and air saturated distilled water and was made up according to reference (27). The same resistance thermometer was also used to check the ice bath for the reference junction of the window thermocouple. This last check was done regularly over a period of two months.

The final results of these tests gave an absolute uncertainty of ± 0.03° C in the ice point and ± 0.10° C in the boiling point of water as measured by the window thermocouple. The maximum measured instability of the ice bath in any 24 hour period was ± 0.01° C, and the maximum instability over the entire 2 month period was ± 0.02° C.

The final and corrected temperature data for the complete experimental series is given in Table 3-2.

Table 3-2

Corrected Experimental Temperature Data

Run Number	Surface Temp. (°C)	Max. Temp. Dev. (°C)	Uncertainty in Absolute Temp. (°C)	Total Time of Control (hours)
MM00A (1-7)	0.06	± 0.14	± 0.04	77
MM30A (1-6)	29.83	± 0.01	± 0.05	81
MM50B (1-6)	49.76	± 0.04	± 0.08	76
MG00A (1-6)	0.11	± 0.16	± 0.04	77
MG30A (1-6)	29.87	± 0.06	± 0.06	75
MG50A (1-6)	49.77	± 0.03	± 0.08	78
GM00A (1-6)	0.04	± 0.45	± 0.04	65
GM30A (1-6)	29.85	± 0.04	± 0.05	77
GM50A (1-6)	49.77	± 0.03	± 0.08	76

Prior to any experimental runs with the sample assembly the angle of incidence of the x-ray beam to a horizontal surface at the goniometer center was determined. The procedure used for the initial alignment of the goniometer to set a 0° reference line was that supplied by Norelco (22). Once this reference line was determined, the angle of incidence was measured using the parafocusing system of the goniometer. A bubble level was placed on a steel flat clipped in the powder specimen holder of the goniometer. The parafocusing system was then adjusted until the bubble level indicated that the bar was horizontal. The diffraction angle as indicated by the goniometer was then just twice the angle of incidence. In the actual measurement of this angle, a series of readings were taken reversing the steel flat and rotating the bubble level to eliminate errors due to imperfections in the steel flat or bubble level. The mean value of these measurements gave an angle of incidence of $4.80 \pm 0.02^{\circ}$.

The sample surface was adjusted to the goniometer axis experimentally by using the scattered x-ray beam. The intersection of the incident beam and the viewing beam, as determined by the scatter slits, defines a scattering volume. Under normal running conditions the scatter slit combinations were so chosen that this scattering volume was wholly contained within the sample cell boundaries. In this way any scattered radiation was totally from the contained sample. Air scatter was eliminated by evacuation of the cell to $\sim 2\mu$ Hg, and gas scatter of the three samples studied was negligible because of the low vapor pressures. This final point was checked experimentally, and there was no measurable scatter from the volume immediately above the sample. The scattering volume

dimension parallel to the goniometer axis was defined by two brass rings on the sample cell. (See Figure 3-5.)

To set the sample level, the cell was rotated raising or lowering the sample in the scattering volume. In either case the scattered intensity approaches a maximum as the sample surface approaches the goniometer center. By a judicious choice of scatter slits and viewing angle 2θ, the maximum could be made quite sharp. The determination of this maximum was repeated many times for each sample and was approached from both a too high and too low liquid level. It was quite important to allow the surface to come to equilibrium because of the large surface tension effects. It was for this reason that approaches were made from both directions and that minor oscillations were induced in the liquid to help in attaining equilibrium. The uncertainty in the liquid level as set by this method was ± 0.003".

For a complete experimental run it was necessary to use six sub-runs. A sub-run was a single run which used a single set of scatter slits and a single angular increment in 2θ. The change in scatter slits was necessary because of the loss in scattered intensity as the viewed area decreased with increasing 2θ. In all sub-runs the initial point viewed an area 0.45" by 0.3" on the sample surface. The 0.45" dimension remained constant for all runs and was defined by the brass rings on the sample cell. The 0.3" dimension, the distance L of Figure 3-1, was defined by the choice of scatter slits. Unfortunately as 2θ was increased, the distance L and the viewed area was decreased, thereby reducing the scattered intensity. For this reason the larger viewing area was periodically

restored before the measured intensity dropped so low that the count times became prohibitively long. Even with these slit changes, a single run of one sample at one temperature took a little over three days of continuous running.

The experimental angular increment $\Delta\theta$ in 2θ was chosen according to the detail and change in the intensity as a function of 2θ. Several preliminary runs were used to determine the general shape of the intensity curve as a function of 2θ. On the basis of these runs, an angular increment was chosen so that experimental detail and resolution, compatible with counting and slit resolution, would not be lost. All sub-runs were overlapped by a given number of points in order to determine normalization factors. These factors were necessary for constructing a single intensity curve from the individual sub-run curves. In theory it should be possible to calculate or experimentally determine the overlap normalization factors just once. In practice this was not possible because of minor changes in slit settings from one run to another, and therefore all runs have their own normalization factors.

The basic counting program followed was essentially the same as that of Rodriguez (28). The final system was a compromise based on the limitations in the automatic counting and angular stepping equipment, the count time available for a given number of points, the necessary accuracy for high S normalization of the i(S) curve, and the desired accuracy for i(S) at low S values where rapid and large variations in i(S) exist.

The counting program and slit combinations used in all the experimental runs are given in Table 3-3.

In operation the equipment was set up to run automatically for any sub-run. A programmer was built to step the detector arm of the goniometer and initiate the count cycle of the counting system. When the count was finished, the time and count were printed and indexed. The programmer then received a signal which restarted the complete cycle. The programmer/goniometer/counting system was built to use either preset count or preset time and to step the detector arm of the goniometer a preset number of cycles to obtain the desired $\Delta\theta$.

Table 3-3

Scanning Program

2θ Scan Interval	2θ Increment	Scatter Slits[1]	Angular Resolution[2]	Count Mode
8°-12°	0.25°	0.0020" 0.0012"	0.13°	900/1000 seconds[3]
11°-18°	0.25°	0.0020" 0.0030"	0.17°	1400/1600 seconds[3]
16°-31°	0.50°	0.0030" 0.0066"	0.38°	1400/1600 seconds[3]
27°-48°	1.00°	0.0066" 0.0087"	0.48°	4000 counts
42°-66°	2.00°	0.0087" 0.0205"	1.16°	10000 counts
58°-102°	4.00°	0.0205" 0.0205"	1.16°	10000 counts

[1] The first slit of each pair listed is the slit nearer the axis of the goniometer.
[2] Mean of total angular aperture and aperture of uniform sensitivity.
[3] First time interval for x-ray tube at 14ma/40KV, second time interval for x-ray tube at 12ma/40KV. (Higher current condition used only for GM00A Series.)

Data Analysis

Experimental Corrections

In order to obtain the final radial distribution function by a Fourier inversion, an explicit evaluation of the i (S) function must be made. It is this function which can be derived from the experimental intensity. The following derivation is carried out for the single element monatomic liquid for simplicity, although the basic results are valid for the two element case when appropriate corrections are made in the physical constants, such as bulk density.

The total measured experimental intensity can be expressed by

$$I_{ex} = K_1 I_{coh} + K_2 I_{mod} + K_3 I_{fl} + K_4 I_{bg} \qquad (4\text{-}1)$$

where I_{ex} = measured experimental intensity

I_{coh} = intensity of coherently scattered radiation

I_{mod} = intensity of modified or incoherently scattered radiation

I_{fl} = intensity of fluorescent radiation

I_{bg} = intensity of background radiation

K_1, K_2, K_3, K_4 are constants or functional expressions of θ and experimental conditions.

Since the evaluation of i (S) contains explicitly only I_{coh}, equation (4-1) can be rewritten

$$I_{coh} = \left[I_{ex} - (K_2 I_{mod} + K_3 I_{fl} + K_4 I_{bg}) \right] \frac{1}{K_1} \qquad (4\text{-}2)$$

or

$$I_{coh} = K_5 I_{ex} - (K_6 I_{mod} + K_7 I_{fl} + K_8 I_{bg}) \qquad (4\text{-}3)$$

where $K_5 = \frac{1}{K_1}$

$K_6 = \frac{K_2}{K_1}$

$K_7 = \frac{K_3}{K_1}$

$K_8 = \frac{K_4}{K_1}$

It is just these constants or expressions that must be determined to evaluate I_{coh}.

As previously mentioned in the experimental section, a judicious choice of x-ray tube and window setting of the pulse height analyzer allows K_7 to be set equal to zero.

By careful design and cell evacuation any cell or gas background scatter had been eliminated. The only remaining backgrounds were local residual radioactives, cosmic rays, and electronic noise, all of which were angle independent. Therefore K_8 is equal to K_5. Equation (4-3) can now be simplified to

$$I_{coh} = K_5 (I_{ex} - I_{bg}) - K_6 I_{mod} \qquad (4\text{-}4)$$

or

$$I_{coh} = K_5' (E_{ex} - E_{bg}) - K_6' E_{mod} \qquad (4\text{-}5)$$

The only difference between the two equations is that intensity I_i is given in terms of cts/sec/unit area and scatter E_i in terms of cts/sec. This substitution is quite convenient since it represents directly the actual counting data.

The terms K_s' and K_i' are expressions containing correction terms for sample, window, and beta filter absorption of incident and scattered radiation. They also contain a polarization factor, a view factor, a normalization factor for matching sub-runs, and a normalization factor for matching to i (S) criteria.

Using the geometry and designations shown in Figure 3-1 and applying the exponential absorption law, the experimental coherent scatter at a particular S is given by

$$E_{c1} = \rho_o F_c(S)\, a\, I_o \iiint e^{-\mu_c\left(\frac{1}{\sin\alpha} + \frac{1}{\sin\phi}\right) z}\, dx\, dy\, dz \quad (4\text{-}6)$$

where ρ_o = atomic density

$F_c(S) = f^2(i(S)+1)$, total coherent scatter per atom in electron units

a = "effective" area of detector (true effective area times detector efficiency)

I_o = incident beam intensity at liquid surface

μ_c = absorption factor for coherent radiation

$\frac{z}{\sin\alpha}$ = distance travelled in the sample by the incident beam

$\frac{z}{\sin\phi}$ = distance travelled in the sample by the scattered beam

α = angle between the incident beam and the liquid surface

ϕ = angle between the scattered beam and the liquid surface, $\phi = (2\theta - \alpha)$.

This equation is strictly valid only if the incident and scattered beams are truly parallel. For the experimental conditions used, the divergence of the beams was sufficiently small so that the equation shown above could still be used quite accurately.

Using equation (4-6) and integrating over length L on x, width W on y, and from z equals zero (liquid surface) to some depth z gives

$$E_{c1} = \rho_o F_c(S)\, a\, I_o \frac{WL}{\mu_c}\left[\frac{\sin\alpha \sin\phi}{\sin\alpha + \sin\phi}\right]$$

$$\times \left[1 - e^{-\mu_c\left(\frac{\sin\alpha + \sin\phi}{\sin\alpha \sin\phi}\right) z}\right] \qquad (4\text{-}7)$$

The mass absorption coefficients of mercury and gallium are 69.90 and 31.04 cm^2/g respectively (29). Assuming the minimum absorption case of $\phi = 90°$ and for an α of 4.80°, the exponential term of equation (4-7) drops to 0.001 at a depth of 2.22×10^{-4} and 1.11×10^{-3} inches for mercury and gallium respectively. Since the depth of all of the liquid samples was much greater than either of these values, the exponential term can be ignored.

The window and beta filter absorption was designed to be invariant with respect to 2θ and therefore can be included as a constant reduction factor b_c. In actual practice this factor can be considered to be entirely due to the beta filter since the window absorption is negligible in comparison. Since the width W

is defined by the parallel brass rings surrounding the cell, it is also angle independent.

Because of the horizontal geometry of the surface, the length L varies with the scanning angle and must be corrected by a view factor. This factor has the form

$$L = \frac{H}{\sin \phi} \tag{4-8}$$

where H is the height of the beam at the liquid surface.

One final angle dependent correction is that of polarization. Assuming the incident beam to be unpolarized, the scattered intensity for a given 2θ is reduced by a factor of $\frac{(1+\cos^2 2\theta)}{2}$.

Combining the view factor and the polarization correction with equation (4-7) and dropping the exponential term gives

$$E_{c2} = \rho_o F_c (S)\, a\, b_c\, I_o \frac{WH}{\mu_c} \left(\frac{\sin \alpha}{\sin \alpha + \sin \phi} \right) \times \left(\frac{1 + \cos^2 2\theta}{2} \right) \tag{4-9}$$

Separating out the terms which are independent of scanning angle and setting them equal to a constant yields

$$C = \frac{2 \mu_c}{\rho_o\, a\, b_c\, I_o WH \sin \alpha} \tag{4-10}$$

such that

$$E_{c2}=\frac{F_c(S)}{C}\left(\frac{1+\cos^2 2\theta}{\sin\alpha+\sin\phi}\right) \qquad (4\text{-}11)$$

The last correction factor needed, and which is angle independent, is the product of two normalization factors. The first of these is just the inter-normalization factor between sub-runs. This factor was derived from the experimentally determined overlap points. The ratio of the net count rates for each overlap point was determined and the arithmetic mean of the ratios was used as a first approximation for the overlap factor. The factor was then applied to the overlap points of the appropriate sub-run, and the results were plotted against the same overlap points of the sub-run to be matched. In almost all instances (44 out of 46) this first value was quite good, and no further corrections were made. In the remaining cases (2 out of 46) it was obvious from the plot that one of the experimental ratio points was significantly different from the remaining points and was discarded. In each instance one or both of the experimental points used to determine the ratio at a given 2θ had a small total count and therefore had a relatively high uncertainty as shown by $\pm\sqrt{N}$, where N is the total number of counts.

The second factor is ultimately used to normalize the i (S) curve for the final inversion and will be explained more fully in the part on normalization.

If these two factors are combined into a single factor A equation (4-11)

can be rewritten

$$E_{c3} = E_{coh} = \frac{F_c(S)}{AC}\left(\frac{1+\cos^2 2\theta}{\sin\alpha + \sin\phi}\right) \qquad (4\text{-}12)$$

A similar derivation can be carried out for the incoherent or modified scatter. An equation for the experimental modified scatter identical in form to that of equation (4-6) can be written

$$E_{m1} = \rho_o F_m(S)\, a\, I_o \iiint e^{-\left(\frac{\mu_c}{\sin\alpha} + \frac{\mu_m}{\sin\phi}\right)z} \, dx\, dy\, dz \qquad (4\text{-}13)$$

where F_m = incoherent scatter per atom in electron units

μ_m = absorption coefficient for incoherent or modified radiation.

Using the same limits as before, integrating, and dropping the exponential term yields

$$E_{m1} = \rho_o F_m(S)\, a\, I_o WL\left(\frac{\sin\alpha \sin\phi}{\mu_m \sin\alpha + \mu_c \sin\phi}\right) \qquad (4\text{-}14)$$

The modified scatter has, in addition to the same polarization factor and view factor, a modified beta filter absorption factor b_m and the Breit-Dirac correction $1/B^2$. This Breit-Dirac factor is used to correct the effect of electron recoil on the observed intensity and is discussed by James (30) and Compton and Allison (31).

The factor B is defined as

$$B = \frac{\lambda_m}{\lambda_c} = 1 + \frac{k \sin^2 \theta}{\lambda_c} \qquad (4\text{-}15)$$

where λ_m = wavelength of modified radiation

λ_c = wavelength of coherent radiation

k = constant (0.04852 Å for wavelength in angstroms (32).

Combining equation (4-14) and the above mentioned corrections yields

$$E_{m2} = \frac{\rho F_m(S)\, a\, b_m\, I_o W H}{B^2} \left(\frac{\sin \alpha}{\mu_m \sin \alpha + \mu_c \sin \phi} \right) \times \left(\frac{1 + \cos^2 2\theta}{2} \right) \qquad (4\text{-}16)$$

Equation (4-16) can be greatly simplified by the use of the previously derived constant C. This substitution gives

$$E_{m2} = \frac{F_m(S)\, b_m}{C B^2 b_c} \left(\frac{1 + \cos^2 2\theta}{\frac{\mu_m}{\mu_c} \sin \alpha + \sin \phi} \right) \qquad (4\text{-}17)$$

Both Kramers (33) and Compton (34) have attempted theoretically to show that the dependence of μ on wavelength for all elements can be approximated by a simple exponential form

$$\frac{\mu_1}{\mu_2} = \left(\frac{\lambda_1}{\lambda_2} \right)^n \qquad (4\text{-}18)$$

with n equals 3.

It has been experimentally verified by Richtmyer (35) that n does have a value of 3 for a few elements. Although this value of n would not be a bad

estimate for elements other than the ones studied, it should only be used as an order of magnitude estimate if no other information were available. Obviously the simple expression given is good only if there are no absorption edges between λ_1 and λ_2. Other values have been suggested by Allen (36, 37) for a better universal number.

If the experimental values for absorption coefficients at various wavelengths are available for the particular element of interest, an exact calculation of the exponent can be made. Fortunately experimental data was available so that it was possible for the author to do these calculations.

Rewriting equation (4-18) in terms of coherent and modified radiation gives

$$\frac{\mu_m}{\mu_c} = \left(\frac{\lambda_m}{\lambda_c}\right)^U = B^U \qquad (4\text{-}19)$$

By use of the exponential absorption law, the absorption terms b_c and b_m for a beta filter of thickness t_β can be written

$$\frac{b_m}{b_c} = \frac{e^{-\mu_{\beta m} t_\beta}}{e^{-\mu_{\beta c} t_\beta}} = e^{-\left[\frac{\mu_{\beta m}}{\mu_{\beta c}} - 1\right]\mu_{\beta c} t_\beta} \qquad (4\text{-}20)$$

where $\mu_{\beta m}$ = beta filter absorption coefficient for modified radiation

$\mu_{\beta c}$ = beta filter absorption coefficient for coherent radiation.

Using equation (4-19) it is possible to write

$$\frac{\mu_{\beta m}}{\mu_{\beta c}} = B^V \qquad (4\text{-}21)$$

The exact numerical values of the exponents u and v are given in Appendix 1.

Combining the normalization factor A and the results of equations (4-17), (4-19), (4-20), and (4-21) gives

$$E_{m3} = E_{mod} = \frac{F_m(S)}{ACB^2}\left[\frac{1+\cos^2 2\theta}{B^U \sin\alpha + \sin\phi}\right] e^{-(B^V-1)\mu_{Bc} t_B} \qquad (4\text{-}22)$$

It is now possible to write an expression for the total experimental scatter.

$$E_{ex} = E_{bg} + \frac{1+\cos^2 2\theta}{AC(\sin\alpha+\sin\phi)}\left[F_c(S)\right.$$

$$\left. + \frac{F_m(S)(\sin\alpha+\sin\phi)}{B^2(B^U\sin\alpha+\sin\phi)} e^{-(B^V-1)\mu_{Bc} t_B}\right] \qquad (4\text{-}23)$$

Solving for $F_c(S)$ yields

$$F_c(S) = \frac{AC(\sin\alpha+\sin\phi)}{1+\cos^2 2\theta}(E_{ex} - E_{bg})$$

$$-\frac{F_m(S)(\sin\alpha+\sin\phi)}{B^2(B^U\sin\alpha+\sin\phi)} e^{-(B^V-1)\mu_{Bc} t_B} \qquad (4\text{-}24)$$

Once an explicit evaluation is made for $F_c(S)$, it is possible to derive $i(S)$ from the relation

$$i(S) = \frac{F_c(S)}{f^2} - 1 \qquad (4\text{-}25)$$

Of the three terms E_{ex}, E_{bg}, and $F_m(S)$, the first two are measured experimental quantities. The third term $F_m(S)$ is based on theoretical calculations.

The specific values for F_m (S) used in this work are given in Appendix II.

A detailed analysis of the errors introduced by surface alignment, surface curvature, and surface oscillations is given by Rodriguez (28). Using the criteria developed in this analysis, it was possible to keep these sources of error well below that of count rate uncertainty. For the three samples used in this work, the problem of surface curvature was much less than that of the pure gallium used by Rodriguez because of the effect of reduced surface tension. Surface alignment was also less of a problem and could be done with somewhat greater accuracy and reproducibility. In all probability this difference was also due to the effect of reduced surface tension.

Normalization

In order to obtain an i (S) function which has physical meaning and can be used for a Fourier inversion, the function F_c (S) must be normalized.

At present there are three methods of normalization. The first method developed by Gordon, Shaw, and Daunt (38), involves the determination of the intensity ratio between a gaseous and liquid sample and solving two simultaneous intensity equations. In effect this technique is similar to the second method discussed below. The difference lies in the fact that the total independent scatter is based on an experimental measurement in the first case, i. e. the scattered intensity of the gas, and on theoretical values for the independent scatter in the second case.

The second technique, as described by Klug and Alexander (39), involves matching the high S region of the experimental coherent scatter to the theoretical independent coherent scatter per atom. The basis for this normalization is the assumption that interatomic interference effects decrease very rapidly with increasing S, and that at high S the total coherent scatter can be approximated by the coherent independent scatter. Using equation (4-25) and defining F_c (S) to be equal to f^2 at high S by the above mentioned approximation yields

$$i(S) = \frac{F_c(S)}{f^2} - 1 = \frac{f^2}{f^2} - 1 = 0 \qquad (4\text{-}26)$$

It was on this basis of i (S) being equal to zero at high S that the constants A and C of equation (4-24) were chosen.

The third method, developed independently by Krogh-Moe (40) and Norman (41), is that of inverting the experimental coherent intensity at a unique radial distance, r=0, and then matching it to a theoretical value at this distance. Formally the criteria of this method which must be satisfied for correct normalization of i (S) can be expressed by the equation

$$\int_0^{S_{max}} S^2 \, i(S) \, dS = -2\pi^2 \rho_o \qquad (4\text{-}27)$$

In the case of the data from the samples containing two components the i (S) requirement at high S of equation (4-26) was applied to the expression

$$i(S) = \frac{F_c(S) - \Sigma X_m f_m^2}{(\Sigma X_m f_m)^2} \qquad (4\text{-}28)$$

The tabulated values of the original counting data, corrected count rates, and resultant i (S) terms are given in Tables III-1 to III-9 in Appendix III.

Inversion

Using equation (2-15) and the derived I (S) function, it was possible to carry out the Fourier inversion to obtain a radial distribution function. The usual method of numerical integration using the given i (S) data points was modified by fitting a polynomial to the i (S) data points to obtain an explicit expression for i (S) and then integrating the entire equation analytically. Since both S and sin Sr are known analytically, there seems little advantage to impose on them the approximations necessary for numerical integration. This technique also has the added theoretical and practical advantage in that the inversion for any radius uses the identical approximation and is consistent for all values of r. Also no reevaluation of the integral need be carried out for discrete points for each r value.

In the actual procedure it was both unnecessary and impractical to attempt to fit a single analytical expression to the entire i (S) curve. Instead the i (S) curve was divided into a series of segments, and then each segment was fitted with a cubic polynomial by least squares. The size of any given segment was chosen such that a cubic polynomial could truly follow the variations within the segment, that the deviation of any experimental point from the analytical curve did not exceed the experimental errors, and that no experimental points were given undue importance in the fitting.

To minimize any discontinuities in slope from one segment to the next, the segments were overlapped to their midpoints. By this technique all data points except for the ones in the first half of the first segment and the last half

of the last segment are weighted equally. The region or panel of any given segment where the analytical expression was actually applied in the integration extended from the midpoint of the first overlap to the midpoint of the second overlap. In this way the panels used in the integration were consecutive and without overlap.

In order to eliminate any step discontinuities between panels, the zeroth order coefficient for each panel was set equal to the analytical numerical value of the preceding panel at the panel boundary. If these discontinuities were not eliminated, spurious ripples would be introduced into the final radial distribution function. These effects can be considered to be a special case of the truncation errors due to a non-zero i (S_{max}) described by Furukawa (2).

The final S values for panel boundaries and polynomial coefficients for all experimental runs are given in Tables IV-1 to IV-9 in Appendix IV. The i (S) curves using analytically determined points are shown in Figure 4-1. An expanded plot of a single i (S) curve including the experimentally determined i (S) points is shown in Figure 4-2 to illustrate the agreement between the analytical expression and the data points calculated from experimental results.

Since the basic computer program used for all calculations was developed by a previous investigator, a more detailed description of the actual inversion calculation can be seen in reference (28).

The direct output of the final inversion as defined by

$$G(r) = 4\pi r^2\left[\Sigma\bar{\rho}_i(r) - \rho_0\right] \qquad (4\text{-}29)$$

is shown for all nine runs in Figure 4-3. Once the numerical values for the

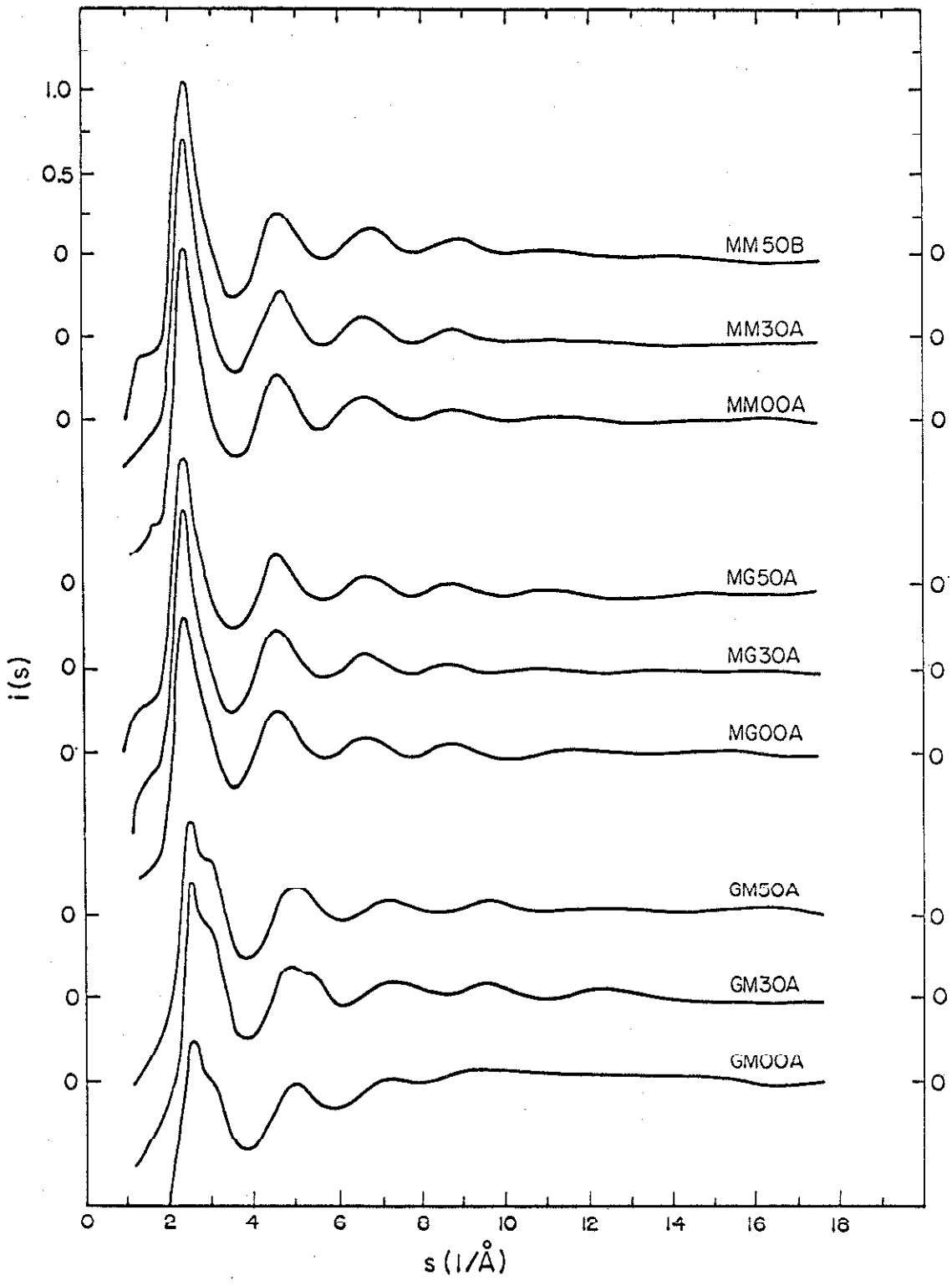

Figure 4-1. Analytical approximations to i (S) curves for all runs.

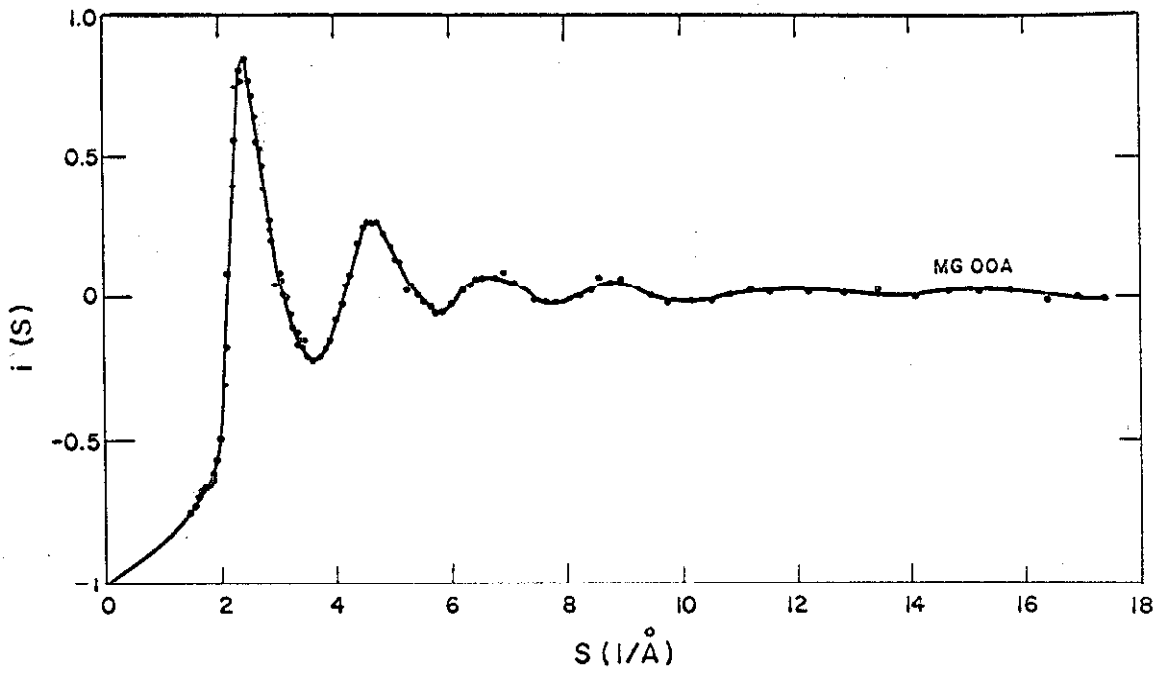

Figure 4-2. Analytical approximation plus experimental data points of a single i (S) curve.

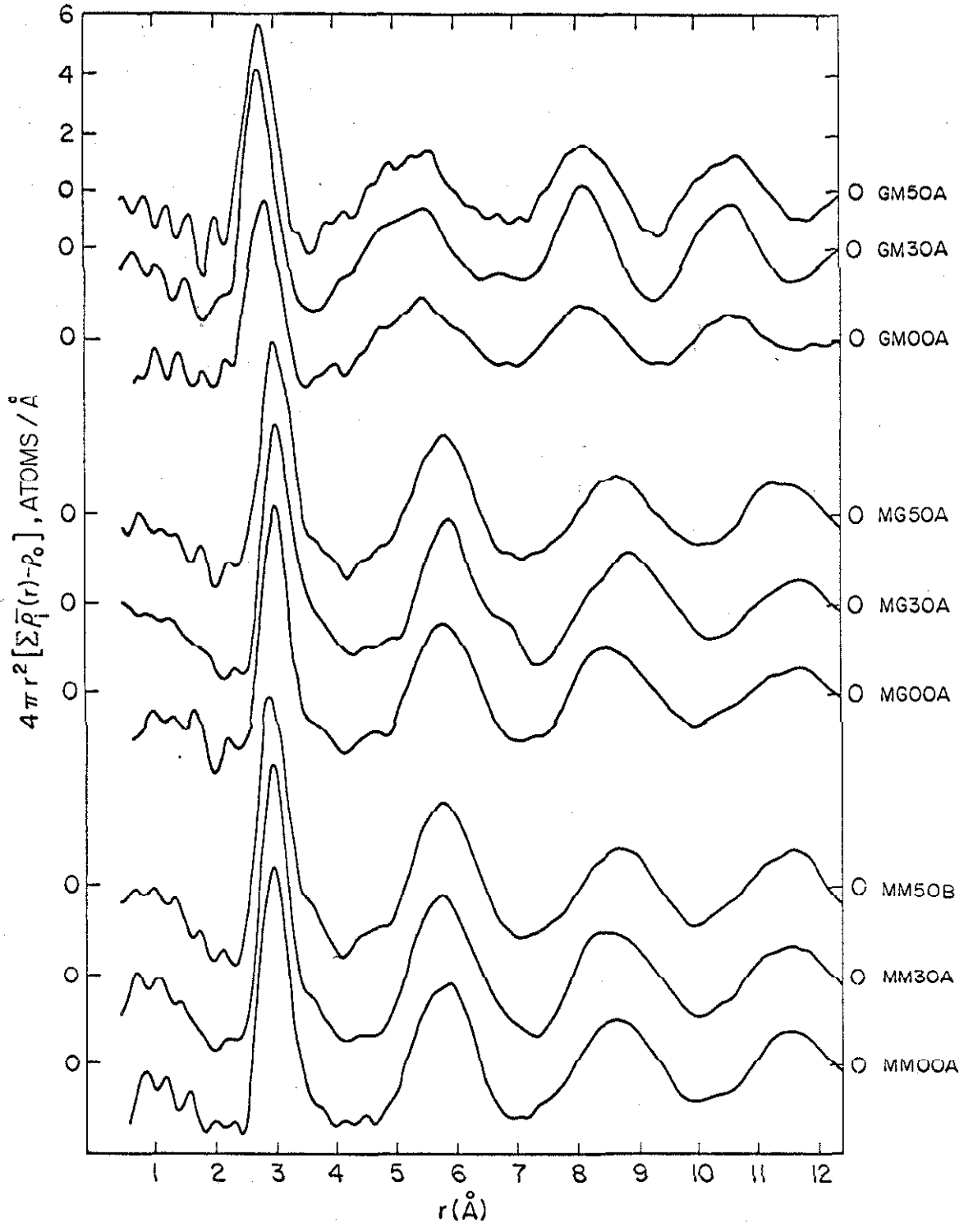

Figure 4-3. Graphical representation of the direct inversion for all runs.

previous expression were obtained, it was possible to calculate the quantity $4\pi r^2 \Sigma \bar{\rho}_i(r)$ as a function of r and then to calculate g (r) as defined by

$$g(r) = \frac{\Sigma \bar{\rho}_i(r)}{\rho_o} \qquad (4\text{-}30)$$

The calculated results for both of these expressions are given in Tables V-1 to V-9 in Appendix V. The graphical representations of these expressions are shown in Figures 5-1 to 5-7 in the following section.

Results and Conclusions

The agreement, or better the disagreement, of the experimentally determined structures of liquid mercury can easily be seen from the results listed in Table 5-1. Several major objections can uniformly be made about almost every source listed in this table. In most cases these objections severely limit the usefulness of the reported findings.

These objections are very brief, if any, experimental corrections of the raw data indicated; atomic scattering factors, dispersion corrections, and incoherent scatter data or even the source references for this information were not given; complete lack of raw data, except for a very few semi-quantitative, partially normalized plots of intensity curves; in several instances arbitrary assignment as to which subsidiary peaks were physically real and which were spurious; general lack of information regarding the method used to determine the coordination number of the first shell; and finally, no error estimates or reasons for their absence were given.

The problem of what values were used for atomic scattering factors, dispersion corrections, and incoherent scatter is vitally important in the normalization of the i (S) curve and in the subsequent inversion. Unfortunately almost all the papers reported did not give values for these necessary factors or the literature sources for the factors. The lack of this information, coupled with the lack of any experimental data or indicated experimental corrections, greatly reduces the usefulness of making comparisons between independent experimental determinations. In general if the plots are shown, a statement to the

Table 5-1

Radial Distribution Data for Mercury

Peak Distances r (Å)	r (Å)	r (Å)	Coord. # 1st peak (atoms)	T (°C)	Method	Reference
3.0	5.6	---	---	(Rm)	x-ray	(1)[1]
3.25	---	---	12	(Rm)	x-ray	(1)[1]
3.23	---	---	10	(Rm)	x-ray	(1)[2]
3.2	6.0	---	---	(Rm)	x-ray	(42)
2.9	5.2	---	6	-36°	x-ray	(43)
3.0	5.8	---	6	30°	x-ray	(43)
3.00	4.08	6.0	6.0	-38°	x-ray	(44)
3.00	4.17	6.1	5.8	0°	x-ray	(44)
3.00	3.95	6.0	5.8	50°	x-ray	(44)
3.00	3.85	6.0	5.5	100°	x-ray	(44)
3.00	3.95	6.0	5.3	150°	x-ray	(44)
3.05	---	---	5.7	200°	x-ray	(44)
3.0	3.47	---	6	18°	x-ray	(45)
---	---	---	8.6	---	x-ray	(46)[3]
3.05	6.0	---	8.3	23°	neutron	(47)
3.0	---	---	---	---	x-ray	(48)
3.1	---	---	8.2	17°	x-ray	(49)
3.12	---	---	8	---	x-ray	(50)[3]
3.15	---	---	8	---	x-ray	(51)[3]
3.05	6.05	---	7.5	---	x-ray	(52)

[1] as interpreted by (45).
[2] as interpreted by (20).
[3] according to (20).

Table 5-1 (Continued)

Radial Distribution Data for Mercury

Peak Distances r (Å)	r (Å)	r (Å)	Coord. # 1st peak (atoms)	T (°C)	Method	Reference
3.03	6.00	---	7.5	-38.9°	x-ray	(53)
3.03	6.00	---	7.5	4°	x-ray	(53)
3.03	6.00	---	7.5	26°	x-ray	(53)
3.05	---	---	10.0	28°	x-ray	(54)[4]

[4] according to (55).

effect that partial or complete normalization has been carried out is made, but there is no mention as to the method or numbers used.

The problem of spurious ripples or peaks introduced by truncation error or normalization uncertainties gives added difficulty in the interpretation of the radial distribution function. In the case of Hendus (45) the choice of spurious versus real peak appears to be quite arbitrary. Out of three equally prominent subsidiary peaks between the first and second major peaks, he considers the first one real and the second two spurious. The only basis used was that this first subsidiary peak coincided with an interatomic crystal distance of mercury, and the other two did not. However, it must be noted that the assignment of this peak did have a "precedent" in the work of Campbell and Hildebrand (44). A number of later determinations, as noted in Table 5-1, have ruled out the existence of this secondary peak. The determination by Vineyard (47) using neutron diffraction is of particular interest since the problem of normalization using angular dependent scattering factors does not exist.

A large area of uncertainty exists in the calculation of the coordination number of the first shell. The primary problem is due solely to the lack of uniformity in definition of the first shell. Basically three different methods are used. The first method defines the coordination number of the first shell as the area contained under the symmetrical curve formed by mirroring the $4\pi r^2 \rho(r)$ curve about the r value for the maximum of the first physically real peak in the $4\pi r^2 \rho(r)$ versus r plot.

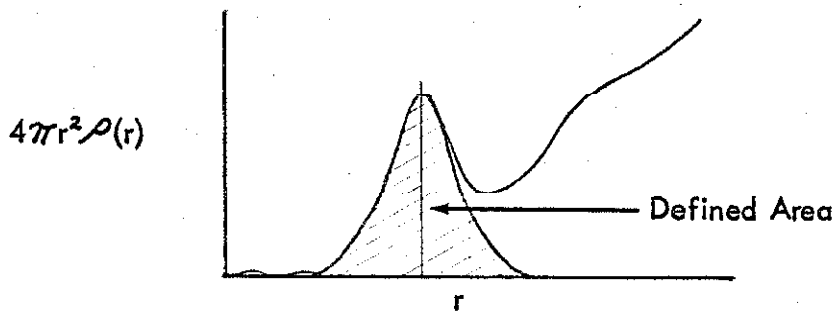

The second method defines the coordination number as the area under the $4\pi r^2\rho(r)$ curve minus the extrapolated leading edge of the second peak.

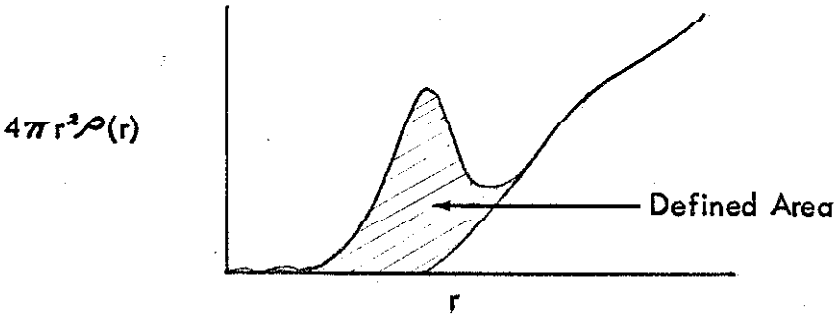

The third method defines the coordination number as the area under the $4\pi r^2\rho(r)$ curve bounded on the high r side by a vertical line dropped from the first physically real minimum.

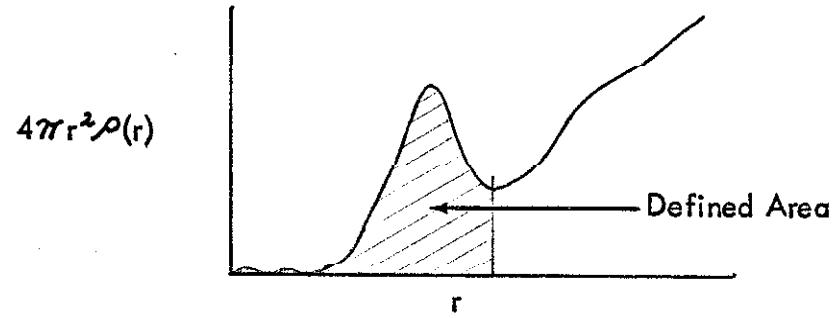

Regardless of the method used, care must be exercised in determining the area boundaries if error ripples are present.

Although each method has its own uncertainty as a means of coordination number determination, the greatest uncertainty of the literature values is caused

by the general lack of information as to which method the investigator used. Of all the references listed in Table 5-1, only Campbell and Hildebrand (44) used two of the methods and specifically defined them. The coordination numbers from their work listed in Table 5-1 were derived using the symmetrical curve technique. For lack of other information all remaining tabulated values were assumed to be based on the symmetrical curve method. This method is used most often by investigators in the field, but it is by no means the universal one.

All three of the above mentioned techniques were used to determine the first shell coordination number for the systems studied for this thesis. Nevertheless, it is the opinion of the author that the symmetrical curve method offers several advantages. The $4\pi r^2 \rho(r)$ curve up to the r of the first peak maximum has sharper definition than any subsequent peak, and therefore any necessary extrapolation is relatively easy and straightforward. In comparison, the extrapolation of the leading edge of the second peak is quite difficult, and slight changes in this extrapolation will change the bounded area quite markedly. The difficulty of the third technique for most cases is choosing the r value of the true minimum at which to draw the vertical line. This problem is particularly bad when the first minimum is a rather broad and shallow one, and when it is obscured by error ripples. The final results for the distances and values of the first three peak maximums and the coordination numbers of the first shell of all nine experimental runs are given in Table 5-2 and 5-3. In the case of the two element mixtures the coordination number can be considered to be an average of the different distributions making up the sample. A plot of $4\pi r^2 \Sigma \bar{\rho}_i(r)$ versus r for

Table 5-2

Summary Data of g (r) Curves

Series	Peak Distance			Peak Magnitude		
	1st peak (Å)	2nd peak (Å)	3rd peak (Å)	1st peak	2nd peak	3rd peak
MM00A	3.02	5.82	8.60	2.42	1.15	1.040
MM30A	3.02	5.80	8.50	2.53	1.17	1.041
MM50B	2.98	5.80	8.70	2.37	1.17	1.031
MG00A	2.98	5.78	8.44	2.37	1.14	1.040
MG30A	3.00	5.86	8.84	2.27	1.16	1.045
MG50A	2.98	5.82	8.62	2.27	1.15	1.033
GM00A	2.86	5.47	8.12	1.88	1.070	1.030
GM30A	2.74	5.45	8.14	2.26	1.068	1.053
GM50A	2.75	5.48	8.14	2.17	1.068	1.038

Table 5-3

Summary Data of $4\pi r^2 \Sigma \bar{\rho}_i(r)$ Curves

Series	Coordination Number			1st peak zero intercept (Å)	1st peak maximum (Å)
	(atoms)[1]	(atoms)[2]	(atoms)[3]		
MM00A	7.5	8.5	8.7	2.00	3.06
MM30A	7.3	8.3	8.4	2.13	3.05
MM50B	7.0	8.1	8.4	2.12	3.01
MG00A	7.8	10.0	8.3	2.08	3.00
MG30A	7.0	9.0	8.5	2.25	3.05
MG50A	7.1	8.4	7.7	2.10	3.02
GM00A	8.5	9.9	8.3	1.70	2.90
GM30A	7.7	8.8	8.7	1.95	2.80
GM50A	7.9	9.3	8.4	1.91	2.79

[1] Symmetrical curve method.
[2] Second peak extrapolation method.
[3] Vertical boundary method.

all the samples at each run temperature is shown in Figure 5-1. The function g (r) for all the samples used by the author plus a series of pure gallium runs from Rodriguez (28) is shown graphically in Figures 5-2 to 5-7 at the end of this section. The labelling of the gallium series was carried out to be consistent with the system used for the other runs and was not that used by Rodriguez. The two digit temperature designation can be identified with the correct run in reference (28). The redundancy of plotting the different runs, segregated first as to composition and then as to temperature, was done to simplify and aid in making comparisons between runs.

Three techniques were used to determine whether the microdroplet dispersion or the true solution hypothesis was the more probable for the two element mixtures.

The first method involved the determination of that part of the first peak coordination number due to just the solvent atoms for a truly random model and for a droplet model. In both models the distribution for the solvent atoms was assumed to be the same as that for the pure liquids. Due to the uncertainties involved in the determination of the coordination number and the small amount of solute, the results were inconclusive.

The second method was a graphical one in which the appropriate $4\pi r^2 \Sigma \bar{\rho}_i(r)$ curve of the pure liquid of the solvent metal was normalized with the factor $K_i^2 X_i^2 / (\Sigma K_i X_i)^2$ and then subtracted from the solution curve. The results for all six runs of the two element mixtures were surprisingly similar. They all gave residual first peaks which clustered around 2.55 Å. The two extreme

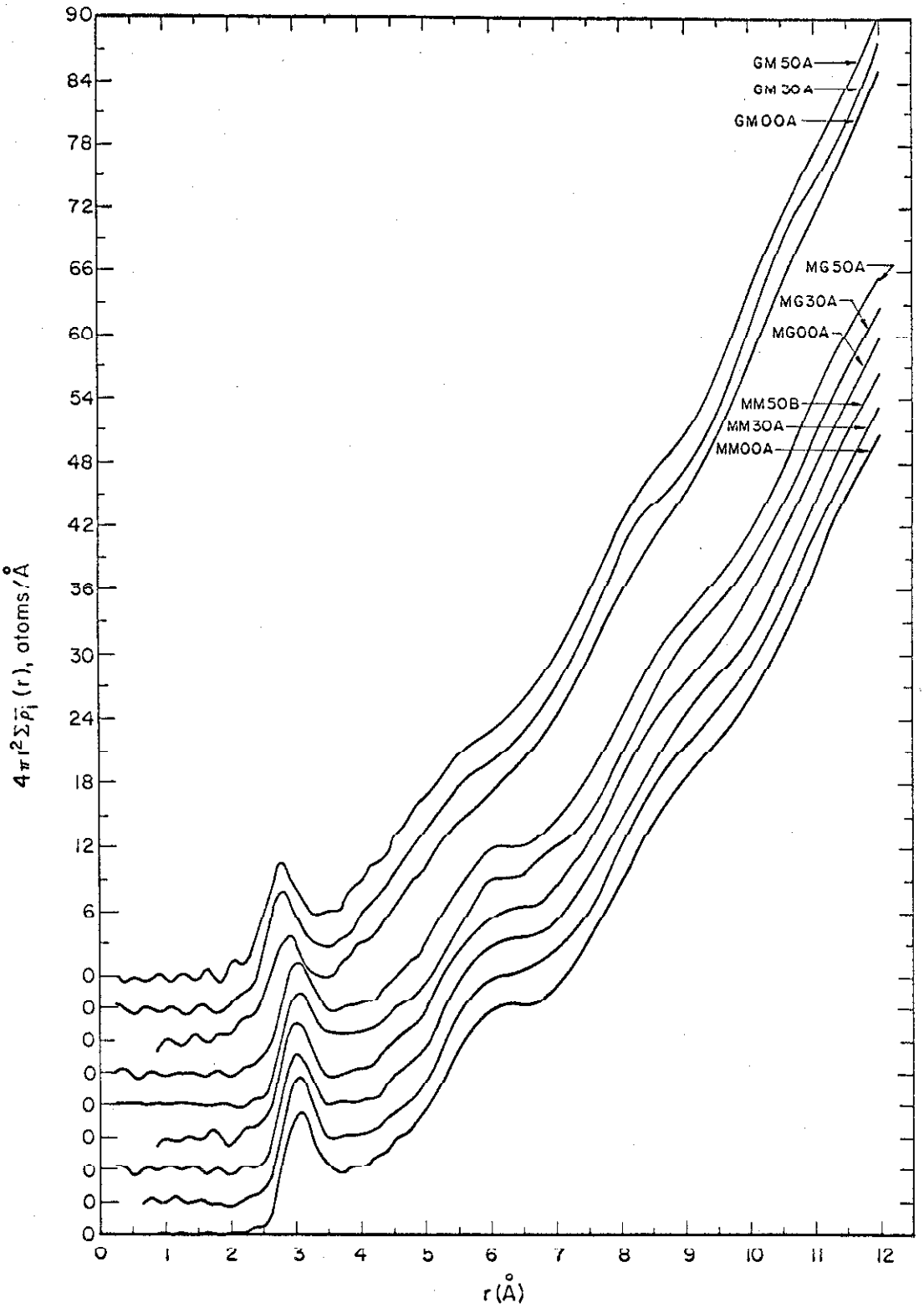

Figure 5-1. $4\pi r^2 \Sigma \bar{\rho}_i(r)$ versus r for all runs.

values were 2.35 Å and 2.65 Å. As can readily be seen, even the maximum value of 2.65 Å does not match the lowest first peak values for mercury, 2.98Å, or gallium, 2.80Å (28). Although it would be presumptuous to say that this distance must be the gallium-mercury distance, particularly with the f value approximation which had to be used, it can be said with fair certainty that mercury-mercury or gallium-gallium interactions due to a dispersion of spherical droplets containing more than 50 atoms were absent in both the high mercury and high gallium sample mixtures. This latter calculation was based on a simple model assuming a monodisperse population of spherical droplets in the solvent metal, summing all pair interactions from the droplet interior, and comparing it to the sum of all droplet surface pair interactions. Using this model, a monodisperse droplet population containing 50 atoms per droplet would have a ratio of approximately two to one for a surface to volume pair interaction ratio. Since the two residual peaks for these interactions would be well separated, it was felt that the above mentioned ratio would allow easy identification if both peaks were present.

The third and final technique involved the direct comparison of the i (S) curves of the two element mixtures with those of the pure substances.

In the case of the high mercury sample, the comparison with the pure mercury sample showed only minor variations. The first peak was significantly lower and the high S shoulder was slightly more pronounced for the mixture, but the overall changes were not sufficiently great to draw any direct conclusions about the atomic structure. The primary reason for this difficulty was the high concentration of mercury coupled with its relatively much greater scattering

power which tended to minimize the mercury-gallium interactions. Differences were present, but the inversion of the i (S) curves was necessary in order to make a more positive statement about the structure.

In contrast, the high gallium i (S) curves showed marked differences from the pure gallium curves of reference (28). The first and second peaks were greatly reduced, the first minimum was more negative, and the high S shoulder of the first peak was quite pronounced. A semi-quantitative model of an i (S) curve was constructed using appropriately weighted i (S) curves of the pure components. The construction was based on the extreme case of two separate phases where gallium-mercury interactions would be negligible. The disagreement was great both from a quantitative and qualitative standpoint. And so by default, a prominent interaction other than the gallium-gallium or mercury-mercury interaction must be postulated. For this reason a large component of gallium-mercury interactions is proposed, and consequently the solution versus the droplet hypothesis is preferred. This result is in agreement with the previous conclusions. Unfortunately no quantitative lower limit can be set for a recognizable spherical droplet as was done in the previous case.

As was mentioned earlier, there is a notable lack of error discussion or the reason for its omission in the papers on liquid mercury. This lack seems to be quite widespread in other papers dealing with the problems of x-ray diffraction and liquid structure of other substances. This thesis will also be partially subject to this same difficulty.

The basic problem which all investigators in this field face whenever accurate analytical error analysis is attempted is the Fourier inversion between the experimental data and the final radial distribution functions. In order to determine the true uncertainty introduced into the final distribution functions, peak positions, and coordination numbers, it is necessary to run a complete inversion for each change or uncertainty in question. Considering the variety and complexity of the various uncertainties present in a study of this kind, the computational work involved in presenting a reasonably complete error analysis is a great deal more complex and time consuming than the original basic calculations. For specific points in question, such as a well defined ripple or a questionable isolated peak, it is usually possible to trace a probable cause by criteria explained in Furukawa (2) or Klug and Alexander (13). But at present, no general error analysis can be made without using involved and time consuming test inversions.

It is possible to give semi-quantitative minimum values of uncertainties based on the calculated values for peak positions and coordination numbers. Although these numbers represent minimal uncertainties and are made on the assumption that no error exists in the experimental data, their order of magnitude should be fiarly accurate with respect to the actual but unknown uncertainties. These estimated uncertainties of the first, second, and third peak positions are ± 0.05Å, ± 0.05Å, and ± 0.15Å respectively, and the uncertainty in the coordination number is ± 0.15 atom.

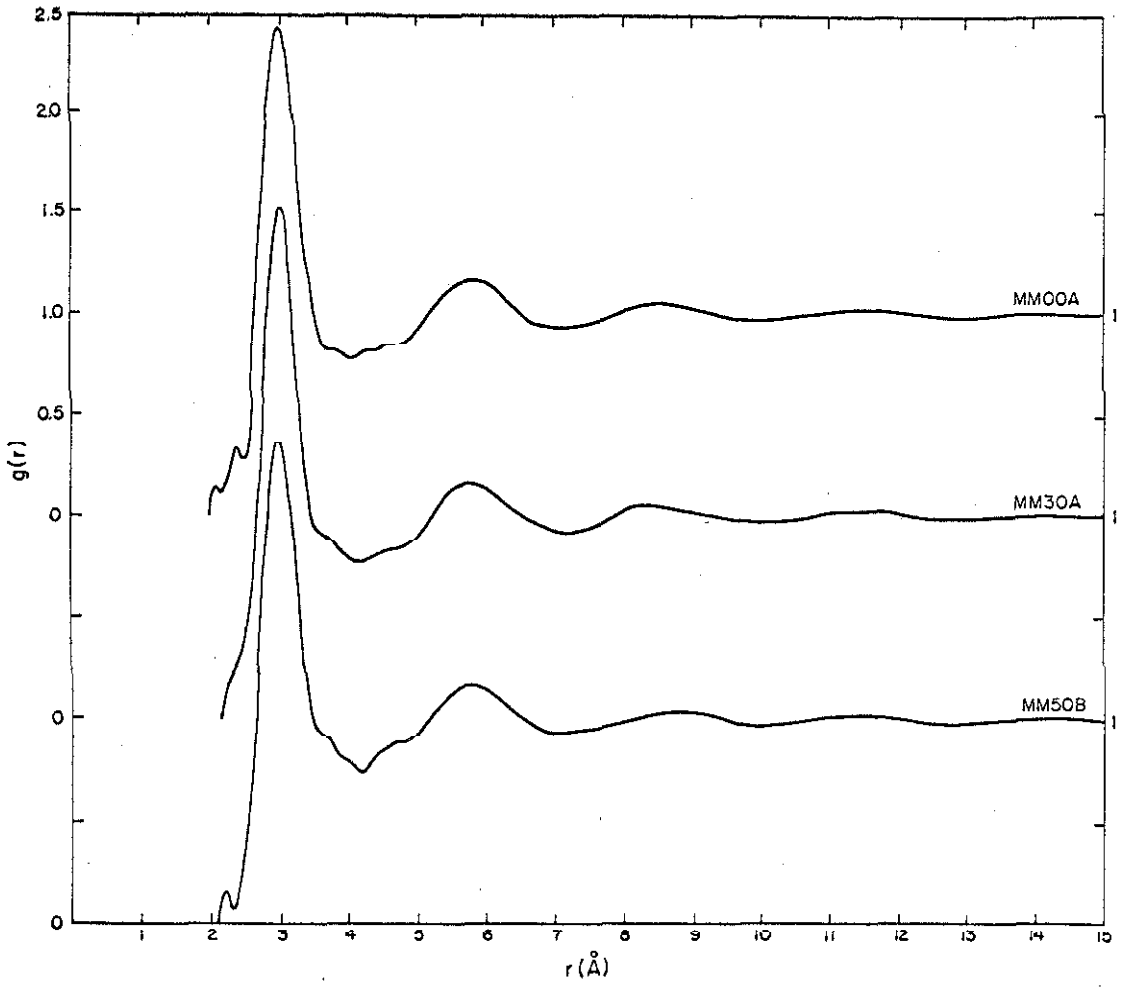

Figure 5-2. g (r) versus r for pure mercury at three temperatures.

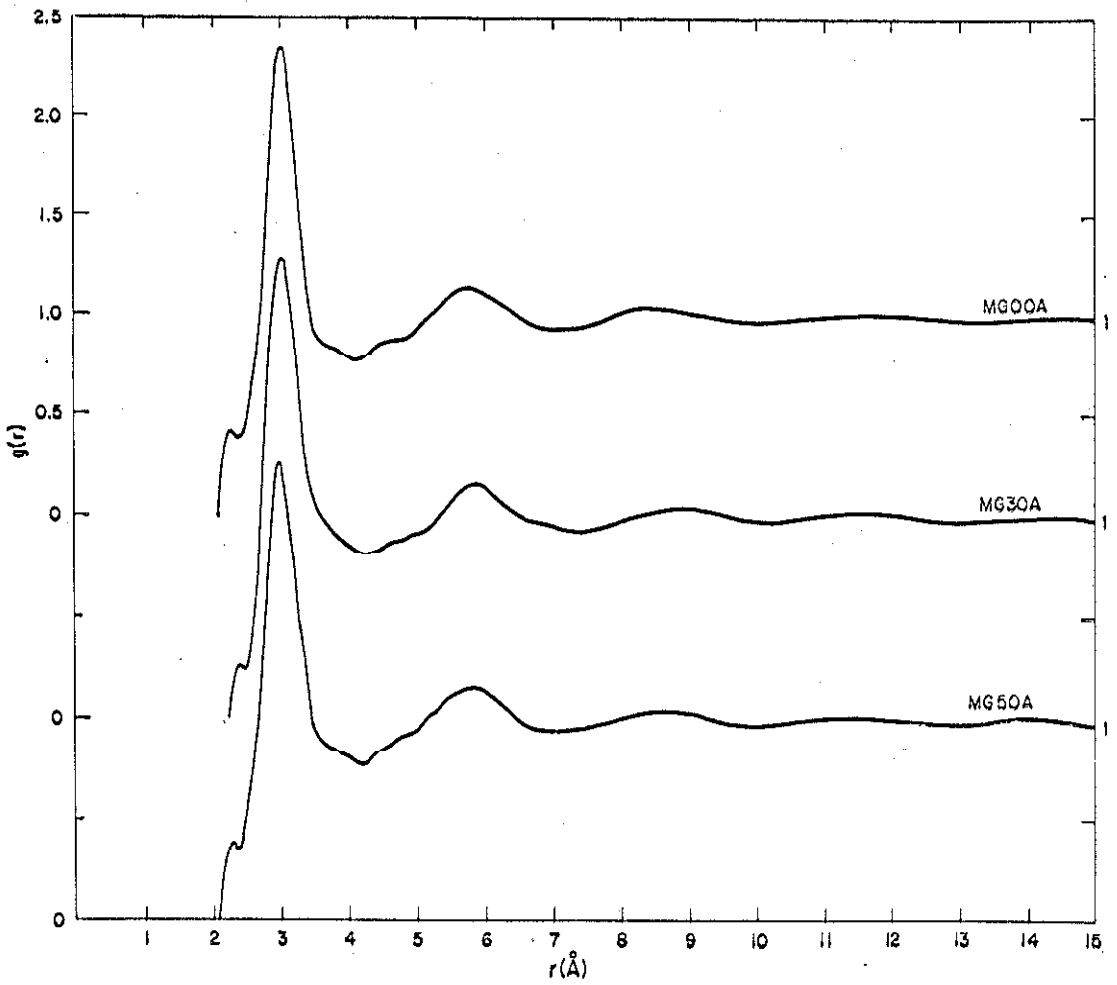

Figure 5-3. g (r) versus r for high mercury-low gallium at three temperatures.

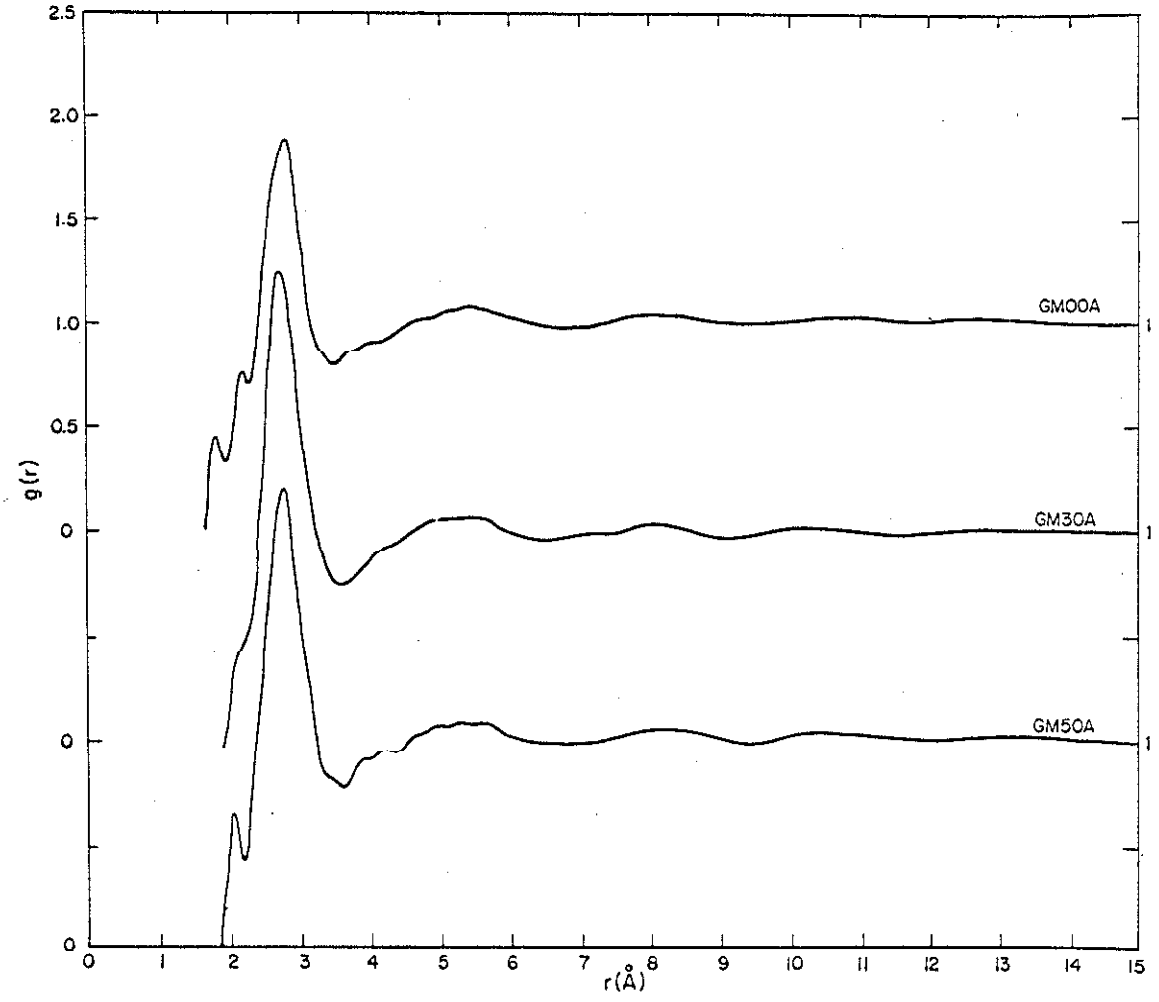

Figure 5-4. g (r) versus r for high gallium-low mercury at three temperatures.

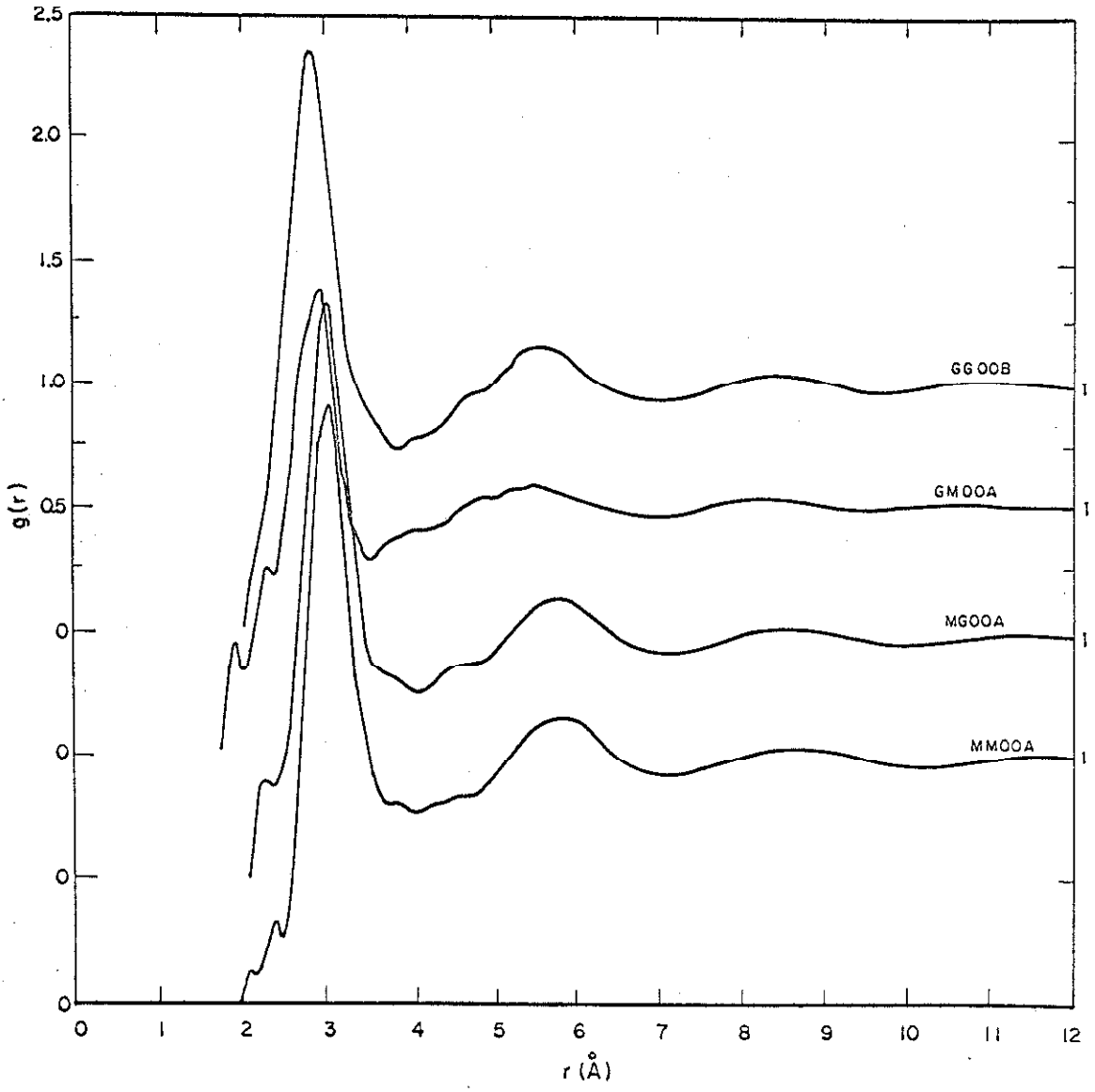

Figure 5-5. g (r) versus r for four samples at 0° C.

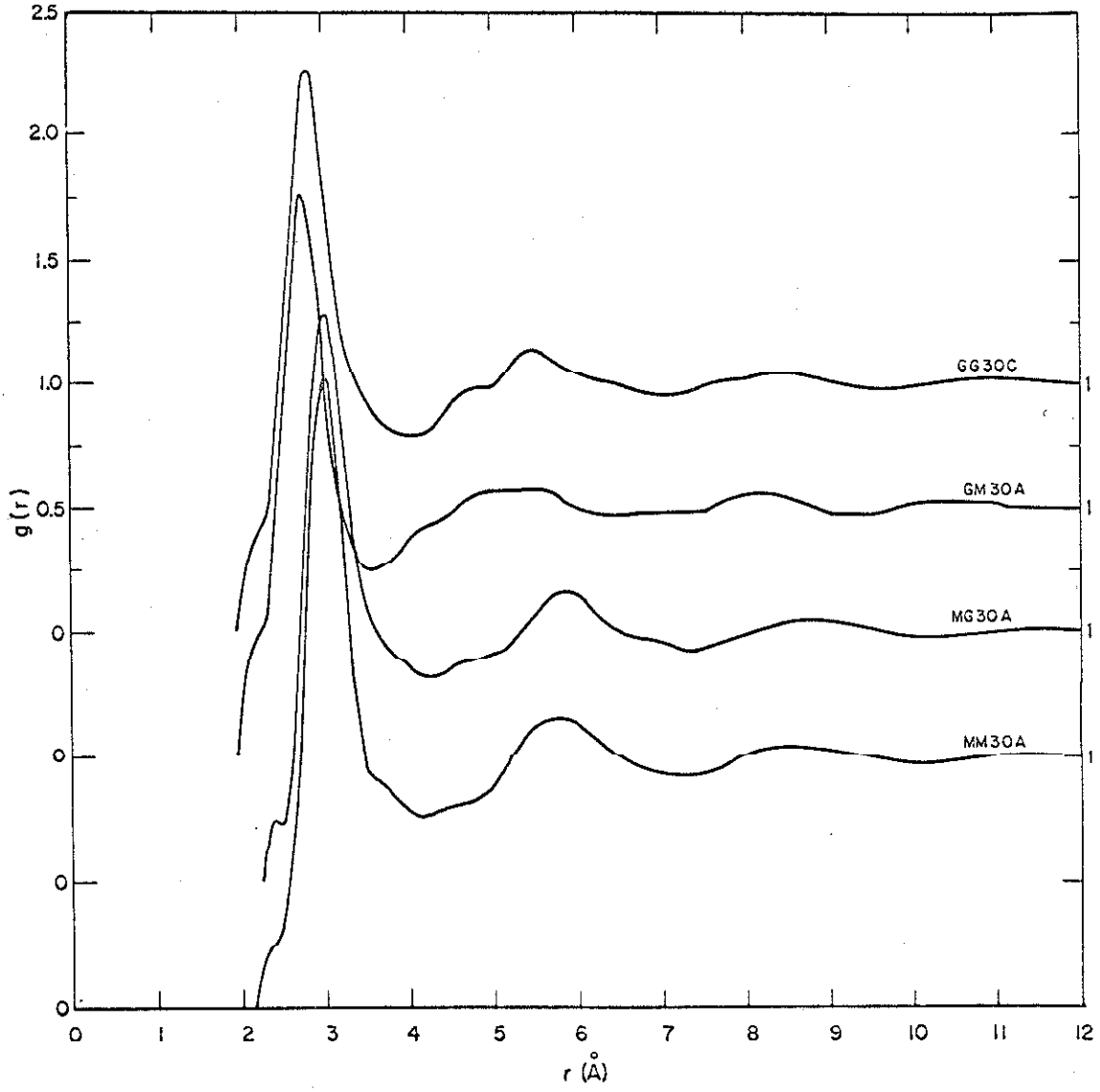

Figure 5-6. g (r) versus r for four samples at 30° C.

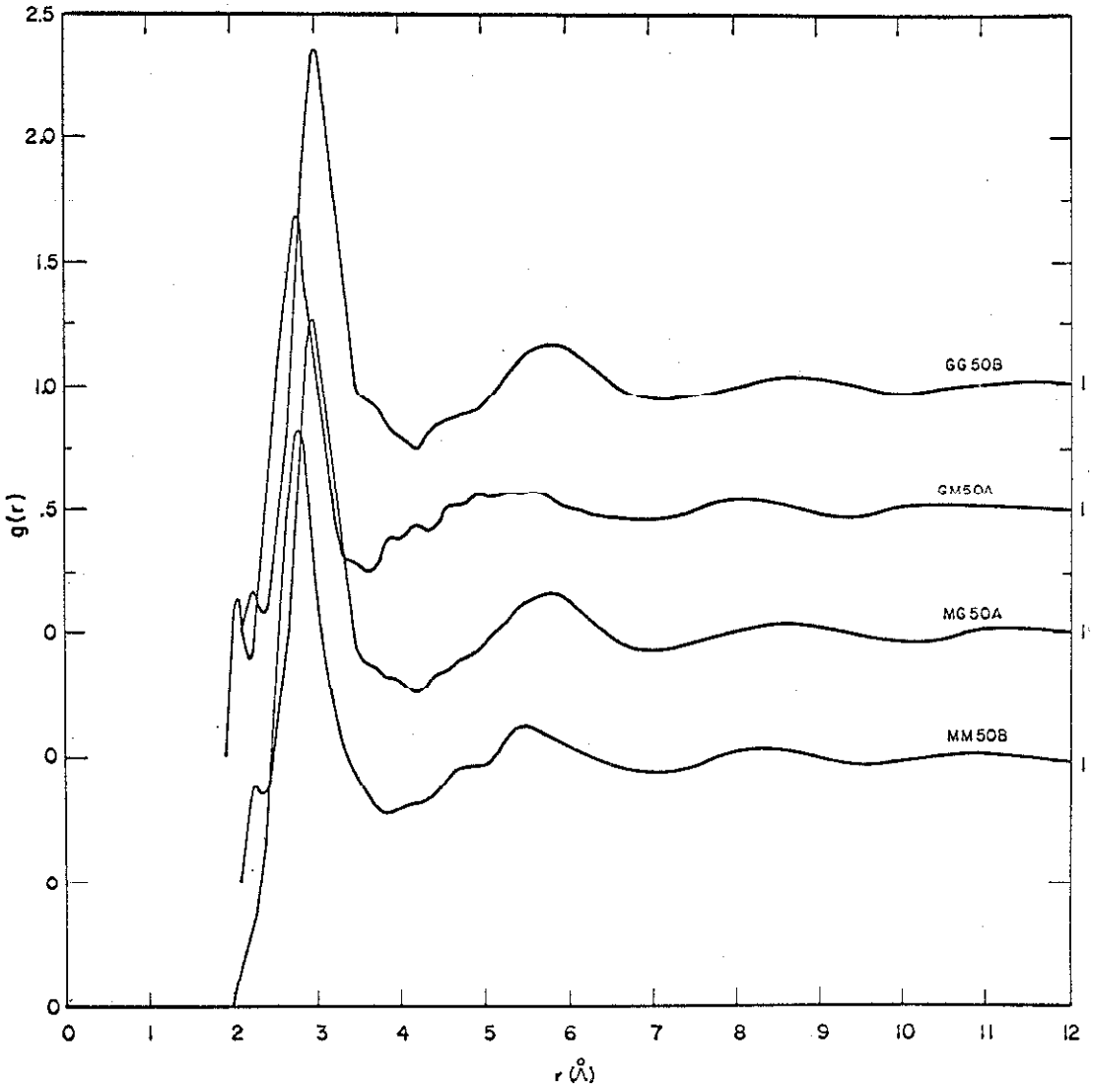

Figure 5-7. g (r) versus r for four samples at 50° C.

References

(1) P. Debye and H. Menke, Phys. Z., 31, 797 (1930).

(2) K. Furukawa, Rep. Prog. Phys., 25, 395 (1962).

(3) W. M. Spicer and H. W. Bartholomay, J. Am. Chem. Soc., 73, 868 (1951).

(4) Y. S. Kim, C. L. Standley, R. F. Kruh, and G. T. Clayton, J. Chem. Phys., 34, 1464 (1961).

(5) P. Debye, Ann. Physik , 46, 809 (1915).

(6) F. Zernike and J. A. Prins, Z. Physik , 41, 184 (1927).

(7) B. E. Warren and N. S. Gingrich, Phys. Rev., 46, 368 (1934).

(8) B. E. Warren, J. Appl. Phys., 8, 645 (1937).

(9) J. T. Randall, The Diffraction of X-Rays and Electrons by Amorphous Solids, Liquids and Gases, p. 104, John Wiley & Sons, Inc., New York (1934).

(10) R. W. James, The Optical Principles of the Diffraction of X-Rays, (Vol. II of The Crystalline State) p. 458, G. Bell & Sons Ltd., London (1954).

(11) H. H. Paalman and C. J. Pings, Rev. Mod. Phys., 35, 389 (1963).

(12) J. Waser and V. Schomaker, Rev. Mod. Phys., 25, 671 (1953).

(13) H. P. Klug and L. E. Alexander, X-Ray Diffraction Procedures, p. 607, John Wiley & Sons, Inc., New York (1954).

(14) B. E. Warren, H. Krutter, and O. Morningstar, J. Am. Ceram. Soc., 19, 202 (1936).

(15) H. W. Furumoto, Diffraction of X-Rays by Liquids-Nitrogen, Oxygen, and Their Mixtures, Ph. D. Thesis, Ohio State Univ. (1963).

(16) J. D. Mackenzie, Modern Aspects of the Vitreous State, p. 14, Butterworth Inc., Washington, D. C. (1960).

References (Continued)

(17) H. P. Klug and L. E. Alexander, X-Ray Diffraction Procedures, p. 592, John Wiley & Sons, Inc., New York (1954).

(18) H. S. Peiser, H. P. Rooksby, and A. J. C. Wilson, X-Ray Diffraction of Polycrystalline Materials, p. 445, The Institute of Physics, London (1955).

(19) J. Zarzycki, Non-Crystalline Solids, p. 117, John Wiley & Sons, Inc., New York (1960).

(20) R. F. Kruh, Chem. Rev., 62, 319 (1962).

(21) W. I. Honeywell, C. M. Knobler, B. L. Smith, and C. J. Pings, Rev. Sci. Instr., 35 (1964).

(22) Handbook of Instruction for the Norelco X-Ray Diffractometer, Philips Electronics, Inc., New York.

(23) S. E. Rodriguez and C. J. Pings, Rev. Sci. Instr., 33, 1469 (1962).

(24) L. J. Briggs, J. Chem. Phys., 26, 784 (1957).

(25) S. Boyer, Ind. Eng. Chem., 17, 1252 (1925).

(26) Temperature, Its Measurement and Control in Science and Industry, p. 1306, Reinhold Publishing Corp., New York (1941).

(27) Temperature, Its Measurement and Control in Science and Industry, p. 241, Reinhold Publishing Corp., New York (1941).

(28) S. E. Rodriguez, X-Ray Diffraction Studies of Stable and Supercooled Liquid Gallium, Ph. D. Thesis, Calif. Inst. of Tech. (1964).

(29) A. Taylor, X-Ray Metallography, p. 936, John Wiley & Sons, Inc., New York (1961).

(30) R. W. James, The Optical Principles of the Diffraction of X-Rays, (Vol. II of The Crystalline State) p. 463, G. Bell & Sons Ltd., London (1954).

(31) A. H. Compton and S. K. Allison, X-Rays in Theory and Experiment, 2nd Ed., p. 234, D. van Nostrand Co. Inc., Princeton (1935).

References (Continued)

(32) R. B. Leighton, Principles of Modern Physics, p. 433, McGraw-Hill, New York (1959).

(33) H. A. Kramers, Phil. Mag., 46, 836 (1923).

(34) A. H. Compton, Phys. Rev., 14, 249 (1919).

(35) F. K. Richtmyer, Phys. Rev., 27, 1 (1926).

(36) S. J. M. Allen, Phys. Rev., 27, 266 (1926).

(37) S. J. M. Allen, Phys. Rev., 28, 907 (1926).

(38) W. L. Gordon, C. H. Shaw, and J. G. Daunt, J. Phys. Chem. Solids, 5, 117 (1958).

(39) H. P. Klug and L. E. Alexander, X-Ray Diffraction Procedures, p. 594, John Wiley & Sons, Inc. New York (1954).

(40) J. Krogh-Moe, Acta Cryst., 9, 951 (1956).

(41) N. Norman, Acta Cryst., 10, 370 (1957).

(42) H. Menke, Phys. Z., 33, 593 (1932).

(43) R. N. Boyd and H. R. R. Wakeham, J. Chem. Phys., 7, 958 (1939).

(44) J. A. Campbell and J. H. Hildebrand, J. Chem. Phys., 11, 330 (1943).

(45) H. Hendus, Z. Naturforsch., 3a, 416 (1948).

(46) R. E. Jennings, Acta Cryst., 5, 1 (1952).

(47) G. H. Vineyard, J. Chem. Phys., 22, 1665 (1954).

(48) J. S. Lukesh, W. H. Howland, L. F. Epstein, and M. D. Powers, J. Chem. Phys., 23, 1923 (1955).

(49) R. E. Smallman and B. R. T. Frost, Acta Met., 4, 611 (1956).

(50) A. F. Skrishevskii and D. M. Karlikov, Ukrain. Fiz. Zhur. (Suppl.), 2, No. 2, 49 (1957).

References (Continued)

(51) J. I. Petz, C. L. Standley, and R. F. Kruh, unpublished results.

(52) O. Pfannenschmid, Z. Naturforsch., 15a, 603 (1960).

(53) R. F. Kruh, G. T. Clayton, C. Head, and G. Sandlin, Phys. Rev., 129, 1479 (1963).

(54) C. N. J. Wagner, H. Ocken, & M. L. Joshi, "The Structure of Liquid Copper, Silver, Tin, and Mercury", Technical Report #4, Yale Univ., New Haven (Jan. 1964).

(55) Nuclear Science Abstracts, 18, 1950 (1964).

(56) B. D. Cullity, Elements of X-Ray Diffraction, p. 464, Addison-Wesley Publishing Co. Inc., Reading (1956).

(57) A. Taylor, X-Ray Metallography, p. 22, John Wiley and Sons, Inc., New York (1961).

(58) A. Taylor, X-Ray Metallography, p. 936, John Wiley and Sons, Inc., New York (1961).

(59) Handbook of Chemistry and Physics, 40th Ed., Chemical Rubber Publishing Co., Cleveland (1958).

(60) A. H. Compton and S. K. Allison, X-Rays in Theory and Experiment, 2nd Ed., p. 782, D. van Nostrand Co. Inc., Princeton (1935).

(61) A. J. Freeman, Acta Cryst., 12, 274 (1959).

(62) A. J. Freeman, Acta Cryst., 12, 929 (1959).

(63) A. J. Freeman, Acta Cryst., 13, 190 (1960).

(64) J. A. Ibers, Acta Cryst., 11, 447 (1958).

(65) A. J. Freeman, Acta Cryst., 12, 261 (1959).

(66) D. T. Cromer, "Anomalous Dispersion Corrections Computed from Relativistic Hartree-Dirac-Slater Wave Equations", unpublished.

References (Continued)

(67) W. G. Davies and E. S. Keeping, Phil. Mag., 7, 145 (1929).

Appendix I

Table I-1

General Constants

$\lambda = 0.56083$ Å	Weighted mean of Ag $K_{\alpha 1}$ and Ag $K_{\alpha 2}$ lines. Reference (56).
$\alpha = 4.80°$	Measured angle between sample surface and incident x-ray beam.
$t_\beta = 0.0031"$	Measured thickness of rhodium beta filter.
$\mu_{Rh} = 164$ cm^{-1}	Linear absorption coefficient for Ag K_α by rhodium. Based on mass absorption coefficient of reference (57).
u (Hg) = 2.73	Exponent of B for mercury. Determined graphically from data of reference (58).
u (Ga) = 2.73	Exponent of B for gallium. Determined graphically from data of reference (58).
v (Rh) = 2.71	Exponent of B for rhodium beta filter. Determined graphically from data of reference (58).
ρ(Hg) = 0.04068 atoms/Å^3	Based on bulk liquid density of mercury from reference (59).
ρ(Ga) = 0.05265 atoms/Å^3	Based on bulk liquid density of gallium from reference (59).
ρ(MG Series) = 0.04100 atoms/Å^3	Both values are calculated from atomic densities of pure substances assumed $\Delta V_{mix} = 0$ from reference (67).
ρ(GM Series) = 0.05235 atoms/Å^3	

Table I-1 (Continued)

MG Series	
X (Hg) = 0.9658	Mole fractions determined experimentally.
X (Ga) = 0.0342	
GM Series	
X (Hg) = 0.0197	Mole fractions determined experimentally.
X (Ga) = 0.9803	
MG Series	
K (Hg) = 80.0	Effective atomic numbers determined graphically from atomic scattering factor data.
K (Ga) = 39.6	
GM Series	
K (Hg) = 63.7	Effective atomic numbers determined graphically from atomic scattering factor data.
K (Ga) = 31.0	

Appendix II

Atomic Scattering Factor, Incoherent Scatter, and Dispersion Correction Data

The atomic scattering factor f used in the text is composed of three distinct parts which can be represented by the equation

$$f = f_o + \Delta f' + i\Delta f''$$

where $\Delta f'$ and $\Delta f''$ are respectively the real and imaginary dispersion corrections. For the particular systems studied, both dispersion corrections can be considered to be constants independent of angle θ and only dependent on the sample element and radiation used.

Both dispersion corrections are constants which are dependent on the sample element and wavelength of radiation used but independent of angle θ.

The incoherent scatter data for mercury is the result of interpolation and extrapolation of incoherent scatter data of a series of elements for which both Compton and Allison (60) and Freeman (61, 62, 63) have made calculations. This technique was necessary because the only incoherent data for mercury was calculated by Compton and Allison, and the more recent and sophisticated calculations of Freeman are considered to be a great deal more accurate, particularly for the heavier elements.

In the case of the incoherent scatter data for gallium, a simple linear interpolation between the corresponding values for copper and germanium as calculated by Freeman (61, 62) was used.

Table II-1

	Atomic Scattering Factor		Incoherent Scatter	
$\frac{\sin\theta}{\lambda}$	f_o (Hg) Ref. (64)	f_o (Ga) Ref. (65)	F_m (Hg)	F_m (Ga)
0.00	80.00	31.00	0.0	0.00
0.05	78.72	-----	---	----
0.10	75.48	28.31	4.4	1.72
0.15	71.37	-----	---	----
0.20	67.14	24.49	16.0	4.92
0.25	63.09	-----	----	----
0.30	59.31	20.96	19.8	7.64
0.35	55.84	-----	----	----
0.40	52.65	17.73	26.6	10.25
0.50	47.04	14.90	31.7	12.66
0.60	42.31	12.57	36.2	14.76
0.70	38.22	10.74	39.5	16.55
0.80	34.64	9.36	42.3	-----
0.90	31.43	8.35	44.6	19.40
1.00	28.59	7.59	46.6	-----
1.10	26.07	7.03	48.7	21.53
1.20	23.88	----	50.6	-----
1.30	21.99	6.22	52.4	-----
1.40	-----	----	54.3	-----
1.50	-----	5.59	56.0	-----
1.60	-----	----	----	-----
1.70	-----	4.99	----	-----
1.80	-----	----	----	-----
1.90	-----	4.43	----	-----

Dispersion Corrections: Ag K_α line, reference (66).

$\Delta f'$ (Hg) = -0.94

$\Delta f''$ (Hg) = 6.58

$\Delta f'$ (Ga) = 0.38

$\Delta f''$ (Ga) = 1.16

Appendix III

Experimental Diffraction Data

The following nine tables cover all nine experimental series. Each experimental run is tabulated separately. The normalization factor $\bar{A}$ is the combined normalization factors A and C described in the Data Analysis section.

The Counts or Seconds tabulated for the given counting cycle are the direct output of the counting system.

The intensity is the total corrected experimental intensity normalized to give in electron units the scatter expected from a single atom. All angular corrections, e.g. polarization, view factor, etc., have been applied in the intensity corrections.

MM00A: Table III-1

MM30A: Table III-2

MM50B: Table III-3

MG00A: Table III-4

MG30A: Table III-5

MG50A: Table III-6

GM00A: Table III-7

GM30A: Table III-8

GM50A: Table III-9

Table III-1

Run: MM00A1
Normalization factor Ā: 23053.54
Background: 0.025 cts/sec
Counting for 1600.0 seconds

2Θ(°)	Counts	S(1/Å)	Intensity	i(S)
11.000	4296	2.148	5986.02	0.2556
11.250	5039	2.196	7196.18	0.5243
11.500	5866	2.245	8579.51	0.8352
11.750	6325	2.294	9463.90	1.0441
12.000	6154	2.342	9409.62	1.0518
12.250	5842	2.391	9122.69	1.0083
12.500	5624	2.439	8966.30	0.9929
12.750	5060	2.488	8228.60	0.8464
13.000	4679	2.537	7759.60	0.7577
13.250	4454	2.585	7531.55	0.7224
13.500	4162	2.634	7172.13	0.6559
13.750	3963	2.682	6958.29	0.6219
14.000	3524	2.731	6297.50	0.4817
14.250	3264	2.779	5936.88	0.4101
14.500	2986	2.828	5525.10	0.3247
14.750	2734	2.876	5144.29	0.2450
15.000	2497	2.925	4775.66	0.1667
15.250	2308	2.973	4485.97	0.1063
15.500	2119	3.022	4183.52	0.0414
15.750	2025	3.070	4062.69	0.0209
16.000	1887	3.118	3843.98	-0.0250
16.250	1769	3.167	3658.23	-0.0634
16.500	1626	3.215	3410.69	-0.1187
16.750	1574	3.264	3352.22	-0.1255
17.000	1509	3.312	3261.41	-0.1412
17.250	1400	3.360	3066.98	-0.1849
17.500	1320	3.409	2931.46	-0.2137
17.750	1265	3.457	2848.58	-0.2288
18.000	1351	3.505	3094.80	-0.1537

Table III-1 (Continued)

Run: MM00A2
Normalization factor Ā: 7165.05
Background: 0.025 cts/sec
Counting for 1600.0 seconds

2Θ(°)	Counts	S(1/Å)	Intensity	i(S)
16.000	5897	3.118	3788.54	−0.0391
16.500	5161	3.215	3422.75	−0.1155
17.000	4670	3.312	3194.82	−0.1588
17.500	4280	3.409	3018.01	−0.1904
18.000	3992	3.505	2899.53	−0.2074
18.500	3770	3.602	2818.77	−0.2149
19.000	3569	3.698	2745.02	−0.2210
19.500	3552	3.795	2810.03	−0.1874
20.000	3516	3.891	2859.12	−0.1576
20.500	3583	3.987	2994.11	−0.1011
21.000	3797	4.083	3260.20	−0.0024
21.500	3763	4.179	3315.69	0.0334
22.000	4031	4.275	3646.08	0.1580
22.500	4045	4.371	3751.50	0.2135
23.000	4101	4.467	3898.50	0.2843
23.500	3964	4.563	3858.94	0.2943
24.000	3745	4.659	3731.00	0.2737
24.500	3488	4.754	3554.11	0.2347
25.000	3234	4.850	3368.71	0.1908
25.500	3004	4.945	3197.53	0.1499
26.000	2871	5.040	3122.74	0.1426
26.500	2604	5.136	2890.89	0.0757
27.000	2375	5.231	2690.16	0.0178
27.500	2198	5.326	2539.75	−0.0229
28.000	2145	5.421	2529.95	−0.0099
28.500	2015	5.515	2423.40	−0.0358
29.000	1931	5.610	2368.27	−0.0419
29.500	1831	5.705	2288.78	−0.0587
30.000	1732	5.799	2205.82	−0.0779
30.500	1711	5.894	2221.77	−0.0556
31.000	1737	5.988	2300.69	−0.0053

Table III-1 (Continued)

Run: MM00A3
Normalization factor Ā: 1929.56
Background: 0.025 cts/sec
Counting for 4000 counts

2Θ(°)	Seconds	S(1/Å)	Intensity	i(S)
27.000	724.6	5.231	2727.99	0.0323
28.000	826.4	5.421	2493.68	-0.0243
29.000	911.2	5.610	2355.41	-0.0471
30.000	991.3	5.799	2252.60	-0.0581
31.000	1022.9	5.988	2269.75	-0.0189
32.000	1026.1	6.176	2350.88	0.0505
33.000	1033.8	6.364	2422.21	0.1183
34.000	1128.4	6.551	2300.56	0.0957
35.000	1171.7	6.738	2295.86	0.1283
36.000	1240.8	6.924	2244.66	0.1377
37.000	1399.7	7.110	2057.66	0.0742
38.000	1558.8	7.295	1909.41	0.0265
39.000	1657.3	7.480	1855.56	0.0278
40.000	1794.8	7.664	1768.85	0.0087
41.000	1902.3	7.847	1722.28	0.0113
42.000	2044.9	8.030	1652.18	-0.0017
43.000	2096.1	8.212	1662.25	0.0343
44.000	2207.6	8.394	1626.24	0.0411
45.000	2301.2	8.575	1606.90	0.0582
46.000	2436.8	8.755	1561.86	0.0574
47.000	2550.4	8.935	1535.45	0.0688
48.000	2680.0	9.114	1502.61	0.0750

Table III-1 (Continued)

Run: MM00A4
Normalization factor $\bar{A}$: 609.54
Background: 0.025 cts/sec
Counting for 10000 counts

2Θ(°)	Seconds	S(1/Å)	Intensity	i(S)
42.000	1639.3	8.030	1641.95	-0.0080
44.000	1749.1	8.394	1636.47	0.0477
46.000	1935.5	8.755	1569.33	0.0626
48.000	2149.5	9.114	1496.67	0.0707
50.000	2540.3	9.469	1338.33	0.0087
52.000	2854.7	9.822	1256.59	-0.0023
54.000	3166.5	10.172	1193.21	-0.0024
56.000	3545.5	10.519	1120.25	-0.0150
58.000	3847.8	10.863	1083.33	0.0025
60.000	4181.8	11.203	1044.07	0.0162
62.000	4652.9	11.540	980.58	0.0013
64.000	5103.7	11.874	932.28	-0.0020
66.000	5500.5	12.204	900.25	0.0100

Table III-1 (Continued)

Run: MM00A5
Normalization factor $\bar{A}$: 64757.39
Background: 0.025 cts/sec
Counting for 1000.0 seconds

2Θ(°)	Counts	S(1/Å)	Intensity	i(S)
8.000	423	1.563	1815.27	-0.6597
8.250	419	1.612	1854.28	-0.6494
8.500	393	1.661	1785.48	-0.6595
8.750	396	1.709	1854.12	-0.6432
9.000	395	1.758	1903.16	-0.6305
9.250	419	1.807	2084.24	-0.5915
9.500	400	1.855	2038.68	-0.5968
9.750	430	1.904	2261.23	-0.5485
10.000	465	1.953	2521.35	-0.4918
10.250	651	2.002	3679.42	-0.2504
10.500	604	2.050	3488.63	-0.2828
10.750	808	2.099	4833.58	0.0039
11.000	991	2.148	6106.41	0.2809
11.250	1176	2.196	7446.74	0.5775
11.500	1377	2.245	8948.29	0.9142
11.750	1378	2.294	9156.60	0.9776
12.000	1306	2.342	8860.69	0.9320

Table III-1 (Continued)

Run: MM00A6
Normalization factor Ā: 279.97
Background: 0.025 cts/sec
Counting for 10000 counts

2Θ(°)	Seconds	S(1/Å)	Intensity	i(S)
58.000	1750.5	10.863	1099.53	0.0181
62.000	2137.1	11.540	986.82	0.0080
66.000	2598.7	12.204	881.65	-0.0119
70.000	2984.6	12.852	826.41	0.0155
74.000	3473.5	13.485	756.33	0.0127
78.000	4018.3	14.101	688.25	-0.0017
82.000	4455.9	14.700	645.35	0.0113

Table III-1 (Continued)

Run: MM00A7
Normalization factor Ā: 279.97
Background: 0.025 cts/sec
Counting for 10000 counts

2Θ(°)	Seconds	S(1/Å)	Intensity	i(S)
86.000	4835.1	15.281	610.19	0.0270
90.000	5194.5	15.844	574.62	0.0340
94.000	5583.5	16.387	533.15	0.0200
98.000	5819.2	16.911	503.29	0.0232
102.000	6074.9	17.413	468.03	0.0037

Table III-2

Run: MM30A1
Normalization factor $\bar{A}$: 25047.67
Background: 0.024 cts/sec
Counting for 1600.0 seconds

2Θ(°)	Counts	S(1/Å)	Intensity	i(S)
11.000	4548	2.148	6891.35	0.4459
11.250	5377	2.196	8349.80	0.7691
11.500	5839	2.245	9281.00	0.9855
11.750	5895	2.294	9581.65	1.0695
12.000	6065	2.342	10077.40	1.1977
12.250	5782	2.391	9812.03	1.1603
12.500	5377	2.439	9313.76	1.0703
12.750	4939	2.488	8727.73	0.9586
13.000	4654	2.537	8388.28	0.9004
13.250	4295	2.585	7891.23	0.8049
13.500	4060	2.634	7602.72	0.7555
13.750	3791	2.682	7231.80	0.6858
14.000	3360	2.731	6523.30	0.5350
14.250	3090	2.779	6105.49	0.4503
14.500	2868	2.828	5765.83	0.3826
14.750	2625	2.876	5366.44	0.2990
15.000	2388	2.925	4961.94	0.2124
15.250	2266	2.973	4787.19	0.1808
15.500	2083	3.022	4470.18	0.1130
15.750	1959	3.070	4270.90	0.0735
16.000	1791	3.118	3963.03	0.0054
16.250	1756	3.167	3948.46	0.0113
16.500	1540	3.215	3508.51	-0.0932
16.750	1507	3.264	3486.91	-0.0902
17.000	1396	3.312	3274.81	-0.1376
17.250	1372	3.360	3267.59	-0.1313
17.500	1270	3.409	3064.60	-0.1778
17.750	1210	3.457	2960.06	-0.1984
18.000	1114	3.505	2758.73	-0.2462

Table III-2 (Continued)

Run: MM30A2
Normalization factor Ā: 7724.80
Background: 0.024 cts/sec
Counting for 1600.0 seconds

2Θ(°)	Counts	S(1/Å)	Intensity	i(S)
16.000	5619	3.118	3891.75	-0.0128
16.500	4918	3.215	3516.19	-0.0912
17.000	4337	3.312	3197.87	-0.1580
17.500	3985	3.409	3028.63	-0.1875
18.000	3722	3.505	2913.75	-0.2035
18.500	3602	3.602	2903.41	-0.1912
19.000	3389	3.698	2809.86	-0.2025
19.500	3310	3.795	2822.18	-0.1838
20.000	3355	3.891	2941.13	-0.1332
20.500	3453	3.987	3111.04	-0.0657
21.000	3475	4.083	3215.14	-0.0163
21.500	3659	4.179	3476.41	0.0838
22.000	3694	4.275	3600.57	0.1434
22.500	3737	4.371	3735.15	0.2082
23.000	3606	4.467	3692.40	0.2160
23.500	3647	4.563	3826.01	0.2832
24.000	3558	4.659	3821.19	0.3047
24.500	3281	4.754	3603.51	0.2520
25.000	3190	4.850	3583.67	0.2673
25.500	2782	4.945	3190.99	0.1475
26.000	2637	5.040	3090.33	0.1307
26.500	2408	5.136	2880.42	0.0718
27.000	2316	5.231	2829.03	0.0709
27.500	2068	5.326	2575.24	-0.0091
28.000	1892	5.421	2401.84	-0.0606
28.500	1883	5.515	2440.22	-0.0290
29.000	1778	5.610	2348.86	-0.0498
29.500	1743	5.705	2348.55	-0.0338
30.000	1760	5.799	2419.74	0.0127
30.500	1570	5.894	2195.52	-0.0669
31.000	1589	5.988	2266.44	-0.0203

Table III-2 (Continued)

Run: MM30A3
Normalization factor Ā: 83649.05
Background: 0.024 cts/sec
Counting for 1000.0 seconds

2Θ(°)	Counts	S(1/Å)	Intensity	i(S)
8.000	359	1.563	1973.67	-0.6299
8.250	399	1.612	2279.73	-0.5686
8.500	374	1.661	2193.55	-0.5813
8.750	341	1.709	2046.43	-0.6061
9.000	367	1.758	2278.97	-0.5572
9.250	374	1.807	2391.62	-0.5310
9.500	375	1.855	2464.89	-0.5121
9.750	405	1.904	2747.81	-0.4509
10.000	453	1.953	3175.48	-0.3593
10.250	506	2.002	3659.52	-0.2545
10.500	586	2.050	4374.06	-0.1002
10.750	707	2.099	5446.28	0.1315
11.000	818	2.148	6483.37	0.3601
11.250	941	2.196	7663.58	0.6235
11.500	1063	2.245	8882.82	0.9002
11.750	1128	2.294	9651.11	1.0845
12.000	1196	2.342	10471.71	1.2838

Table III-2 (Continued)

Run: MM30A4
Normalization factor Ā: 2048.64
Background: 0.024 cts/sec
Counting for 4000 counts

2Θ(°)	Seconds	S(1/Å)	Intensity	i(S)
27.000	731.7	5.231	2868.63	0.0860
28.000	887.7	5.421	2464.34	-0.0359
29.000	939.8	5.610	2424.80	-0.0187
30.000	1042.4	5.799	2274.24	-0.0490
31.000	1093.4	5.988	2254.06	-0.0257
32.000	1082.8	6.176	2365.05	0.0569
33.000	1117.0	6.364	2379.56	0.0983
34.000	1177.2	6.551	2341.25	0.1153
35.000	1238.1	6.738	2306.57	0.1337
36.000	1349.2	6.924	2190.96	0.1101
37.000	1505.5	7.110	2030.53	0.0598
38.000	1622.1	7.295	1948.15	0.0477
39.000	1839.7	7.480	1773.53	-0.0185
40.000	1967.8	7.664	1711.88	-0.0244
41.000	2075.3	7.847	1675.17	-0.0169
42.000	2193.0	8.030	1635.05	-0.0122
43.000	2303.8	8.212	1604.55	-0.0024
44.000	2358.6	8.394	1615.48	0.0340
45.000	2483.5	8.575	1580.00	0.0401
46.000	2520.9	8.755	1603.10	0.0860
47.000	2738.0	8.935	1517.75	0.0562
48.000	2932.2	9.114	1456.88	0.0415
49.000	3204.7	9.292	1369.01	0.0045
50.000	3408.3	9.469	1321.99	-0.0040

Table III-2 (Continued)

Run: MM30A5
Normalization factor Ā: 663.14
Background: 0.024 cts/sec
Counting for 10000 counts

2Θ(°)	Seconds	S(1/Å)	Intensity	i(S)
42.000	1782.4	8.030	1642.61	-0.0076
44.000	1903.2	8.394	1635.89	0.0474
46.000	2130.6	8.755	1550.55	0.0496
48.000	2401.2	9.114	1457.02	0.0416
50.000	2748.5	9.469	1345.39	0.0141
52.000	3195.7	9.822	1220.56	-0.0318
54.000	3505.4	10.172	1172.05	-0.0207
56.000	3794.7	10.519	1138.44	0.0016
58.000	4142.8	10.863	1094.31	0.0131
60.000	4709.3	11.203	1007.78	-0.0205
62.000	5227.5	11.540	948.66	-0.0326
64.000	5622.0	11.874	920.07	-0.0157
66.000	6226.2	12.204	864.21	-0.0323

Table III-2 (Continued)

Run: MM30A6
Normalization factor $\bar{A}$: 309.62
Background: 0.024 cts/sec
Counting for 10000 counts

2Θ(°)	Seconds	S(1/Å)	Intensity	i(S)
58.000	1958.7	10.863	1086.37	0.0055
62.000	2429.4	11.540	959.56	-0.0210
66.000	2941.0	12.204	861.06	-0.0360
70.000	3349.8	12.852	813.82	-0.0007
74.000	4026.4	13.485	720.86	-0.0375
78.000	4638.0	14.101	658.73	-0.0472
82.000	5036.6	14.700	630.81	-0.0130
86.000	5632.5	15.281	578.45	-0.0302
90.000	6060.1	15.844	543.85	-0.0255
94.000	6279.2	16.387	523.70	0.0004
98.000	6700.2	16.911	482.66	-0.0224
102.000	6725.8	17.413	467.05	0.0014

Table III-3

Run: MM50B1
Normalization factor A: 1997.08
Background: 0.026 cts/sec
Counting for 4000 counts

2Θ(°)	Seconds	S(1/Å)	Intensity	i(S)
27.000	695.1	5.231	2943.30	0.1146
28.000	831.4	5.421	2564.80	0.0039
29.000	941.1	5.610	2359.37	-0.0455
30.000	980.1	5.799	2357.65	-0.0136
31.000	1049.0	5.988	2289.75	-0.0101
32.000	1047.2	6.176	2383.17	0.0651
33.000	1082.1	6.364	2393.69	0.1050
34.000	1127.0	6.551	2383.37	0.1357
35.000	1178.9	6.738	2360.88	0.1607
36.000	1285.7	6.924	2240.71	0.1356
37.000	1355.5	7.110	2198.97	0.1492
38.000	1525.5	7.295	2019.01	0.0865
39.000	1657.1	7.480	1919.92	0.0641
40.000	1777.0	7.664	1848.46	0.0550
41.000	1968.6	7.847	1720.93	0.0105
42.000	1999.6	8.030	1748.35	0.0577
43.000	2129.7	8.212	1692.00	0.0532
44.000	2267.7	8.394	1636.98	0.0481
45.000	2310.8	8.575	1655.15	0.0907
46.000	2415.2	8.755	1630.20	0.1048
47.000	2552.3	8.935	1586.94	0.1055
48.000	2797.8	9.114	1487.54	0.0640
49.000	2887.0	9.292	1482.12	0.0898

Table III-3 (Continued)

Run: MM50B2
Normalization factor Ā: 26028.23
Background: 0.026 cts/sec
Counting for 1600.0 seconds

2Θ(°)	Counts	S(1/Å)	Intensity	i(S)
11.000	3912	2.148	6146.10	0.2892
11.250	4561	2.196	7345.25	0.5559
11.500	5264	2.245	8682.99	0.8574
11.750	5402	2.294	9113.16	0.9682
12.000	5211	2.342	8982.43	0.9585
12.250	5170	2.391	9104.04	1.0042
12.500	4784	2.439	8597.52	0.9108
12.750	4410	2.488	8084.47	0.8140
13.000	4020	2.537	7513.29	0.7018
13.250	3874	2.585	7382.95	0.6884
13.500	3634	2.634	7057.19	0.6293
13.750	3531	2.682	6987.83	0.6288
14.000	2954	2.731	5943.58	0.3982
14.250	2896	2.779	5934.51	0.4095
14.500	2518	2.828	5243.67	0.2570
14.750	2379	2.876	5039.27	0.2195
15.000	2229	2.925	4800.25	0.1727
15.250	2103	2.973	4603.44	0.1353
15.500	1843	3.022	4092.65	0.0186
15.750	1793	3.070	4047.11	0.0170
16.000	1635	3.118	3744.09	-0.0504
16.250	1567	3.167	3643.90	-0.0670
16.500	1448	3.215	3414.72	-0.1176
16.750	1317	3.264	3146.74	-0.1794
17.000	1235	3.312	2991.42	-0.2127
17.250	1202	3.360	2954.52	-0.2150
17.500	1120	3.409	2788.44	-0.2523
17.750	1160	3.457	2936.27	-0.2049
18.000	1122	3.505	2879.53	-0.2129

Table III-3 (Continued)

Run: MM50B3
Normalization factor $\bar{A}$: 71187.22
Background: 0.026 cts/sec
Counting for 1000.0 seconds

2Θ(°)	Counts	S(1/Å)	Intensity	i(S)
8.000	407	1.563	1910.27	-0.6418
8.250	408	1.612	1976.31	-0.6262
8.500	425	1.661	2128.11	-0.5939
8.750	444	1.709	2296.43	-0.5577
9.000	431	1.758	2290.03	-0.5550
9.250	425	1.807	2320.26	-0.5450
9.500	397	1.855	2217.20	-0.5614
9.750	417	1.904	2399.82	-0.5207
10.000	484	1.953	2885.08	-0.4181
10.250	569	2.002	3508.47	-0.2854
10.500	619	2.050	3927.75	-0.1923
10.750	808	2.099	5306.73	0.1024
11.000	881	2.148	5941.38	0.2462
11.250	1060	2.196	7354.00	0.5578
11.500	1231	2.245	8767.25	0.8754
11.750	1260	2.294	9180.46	0.9827
12.000	1228	2.342	9139.77	0.9929

Table III-3 (Continued)

Run: MM50B4
Normalization factor Ā: 7657.62
Background: 0.026 cts/sec
Counting for 1600.0 seconds

2Θ(°)	Counts	S(1/Å)	Intensity	i(S)
16.000	5322	3.118	3650.38	-0.0743
16.500	4675	3.215	3309.74	-0.1449
17.000	4263	3.312	3113.12	-0.1804
17.500	3832	3.409	2883.47	-0.2267
18.000	3659	3.505	2836.49	-0.2248
18.500	3294	3.602	2626.82	-0.2687
19.000	3284	3.698	2695.48	-0.2352
19.500	3178	3.795	2682.02	-0.2246
20.000	3230	3.891	2802.85	-0.1743
20.500	3288	3.987	2932.07	-0.1198
21.000	3360	4.083	3077.56	-0.0587
21.500	3546	4.179	3335.57	0.0396
22.000	3676	4.275	3548.56	0.1268
22.500	3710	4.371	3672.43	0.1878
23.000	3704	4.467	3757.55	0.2376
23.500	3643	4.563	3785.17	0.2694
24.000	3316	4.659	3524.06	0.2026
24.500	3361	4.754	3656.77	0.2706
25.000	3084	4.850	3429.41	0.2124
25.500	2870	4.945	3261.01	0.1729
26.000	2659	5.040	3085.61	0.1289
26.500	2444	5.136	2894.89	0.0772
27.000	2356	5.231	2849.74	0.0788
27.500	2224	5.326	2745.04	0.0569
28.000	2050	5.421	2579.79	0.0098
28.500	1909	5.515	2448.90	-0.0255
29.000	1842	5.610	2409.82	-0.0248
29.500	1836	5.705	2450.77	0.0088
30.000	1757	5.799	2390.06	0.0001
30.500	1701	5.894	2358.03	0.0031
31.000	1608	5.988	2269.63	-0.0189

Table III-3 (Continued)

Run: MM50B5
Normalization factor Ā: 582.55
Background: 0.026 cts/sec
Counting for 10000 counts

2Θ(°)	Seconds	S(1/Å)	Intensity	i(S)
42.000	1513.0	8.030	1700.50	0.0282
44.000	1646.8	8.394	1661.30	0.0640
46.000	1799.2	8.755	1613.71	0.0934
48.000	2017.0	9.114	1524.55	0.0911
50.000	2341.8	9.469	1387.85	0.0470
52.000	2642.3	9.822	1297.83	0.0315
54.000	2922.9	10.172	1235.80	0.0343
56.000	3181.7	10.519	1193.76	0.0520
58.000	3555.2	10.863	1120.99	0.0387
60.000	3888.6	11.203	1073.45	0.0459
62.000	4302.5	11.540	1013.93	0.0368
64.000	4694.1	11.874	969.29	0.0394
66.000	5293.6	12.204	894.00	0.0026

Table III-3 (Continued)

Run: MM50B6
Normalization factor Ā: 259.52
Background: 0.026 cts/sec
Counting for 10000 counts

2Θ(°)	Seconds	S(1/Å)	Intensity	i(S)
58.000	1581.5	10.863	1128.45	0.0459
62.000	1943.4	11.540	1006.22	0.0286
66.000	2374.8	12.204	894.61	0.0033
70.000	2777.7	12.852	823.32	0.0115
74.000	3163.4	13.485	770.18	0.0323
78.000	3696.7	14.101	693.80	0.0069
82.000	4230.6	14.700	630.17	-0.0141
86.000	4581.7	15.281	597.02	0.0033
90.000	5057.9	15.844	546.95	-0.0195
94.000	5349.0	16.387	515.91	-0.0157
98.000	5584.7	16.911	486.14	-0.0147
102.000	5671.0	17.413	464.96	-0.0035

Table III-4

Run: MG00A1
Normalization factor Ā: 272.56
Background: 0.024 cts/sec
Counting for 10000 counts

2Θ(°)	Seconds	S(1/Å)	Intensity	i(S)
58.000	1736.5	10.863	1079.30	0.0324
62.000	2116.4	11.540	970.37	0.0239
66.000	2550.3	12.204	874.95	0.0133
70.000	2989.0	12.852	803.60	0.0194
74.000	3412.6	13.485	749.84	0.0378
78.000	3998.0	14.101	673.76	0.0089
82.000	4416.1	14.700	634.30	0.0266
86.000	4858.5	15.281	591.45	0.0271
90.000	5186.1	15.844	560.63	0.0415
94.000	5781.0	16.387	501.36	-0.0139
98.000	5947.2	16.911	479.57	0.0036
102.000	6123.1	17.413	452.29	-0.0005

Table III-4 (Continued)

Run: MG00A2
Normalization factor A: 1998.68
Background: 0.024 cts/sec
Counting for 4000 counts

2Θ(°)	Seconds	S(1/Å)	Intensity	i(S)
27.000	766.6	5.231	2670.70	0.0426
28.000	870.4	5.421	2452.28	-0.0107
29.000	963.2	5.610	2307.87	-0.0378
30.000	1037.9	5.799	2228.46	-0.0396
31.000	1096.2	5.988	2193.44	-0.0227
32.000	1114.6	6.176	2241.12	0.0330
33.000	1174.5	6.364	2207.11	0.0508
34.000	1217.1	6.551	2208.74	0.0862
35.000	1301.1	6.738	2140.54	0.0858
36.000	1376.8	6.924	2094.33	0.0958
37.000	1524.1	7.110	1956.61	0.0542
38.000	1629.5	7.295	1891.93	0.0505
39.000	1844.6	7.480	1725.63	-0.0150
40.000	1961.1	7.664	1675.91	-0.0147
41.000	2066.5	7.847	1641.37	-0.0060
42.000	2182.7	8.030	1602.81	-0.0007
43.000	2309.2	8.212	1561.70	0.0020
44.000	2426.6	8.394	1531.29	0.0110
45.000	2428.7	8.575	1576.78	0.0731
46.000	2590.9	8.755	1521.10	0.0639
47.000	2700.2	8.935	1501.81	0.0804
48.000	2908.2	9.114	1433.29	0.0588

Table III-4 (Continued)

Run: MG00A3
Normalization factor Ā: 672.17
Background: 0.024 cts/sec
Counting for 10000 counts

2Θ(°)	Seconds	S(1/Å)	Intensity	i(S)
42.000	1868.6	8.030	1587.83	-0.0104
44.000	1998.6	8.394	1578.64	0.0436
46.000	2210.1	8.755	1514.83	0.0594
48.000	2514.3	9.114	1410.03	0.0409
50.000	2888.1	9.469	1297.35	0.0092
52.000	3313.5	9.822	1192.84	-0.0236
54.000	3629.9	10.172	1146.90	-0.0109
56.000	4026.6	10.519	1086.86	-0.0139
58.000	4338.6	10.863	1058.64	0.0116
60.000	4670.4	11.203	1030.11	0.0361
62.000	5167.5	11.540	972.88	0.0267
64.000	5539.4	11.874	946.69	0.0488
66.000	6131.5	12.204	889.71	0.0315

Table III-4 (Continued)

Run: MG00A4
Normalization factor Ā: 78409.22
Background: 0.024 cts/sec
Counting for 1000.0 seconds

2Θ(°)	Counts	S(1/Å)	Intensity	i(S)
8.000	293	1.563	1485.55	-0.7228
8.250	306	1.612	1606.97	-0.6963
8.500	306	1.661	1656.66	-0.6836
8.750	311	1.709	1736.70	-0.6645
9.000	301	1.758	1725.17	-0.6638
9.250	302	1.807	1780.63	-0.6492
9.500	303	1.855	1836.54	-0.6343
9.750	301	1.904	1872.61	-0.6233
10.000	334	1.953	2150.90	-0.5610
10.250	372	2.002	2476.64	-0.4874
10.500	477	2.050	3304.86	-0.3042
10.750	545	2.099	3894.24	-0.1695
11.000	653	2.148	4814.34	0.0404
11.250	837	2.196	6368.82	0.3948
11.500	883	2.245	6683.90	0.5234
11.750	988	2.294	7899.35	0.7675
12.000	956	2.342	7805.70	0.7633
12.250	964	2.391	8043.08	0.8351

Table III-4 (Continued)

Run: MG00A5
Normalization factor $\bar{A}$: 7931.35
Background: 0.024 cts/sec
Counting for 1600.0 seconds

2Θ(°)	Counts	S(1/Å)	Intensity	i(S)
16.000	5427	3.118	3858.34	0.0087
16.500	4735	3.215	3474.82	-0.0756
17.000	4376	3.312	3313.17	-0.1022
17.500	3843	3.409	2997.73	-0.1736
18.000	3539	3.505	2843.03	-0.2019
18.500	3270	3.602	2703.32	-0.2273
19.000	3187	3.698	2711.07	-0.2100
19.500	3192	3.795	2793.13	-0.1698
20.000	3089	3.891	2777.58	-0.1588
20.500	3234	3.987	2989.36	-0.0759
21.000	3267	4.083	3101.31	-0.0224
21.500	3358	4.179	3272.62	0.0521
22.000	3333	4.275	3331.77	0.0915
22.500	3486	4.371	3574.76	0.1944
23.000	3525	4.467	3705.05	0.2617
23.500	3418	4.563	3679.03	0.2757
24.000	3232	4.659	3559.96	0.2563
24.500	3107	4.754	3501.32	0.2577
25.000	2915	4.850	3358.43	0.2273
25.500	2704	4.945	3183.17	0.1830
26.000	2498	5.040	3003.23	0.1347
26.500	2415	5.136	2966.18	0.1405
27.000	2103	5.231	2633.03	0.0276
27.500	2082	5.326	2662.34	0.0577
28.000	1981	5.421	2584.47	0.0440
28.500	1806	5.515	2400.88	-0.0150
29.000	1753	5.610	2377.01	-0.0081
29.500	1596	5.705	2203.40	-0.0667
30.000	1542	5.799	2169.85	-0.0655
30.500	1575	5.894	2261.58	-0.0082
31.000	1436	5.988	2097.43	-0.0667

Table III-4 (Continued)

Run: MG00A6
Normalization factor Ā: 26106.84
Background: 0.024 cts/sec
Counting for 1600.0 seconds

2Θ(°)	Counts	S(1/Å)	Intensity	i(S)
11.000	3329	2.148	5241.17	0.1341
11.250	3933	2.196	6348.90	0.3904
11.500	4356	2.245	7200.31	0.5942
11.750	4597	2.294	7773.44	0.7390
12.000	4523	2.342	7816.04	0.7656
12.250	4414	2.391	7791.11	0.7770
12.500	4444	2.439	8011.05	0.8455
12.750	4147	2.488	7626.63	0.7733
13.000	3898	2.537	7310.95	0.7157
13.250	3606	2.585	6893.58	0.6325
13.500	3343	2.634	6511.42	0.5561
13.750	3190	2.682	6330.42	0.5271
14.000	2982	2.731	6025.40	0.4669
14.250	2731	2.779	5615.02	0.3791
14.500	2452	2.828	5126.13	0.2698
14.750	2336	2.876	4968.42	0.2422
15.000	2210	2.925	4779.97	0.2061
15.250	1876	2.973	4116.05	0.0462
15.500	1913	3.022	4271.82	0.0972
15.750	1811	3.070	4108.47	0.0649
16.000	1675	3.118	3857.22	0.0084
16.250	1623	3.167	3796.75	0.0020
16.500	1525	3.215	3620.34	-0.0361
16.750	1384	3.264	3329.97	-0.1062
17.000	1295	3.312	3159.35	-0.1447
17.250	1225	3.360	3030.35	-0.1724
17.500	1204	3.409	3023.01	-0.1664
17.750	1187	3.457	3024.67	-0.1579
18.000	1097	3.505	2829.94	-0.2057

Table III-5

Run: MG30A1
Normalization factor $\bar{A}$: 64596.95
Background: 0.024 cts/sec
Counting for 1000.0 seconds

2Θ(°)	Counts	S(1/Å)	Intensity	i(S)
8.000	390	1.563	1660.63	-0.6884
8.250	410	1.612	1807.44	-0.6565
8.500	436	1.661	1989.17	-0.6171
8.750	445	1.709	2093.81	-0.5925
9.000	380	1.758	1821.48	-0.6442
9.250	439	1.807	2184.61	-0.5662
9.500	465	1.855	2386.13	-0.5203
9.750	480	1.904	2534.10	-0.4848
10.000	523	1.953	2846.64	-0.4140
10.250	680	2.002	3840.33	-0.1965
10.500	737	2.050	4279.36	-0.0943
10.750	959	2.099	5751.44	0.2343
11.000	1063	2.148	6545.28	0.4203
11.250	1244	2.196	7867.14	0.7267
11.500	1310	2.245	8483.78	0.8813
11.750	1305	2.294	8641.10	0.9350
12.000	1276	2.342	8631.74	0.9516

Table III-5 (Continued)

Run: MG30A2
Normalization factor Ā: 22468.50
Background: 0.024 cts/sec
Counting for 1600.0 seconds

2Θ(°)	Counts	S(1/Å)	Intensity	i(S)
11.000	4944	2.148	6722.39	0.4591
11.250	5581	2.196	7773.98	0.7061
11.500	5937	2.245	8463.69	0.8768
11.750	5938	2.294	8655.78	0.9383
12.000	5714	2.342	8510.84	0.9241
12.250	5446	2.391	8284.33	0.8906
12.500	5075	2.439	7879.59	0.8149
12.750	4624	2.488	7323.24	0.7021
13.000	4390	2.537	7091.54	0.6637
13.250	4136	2.585	6811.59	0.6129
13.500	3768	2.634	6321.97	0.5103
13.750	3429	2.682	5858.58	0.4120
14.000	3094	2.731	5380.17	0.3079
14.250	3113	2.779	5515.21	0.3543
14.500	2658	2.828	4785.35	0.1842
14.750	2528	2.876	4630.36	0.1565
15.000	2241	2.925	4169.51	0.0498
15.250	2178	2.973	4121.52	0.0477
15.500	1987	3.022	3818.47	-0.0212
15.750	1856	3.070	3622.48	-0.0633
16.000	1756	3.118	3480.72	-0.0918
16.250	1630	3.167	3278.76	-0.1372
16.500	1545	3.215	3154.36	-0.1625
16.750	1458	3.264	3020.09	-0.1912
17.000	1402	3.312	2947.12	-0.2034
17.250	1342	3.360	2861.67	-0.2195
17.500	1237	3.409	2671.80	-0.2655
17.750	1297	3.457	2848.81	-0.2079
18.000	1209	3.505	2689.55	-0.2460

Table III-5 (Continued)

Run: MG30A3
Normalization factor Ā: 1825.07
Background: 0.024 cts/sec
Counting for 4000 counts

2Θ(°)	Seconds	S(1/Å)	Intensity	i(S)
27.000	725.7	5.231	2576.33	0.0049
28.000	822.2	5.421	2370.75	-0.0445
29.000	877.9	5.610	2312.84	-0.0356
30.000	973.8	5.799	2169.14	-0.0659
31.000	1033.1	5.988	2125.50	-0.0538
32.000	1076.6	6.176	2118.59	-0.0251
33.000	1038.9	6.364	2279.72	0.0864
34.000	1088.5	6.551	2256.31	0.1103
35.000	1177.3	6.738	2161.13	0.0966
36.000	1288.4	6.924	2044.05	0.0687
37.000	1377.7	7.110	1977.58	0.0659
38.000	1530.3	7.295	1839.98	0.0207
39.000	1660.0	7.480	1752.19	0.0008
40.000	1816.1	7.664	1653.22	-0.0285
41.000	1903.9	7.847	1627.62	-0.0147
42.000	2027.3	8.030	1576.45	-0.0178
43.000	2070.9	8.212	1591.62	0.0220
44.000	2257.8	8.394	1503.50	-0.0081
45.000	2319.9	8.575	1507.46	0.0240
46.000	2430.8	8.755	1480.99	0.0347
47.000	2532.4	8.935	1462.79	0.0512
48.000	2694.5	9.114	1413.46	0.0435

Table III-5 (Continued)

Run: MG30A4
Normalization factor Ā: 586.93
Background: 0.024 cts/sec
Counting for 10000 counts

2Θ(°)	Seconds	S(1/Å)	Intensity	i(S)
42.000	1662.4	8.030	1558.98	-0.0291
44.000	1815.8	8.394	1517.63	0.0016
46.000	1971.2	8.755	1483.62	0.0367
48.000	2187.9	9.114	1415.72	0.0453
50.000	2537.2	9.469	1290.28	0.0035
52.000	2921.8	9.822	1182.00	-0.0329
54.000	3171.2	10.172	1147.24	-0.0106
56.000	3460.9	10.519	1105.30	0.0037
58.000	3729.9	10.863	1076.44	0.0296
60.000	4144.5	11.203	1014.49	0.0195
62.000	4605.9	11.540	953.95	0.0056
64.000	5116.0	11.874	895.52	-0.0113
66.000	5546.3	12.204	859.60	-0.0057

Table III-5 (Continued)

Run: MG30A5
Normalization factor Ā: 7279.84
Background: 0.024 cts/sec
Counting for 1600.0 seconds

2Θ(°)	Counts	S(1/Å)	Intensity	i(S)
16.000	5177	3.118	3376.05	-0.1197
16.500	4698	3.215	3163.17	-0.1602
17.000	4317	3.312	2998.52	-0.1892
17.500	3796	3.409	2716.34	-0.2529
18.000	3633	3.505	2678.37	-0.2492
18.500	3443	3.602	2612.86	-0.2538
19.000	3423	3.698	2673.62	-0.2212
19.500	3308	3.795	2656.69	-0.2113
20.000	3362	3.891	2776.23	-0.1592
20.500	3508	3.987	2977.69	-0.0796
21.000	3508	4.083	3057.63	-0.0365
21.500	3580	4.179	3203.23	0.0293
22.000	3711	4.275	3407.47	0.1168
22.500	3758	4.371	3538.46	0.1821
23.000	3717	4.467	3586.41	0.2206
23.500	3637	4.563	3594.04	0.2457
24.000	3464	4.659	3503.27	0.2359
24.500	3315	4.754	3429.87	0.2316
25.000	3032	4.850	3206.22	0.1706
25.500	2793	4.945	3017.49	0.1201
26.000	2644	5.040	2918.37	0.1020
26.500	2385	5.136	2686.32	0.0305
27.000	2205	5.231	2534.27	-0.0119
27.500	2153	5.326	2526.63	0.0024
28.000	2007	5.421	2401.97	-0.0315
28.500	1927	5.515	2352.52	-0.0354
29.000	1836	5.610	2285.33	-0.0474
29.500	1790	5.705	2272.22	-0.0367
30.000	1740	5.799	2251.75	-0.0292
30.500	1619	5.894	2133.09	-0.0662
31.000	1548	5.988	2077.21	-0.0760

Table III-5 (Continued)

Run: MG30A6
Normalization factor Ā: 260.07
Background: 0.024 cts/sec
Counting for 10000 counts

2Θ(°)	Seconds	S(1/Å)	Intensity	i(S)
58.000	1670.2	10.863	1070.72	0.0238
62.000	2047.0	11.540	957.27	0.0093
66.000	2472.0	12.204	861.25	-0.0036
70.000	2869.4	12.852	798.74	0.0128
74.000	3300.8	13.485	739.67	0.0227
78.000	3825.2	14.101	671.95	0.0060
82.000	4326.1	14.700	617.69	-0.0025
86.000	4762.5	15.281	575.58	-0.0029
90.000	5168.4	15.844	536.52	-0.0074
94.000	5374.7	16.387	514.78	0.0153
98.000	5657.9	16.911	481.06	0.0070
102.000	5841.7	17.413	452.39	-0.0003

Table III-6

Run: MG50A1
Normalization factor Ā: 22721.41
Background: 0.025 cts/sec
Counting for 1600.0 seconds

2Θ(°)	Counts	S(1/Å)	Intensity	i(S)
11.000	3372	2.148	4618.91	-0.0025
11.250	4133	2.196	5807.09	0.2703
11.500	4879	2.245	7023.36	0.5546
11.750	5249	2.294	7730.67	0.7294
12.000	5195	2.342	7819.39	0.7664
12.250	5080	2.391	7810.40	0.7815
12.500	4802	2.439	7536.24	0.7351
12.750	4577	2.488	7329.74	0.7036
13.000	4176	2.537	6818.57	0.5990
13.250	3980	2.585	6625.92	0.5685
13.500	3710	2.634	6293.67	0.5035
13.750	3386	2.682	5849.36	0.4097
14.000	3264	2.731	5743.58	0.3974
14.250	2967	2.779	5312.31	0.3038
14.500	2673	2.828	4866.94	0.2047
14.750	2534	2.876	4693.77	0.1726
15.000	2340	2.925	4406.09	0.1104
15.250	2144	2.973	4101.63	0.0425
15.500	1956	3.022	3799.97	-0.0260
15.750	1802	3.070	3554.32	-0.0812
16.000	1695	3.118	3394.77	-0.1147
16.250	1690	3.167	3440.78	-0.0937
16.500	1524	3.215	3145.36	-0.1650
16.750	1443	3.264	3021.78	-0.1907
17.000	1451	3.312	3087.51	-0.1646
17.250	1360	3.360	2933.89	-0.1994
17.500	1208	3.409	2636.42	-0.2755
17.750	1257	3.457	2789.20	-0.2249
18.000	1189	3.505	2673.30	-0.2507

Table III-6 (Continued)

Run: MG50A2
Normalization factor Ā: 1787.79
Background: 0.025 cts/sec
Counting for 4000 counts

2Θ(°)	Seconds	S(1/Å)	Intensity	i(S)
27.000	705.0	5.231	2598.13	0.0136
28.000	820.5	5.421	2327.15	-0.0625
29.000	897.3	5.610	2216.34	-0.0770
30.000	946.5	5.799	2186.49	-0.0582
31.000	1027.0	5.988	2094.53	-0.0680
32.000	1056.5	6.176	2115.06	-0.0267
33.000	1085.4	6.364	2136.85	0.0164
34.000	1125.7	6.551	2136.67	0.0497
35.000	1155.0	6.738	2158.15	0.0950
36.000	1309.6	6.924	1969.62	0.0286
37.000	1380.8	7.110	1932.79	0.0410
38.000	1485.8	7.295	1856.89	0.0304
39.000	1690.5	7.480	1685.10	-0.0389
40.000	1820.4	7.664	1615.57	-0.0515
41.000	1913.1	7.847	1586.61	-0.0405
42.000	2059.4	8.030	1519.87	-0.0544
43.000	2104.2	8.212	1534.11	-0.0164
44.000	2138.6	8.394	1556.05	0.0280
45.000	2291.2	8.575	1495.43	0.0155
46.000	2473.7	8.755	1425.18	-0.0059
47.000	2534.1	8.935	1431.93	0.0281
48.000	2733.6	9.114	1364.44	0.0058

Table III-6 (Continued)

Run: MG50A3
Normalization factor Ā: 6948.23
Background: 0.025 cts/sec
Counting for 1600.0 seconds

2Θ(°)	Counts	S(1/Å)	Intensity	i(S)
16.000	5679	3.118	3537.15	-0.0768
16.500	4927	3.215	3167.51	-0.1590
17.000	4479	3.312	2970.34	-0.1970
17.500	3990	3.409	2726.51	-0.2501
18.000	3651	3.505	2569.17	-0.2806
18.500	3590	3.602	2601.57	-0.2571
19.000	3431	3.698	2557.86	-0.2558
19.500	3407	3.795	2612.49	-0.2248
20.000	3244	3.891	2555.64	-0.2276
20.500	3378	3.987	2735.51	-0.1561
21.000	3481	4.083	2895.63	-0.0887
21.500	3524	4.179	3008.95	-0.0344
22.000	3607	4.275	3160.11	0.0341
22.500	3631	4.371	3261.91	0.0880
23.000	3771	4.467	3473.32	0.1814
23.500	3520	4.563	3318.74	0.1486
24.000	3537	4.659	3414.97	0.2042
24.500	3214	4.754	3172.68	0.1375
25.000	3036	4.850	3064.26	0.1177
25.500	2747	4.945	2831.92	0.0498
26.000	2703	5.040	2848.54	0.0750
26.500	2483	5.136	2671.11	0.0245
27.000	2304	5.231	2529.43	-0.0139
27.500	2191	5.326	2454.91	-0.0267
28.000	2074	5.421	2370.64	-0.0445
28.500	1951	5.515	2273.92	-0.0685
29.000	1898	5.610	2256.53	-0.0598
29.500	1745	5.705	2112.95	-0.1061
30.000	1719	5.799	2122.63	-0.0865
30.500	1645	5.894	2069.44	-0.0949
31.000	1665	5.988	2136.41	-0.0488

Table III-6 (Continued)

Run: MG50A4
Normalization factor Ā: 570.12
Background: 0.025 cts/sec
Counting for 10000 counts

2Θ(°)	Seconds	S(1/Å)	Intensity	i(S)
42.000	1632.8	8.030	1541.89	-0.0402
44.000	1787.7	8.394	1497.43	-0.0123
46.000	1941.4	8.755	1463.35	0.0219
48.000	2207.9	9.114	1362.64	0.0044
50.000	2558.1	9.469	1243.01	-0.0350
52.000	2846.3	9.822	1178.82	-0.0357
54.000	3163.1	10.172	1117.25	-0.0378
56.000	3509.6	10.519	1058.61	-0.0409
58.000	3750.9	10.863	1039.70	-0.0075
60.000	4151.3	11.203	983.80	-0.0131
62.000	4640.1	11.540	919.72	-0.0327
64.000	5122.8	11.874	868.70	-0.0429
66.000	5635.9	12.204	821.52	-0.0526

Table III-6 (Continued)

Run: MG50A5
Normalization factor A: 256.04
Background: 0.025 cts/sec
Counting for 10000 counts

2Θ(°)	Seconds	S(1/Å)	Intensity	i(S)
58.000	1691.2	10.863	1040.97	-0.0062
62.000	2113.6	11.540	912.57	-0.0407
66.000	2535.4	12.204	826.56	-0.0464
70.000	2976.0	12.852	757.98	-0.0425
74.000	3403.1	13.485	706.12	-0.0272
78.000	3974.8	14.101	636.39	-0.0516
82.000	4367.9	14.700	602.22	-0.0297
86.000	4813.8	15.281	560.54	-0.0314
90.000	5125.8	15.844	532.64	-0.0153
94.000	5520.7	16.387	493.21	-0.0316
98.000	5715.2	16.911	468.78	-0.0214
102.000	5765.1	17.413	451.38	-0.0028

Table III-6 (Continued)

Run: MG50A6
Normalization factor Ā: 58280.42
Background: 0.025 cts/sec
Counting for 1000.0 seconds

2Θ(°)	Counts	S(1/Å)	Intensity	i(S)
8.000	368	1.563	1407.94	-0.7380
8.250	406	1.612	1613.76	-0.6949
8.500	363	1.661	1475.90	-0.7197
8.750	377	1.709	1583.22	-0.6955
9.000	406	1.758	1763.73	-0.6559
9.250	400	1.807	1785.32	-0.6483
9.500	378	1.855	1727.14	-0.6570
9.750	402	1.904	1894.37	-0.6188
10.000	446	1.953	2171.18	-0.5567
10.250	499	2.002	2507.36	-0.4808
10.500	615	2.050	3199.35	-0.3269
10.750	770	2.099	4139.01	-0.1162
11.000	871	2.148	4812.96	0.0401
11.250	1045	2.196	5939.15	0.2996
11.500	1176	2.245	6856.02	0.5172
11.750	1242	2.294	7412.43	0.6575
12.000	1287	2.342	7856.17	0.7748

Table III-7

Run: GM00A1
Normalization factor Ā: 6603.12
Background: 0.039 cts/sec
Counting for 900.0 seconds

2Θ(°)	Counts	S(1/Å)	Intensity	i(S)
8.000	247	1.563	109.50	-0.9180
8.250	259	1.612	119.39	-0.9048
8.500	334	1.661	164.30	-0.8479
8.750	298	1.709	148.86	-0.8654
9.000	336	1.758	175.35	-0.8302
9.250	317	1.807	168.95	-0.8363
9.500	293	1.855	158.85	-0.8473
9.750	331	1.904	187.18	-0.8084
10.000	358	1.953	209.64	-0.7763
10.250	336	2.002	200.38	-0.7860
10.500	411	2.050	256.61	-0.7073
10.750	428	2.099	274.79	-0.6788
11.000	469	2.148	310.75	-0.6251
11.250	548	2.196	375.96	-0.5292
11.500	689	2.245	490.33	-0.3615
11.750	764	2.294	558.88	-0.2555
12.000	833	2.342	625.29	-0.1502

Table III-7 (Continued)

Run: GM00A2
Normalization factor $\bar{A}$: 2350.70
Background: 0.039 cts/sec
Counting for 1400.0 seconds

2Θ(°)	Counts	S(1/Å)	Intensity	i(S)
11.000	2001	2.148	319.02	-0.6137
11.250	2321	2.196	380.20	-0.5233
11.500	2792	2.245	469.77	-0.3906
11.750	3208	2.294	553.34	-0.2635
12.000	3586	2.342	633.35	-0.1385
12.250	3964	2.391	716.32	-0.0062
12.500	4417	2.439	816.29	0.1544
12.750	4441	2.488	837.88	0.2009
13.000	4529	2.537	872.17	0.2674
13.250	4432	2.585	870.40	0.2794
13.500	4099	2.634	820.06	0.2160
13.750	3948	2.682	804.76	0.2061
14.000	3692	2.731	766.18	0.1589
14.250	3457	2.779	730.13	0.1145
14.500	3244	2.828	697.06	0.0737
14.750	3076	2.876	672.34	0.0457
15.000	3030	2.925	673.95	0.0608
15.250	2841	2.973	642.26	0.0200
15.500	2720	3.022	625.03	0.0027
15.750	2642	3.070	617.12	0.0010
16.000	2446	3.118	579.99	-0.0510
16.250	2354	3.167	566.95	-0.0634
16.500	2238	3.215	547.17	-0.0875
16.750	2051	3.264	508.40	-0.1466
17.000	1853	3.312	465.29	-0.2151
17.250	1735	3.360	441.61	-0.2493
17.500	1626	3.409	419.38	-0.2818
17.750	1536	3.457	401.44	-0.3070
18.000	1443	3.505	381.94	-0.3359

Table III-7 (Continued)

Run: GM00A3
Normalization factor A: 733.65
Background: 0.039 cts/sec
Counting for 1400.0 seconds

2Θ(°)	Counts	S(1/Å)	Intensity	i(S)
16.000	7805	3.118	586.66	-0.0401
16.500	6846	3.215	531.18	-0.1161
17.000	5898	3.312	471.84	-0.2031
17.500	5129	3.409	422.67	-0.2756
18.000	4492	3.505	380.98	-0.3377
18.500	4093	3.602	357.13	-0.3681
19.000	3623	3.698	324.81	-0.4174
19.500	3488	3.795	321.47	-0.4096
20.000	3286	3.891	311.03	-0.4168
20.500	3293	3.987	320.25	-0.3821
21.000	3165	4.083	315.85	-0.3762
21.500	3244	4.179	332.40	-0.3229
22.000	3257	4.275	342.36	-0.2825
22.500	3344	4.371	360.56	-0.2209
23.000	3382	4.467	373.79	-0.1688
23.500	3357	4.563	380.04	-0.1319
24.000	3276	4.659	379.62	-0.1109
24.500	3334	4.754	395.57	-0.0462
25.000	3241	4.850	393.27	-0.0280
25.500	3143	4.945	389.88	-0.0125
26.000	2881	5.040	364.83	-0.0582
26.500	2840	5.136	367.51	-0.0262
27.000	2641	5.231	348.70	-0.0573
27.500	2534	5.326	341.47	-0.0551
28.000	2336	5.421	320.87	-0.0954
28.500	2191	5.515	306.76	-0.1174
29.000	2087	5.610	297.86	-0.1240
29.500	1950	5.705	283.45	-0.1502
30.000	1850	5.799	273.90	-0.1615
30.500	1839	5.894	277.64	-0.1267
31.000	1699	5.988	260.88	-0.1653

Table III-7 (Continued)

Run: GM00A4
Normalization factor $\bar{A}$: 64.05
Background: 0.039 cts/sec
Counting for 10000 counts

2Θ(°)	Seconds	S(1/Å)	Intensity	i(S)
42.000	1463.7	8.030	192.91	-0.0040
44.000	1630.6	8.394	184.08	0.0278
46.000	1845.8	8.755	172.50	0.0340
48.000	2059.1	9.114	163.73	0.0517
50.000	2267.5	9.469	157.15	0.0799
52.000	2595.3	9.822	144.80	0.0497
54.000	2885.3	10.172	137.13	0.0505
56.000	3209.1	10.519	129.57	0.0434
58.000	3486.0	10.863	125.14	0.0615
60.000	3808.2	11.203	119.93	0.0654
62.000	4166.7	11.540	114.52	0.0607
64.000	4610.3	11.874	107.87	0.0336
66.000	4850.8	12.204	106.70	0.0712

Table III-7 (Continued)

Run: GM00A5
Normalization factor Ā: 189.94
Background: 0.039 cts/sec
Counting for 4000 counts

2Θ(°)	Seconds	S(1/Å)	Intensity	i(S)
27.000	554.5	5.231	350.61	-0.0516
28.000	641.8	5.421	315.73	-0.1115
29.000	706.2	5.610	298.81	-0.1209
30.000	796.2	5.799	275.64	-0.1554
31.000	873.1	5.988	261.21	-0.1641
32.000	933.7	6.176	253.63	-0.1499
33.000	985.4	6.364	249.36	-0.1235
34.000	994.1	6.551	256.38	-0.0494
35.000	1074.2	6.738	245.73	-0.0489
36.000	1122.7	6.924	243.42	-0.0123
37.000	1164.6	7.110	242.80	0.0333
38.000	1276.7	7.295	220.06	0.0124
39.000	1378.3	7.480	218.95	0.0080
40.000	1494.1	7.664	208.46	-0.0030
41.000	1649.5	7.847	194.69	-0.0373
42.000	1726.3	8.030	191.86	-0.0105
43.000	1832.7	8.212	186.24	-0.0019
44.000	1931.9	8.394	182.00	0.0139
45.000	2088.5	8.575	173.23	-0.0030
46.000	2164.1	8.755	172.09	0.0310
47.000	2290.4	8.935	167.21	0.0370
48.000	2359.9	9.114	166.91	0.0766

Table III-7 (Continued)

Run: GM00A6
Normalization factor Ā: 28.82
Background: 0.039 cts/sec
Counting for 10000 counts

2Θ(°)	Seconds	S(1/Å)	Intensity	i(S)
58.000	1589.1	10.863	124.45	0.0540
62.000	1869.5	11.540	115.90	0.0774
66.000	2219.2	12.204	106.05	0.0625
70.000	2604.4	12.852	97.23	0.0365
74.000	2921.0	13.485	92.33	0.0480
78.000	3247.2	14.101	87.44	0.0463
82.000	3609.5	14.700	81.77	0.0191
86.000	3900.7	15.281	77.61	0.0065
90.000	4112.7	15.844	74.48	0.0041
94.000	4350.2	16.387	70.23	-0.0283
98.000	4402.4	16.911	68.30	-0.0181
102.000	4371.3	17.413	66.83	-0.0025

Table III-8

Run: GM30A1
Normalization factor $\bar{A}$: 8699.41
Background: 0.040 cts/sec
Counting for 1000.0 seconds

2θ(°)	Counts	S(1/Å)	Intensity	i(S)
8.000	298	1.563	158.08	-0.8591
8.250	315	1.612	173.87	-0.8380
8.500	360	1.661	208.57	-0.7931
8.750	399	1.709	241.02	-0.7501
9.000	386	1.758	239.08	-0.7496
9.250	361	1.807	228.12	-0.7607
9.500	413	1.855	272.41	-0.7005
9.750	412	1.904	279.02	-0.6884
10.000	428	1.953	298.68	-0.6586
10.250	437	2.002	313.47	-0.6348
10.500	438	2.050	322.15	-0.6187
10.750	440	2.099	331.72	-0.6010
11.000	508	2.148	397.42	-0.5052
11.250	555	2.196	447.61	-0.4290
11.500	646	2.245	538.81	-0.2929
11.750	725	2.294	622.77	-0.1640
12.000	872	2.342	773.11	0.0642

Table III-8 (Continued)

Run: GM30A2
Normalization factor $\bar{A}$: 2890.17
Background: 0.040 cts/sec
Counting for 1600.0 seconds

2Θ(°)	Counts	S(1/Å)	Intensity	i(S)
11.000	2247	2.148	384.92	-0.5225
11.250	2493	2.196	438.36	-0.4419
11.500	2974	2.245	537.24	-0.2951
11.750	3547	2.294	657.51	-0.1142
12.000	4066	2.342	772.16	0.0628
12.250	4704	2.391	914.64	0.2848
12.500	5278	2.439	1049.60	0.5008
12.750	5618	2.488	1141.34	0.6570
13.000	5656	2.537	1172.65	0.7243
13.250	5466	2.585	1155.56	0.7179
13.500	4975	2.634	1071.26	0.6067
13.750	4947	2.682	1085.82	0.6483
14.000	4534	2.731	1012.94	0.5515
14.250	4344	2.779	988.08	0.5296
14.500	4109	2.828	951.07	0.4873
14.750	3839	2.876	903.71	0.4268
15.000	3703	2.925	886.74	0.4153
15.250	3680	2.973	896.66	0.4487
15.500	3561	3.022	882.20	0.4412
15.750	3401	3.070	856.24	0.4135
16.000	3241	3.118	828.93	0.3826
16.250	3120	3.167	810.61	0.3668
16.500	2854	3.215	752.19	0.2787
16.750	2620	3.264	700.25	0.2002
17.000	2348	3.312	635.72	0.0966
17.250	2146	3.360	588.62	0.0227
17.500	2030	3.409	564.47	-0.0102
17.750	1814	3.457	510.17	-0.1010
18.000	1751	3.505	499.26	-0.1110

Table III-8 (Continued)

Run: GM30A3
Normalization factor Ā: 34.76
Background: 0.040 cts/sec
Counting for 10000 counts

2Θ(°)	Seconds	S(1/Å)	Intensity	i(S)
58.000	1966.7	10.863	121.10	0.0175
62.000	2275.8	11.540	114.64	0.0621
66.000	2704.1	12.204	104.75	0.0452
70.000	3190.7	12.852	95.48	0.0112
74.000	3600.9	13.485	90.07	0.0127
78.000	4056.1	14.101	84.14	-0.0087
82.000	4329.5	14.700	81.96	0.0225
86.000	4793.1	15.281	75.89	-0.0257
90.000	5033.8	15.844	73.10	-0.0229
94.000	5113.6	16.387	71.81	0.0042
98.000	5227.6	16.911	69.12	-0.0006
102.000	5260.7	17.413	66.71	-0.0051

Table III-8 (Continued)

Run: GM30A4
Normalization factor Ā: 230.93
Background: 0.040 cts/sec
Counting for 4000 counts

2Θ(°)	Seconds	S(1/Å)	Intensity	i(S)
27.000	568.9	5.231	415.36	0.1414
28.000	641.0	5.421	384.28	0.1034
29.000	706.4	5.610	363.12	0.0910
30.000	799.8	5.799	333.54	0.0451
31.000	933.4	5.988	296.81	-0.0345
32.000	1015.9	6.176	283.11	-0.0371
33.000	1083.6	6.364	275.35	-0.0190
34.000	1130.5	6.551	273.64	0.0235
35.000	1214.6	6.738	263.78	0.0311
36.000	1255.8	6.924	264.15	0.0841
37.000	1357.0	7.110	252.78	0.0819
38.000	1433.5	7.295	247.34	0.1068
39.000	1549.9	7.480	236.23	0.1005
40.000	1693.1	7.664	223.12	0.0790
41.000	1811.5	7.847	215.09	0.0822
42.000	1969.1	8.030	203.91	0.0632
43.000	2114.2	8.212	195.63	0.0581
44.000	2333.3	8.394	182.36	0.0164
45.000	2445.6	8.575	179.11	0.0378
46.000	2594.8	8.755	173.63	0.0421
47.000	2729.5	8.935	169.72	0.0559
48.000	2855.5	9.114	166.75	0.0754

Table III-8 (Continued)

Run: GM30A5
Normalization factor $\bar{A}$: 75.79
Background: 0.040 cts/sec
Counting for 10000 counts

2Θ(°)	Seconds	S(1/Å)	Intensity	i(S)
42.000	1641.4	8.030	203.39	0.0600
44.000	1922.0	8.394	184.55	0.0309
46.000	2181.1	8.755	172.47	0.0338
48.000	2395.9	9.114	166.24	0.0714
50.000	2672.0	9.469	157.51	0.0829
52.000	3004.5	9.822	147.72	0.0761
54.000	3398.8	10.172	137.43	0.0534
56.000	3788.3	10.519	129.53	0.0430
58.000	4239.6	10.863	121.34	0.0201
60.000	4652.9	11.203	115.71	0.0168
62.000	4945.4	11.540	113.76	0.0515
64.000	5326.7	11.874	110.10	0.0620
66.000	5790.5	12.204	105.31	0.0527

Table III-8 (Continued)

Run: GM30A6
Normalization factor Ā: 938.73
Background: 0.040 cts/sec
Counting for 1600.0 seconds

2Θ(°)	Counts	S(1/Å)	Intensity	i(S)
16.000	9802	3.118	825.26	0.3762
16.500	8609	3.215	748.26	0.2717
17.000	7219	3.312	646.84	0.1169
17.500	6020	3.409	555.43	-0.0271
18.000	5303	3.505	503.60	-0.1027
18.500	4756	3.602	464.55	-0.1573
19.000	4206	3.698	422.11	-0.2218
19.500	3904	3.795	402.54	-0.2427
20.000	3652	3.891	386.66	-0.2573
20.500	3563	3.987	387.40	-0.2370
21.000	3464	4.083	386.55	-0.2197
21.500	3406	4.179	389.95	-0.1923
22.000	3366	4.275	395.23	-0.1596
22.500	3508	4.371	422.66	-0.0729
23.000	3532	4.467	436.18	-0.0164
23.500	3584	4.563	453.53	0.0520
24.000	3629	4.659	470.35	0.1220
24.500	3633	4.754	481.99	0.1812
25.000	3510	4.850	476.18	0.1956
25.500	3471	4.945	481.54	0.2410
26.000	3163	5.040	447.86	0.1772
26.500	3020	5.136	436.66	0.1748
27.000	2838	5.231	418.72	0.1514
27.500	2827	5.326	426.03	0.2033
28.000	2578	5.421	395.87	0.1397
28.500	2394	5.515	374.57	0.1005
29.000	2262	5.610	360.65	0.0829
29.500	2079	5.705	337.37	0.0320
30.000	1951	5.799	322.30	0.0062
30.500	1871	5.894	314.78	0.0053
31.000	1738	5.988	297.34	-0.0325

Table III-9

Run: GM50A1
Normalization factor $\bar{A}$: 8210.18
Background: 0.040 cts/sec
Counting for 1000.0 seconds

2Θ(°)	Counts	S(1/Å)	Intensity	i(S)
8.000	265	1.563	130.11	-0.8930
8.250	345	1.612	181.99	-0.8281
8.500	316	1.661	169.78	-0.8412
8.750	374	1.709	211.63	-0.7869
9.000	374	1.758	217.81	-0.7765
9.250	353	1.807	209.92	-0.7839
9.500	343	1.855	208.85	-0.7827
9.750	393	1.904	249.88	-0.7264
10.000	409	1.953	268.08	-0.6991
10.250	401	2.002	269.01	-0.6942
10.500	417	2.050	287.99	-0.6648
10.750	466	2.099	333.41	-0.5986
11.000	487	2.148	358.24	-0.5594
11.250	541	2.196	410.95	-0.4803
11.500	605	2.245	474.11	-0.3845
11.750	759	2.294	616.92	-0.1724
12.000	849	2.342	709.46	-0.0281

Table III-9 (Continued)

Run: GM50A2
Normalization factor $\bar{A}$: 2845.82
Background: 0.040 cts/sec
Counting for 1600.0 seconds

2Θ(°)	Counts	S(1/Å)	Intensity	i(S)
11.000	2160	2.148	363.91	-0.5516
11.250	2350	2.196	406.22	-0.4869
11.500	2807	2.245	498.64	-0.3498
11.750	3289	2.294	599.47	-0.1974
12.000	3696	2.342	690.02	-0.0563
12.250	4491	2.391	859.26	0.2035
12.500	4847	2.439	948.06	0.3500
12.750	5194	2.488	1038.03	0.5017
13.000	5272	2.537	1075.36	0.5764
13.250	5062	2.585	1052.73	0.5598
13.500	4680	2.634	991.46	0.4826
13.750	4459	2.682	962.30	0.4540
14.000	4245	2.731	932.91	0.4242
14.250	3954	2.779	884.26	0.3625
14.500	3746	2.828	852.43	0.3267
14.750	3683	2.876	853.07	0.3434
15.000	3588	2.925	845.54	0.3467
15.250	3476	2.973	833.09	0.3416
15.500	3320	3.022	808.80	0.3161
15.750	3124	3.070	773.11	0.2701
16.000	2998	3.118	753.78	0.2515
16.250	2861	3.167	730.53	0.2254
16.500	2668	3.215	691.27	0.1699
16.750	2595	3.264	682.76	0.1686
17.000	2250	3.312	599.11	0.0296
17.250	2134	3.360	576.25	-0.0002
17.500	2019	3.409	552.70	-0.0322
17.750	1864	3.457	516.69	-0.0887
18.000	1729	3.505	485.19	-0.1380

Table III-9 (Continued)

Run: GM50A3
Normalization factor $\bar{A}$: 230.98
Background: 0.040 cts/sec
Counting for 4000 counts

2Θ(°)	Seconds	S(1/Å)	Intensity	i(S)
27.000	575.2	5.231	410.87	0.1280
28.000	639.2	5.421	385.45	0.1070
29.000	723.4	5.610	354.60	0.0629
30.000	826.3	5.799	322.82	0.0080
31.000	944.1	5.988	293.48	-0.0466
32.000	1048.6	6.176	274.25	-0.0710
33.000	1078.3	6.364	276.78	-0.0132
34.000	1154.4	6.551	267.97	-0.0005
35.000	1205.1	6.738	265.94	0.0407
36.000	1290.2	6.924	257.07	0.0512
37.000	1340.0	7.110	256.08	0.0981
38.000	1465.0	7.295	242.00	0.0795
39.000	1581.4	7.480	231.50	0.0752
40.000	1748.5	7.664	215.97	0.0390
41.000	1840.1	7.847	211.73	0.0625
42.000	2003.0	8.030	200.43	0.0419
43.000	2174.3	8.212	190.14	0.0231
44.000	2310.0	8.394	184.29	0.0292
45.000	2497.5	8.575	175.33	0.0115
46.000	2592.2	8.755	173.85	0.0437
47.000	2789.4	8.935	166.01	0.0280
48.000	2902.3	9.114	164.02	0.0540

Table III-9 (Continued)

Run: GM50A4
Normalization factor A:959.61
Background: 0.040 cts/sec
Counting for 1600.0 seconds

2Θ(°)	Counts	S(1/Å)	Intensity	i(S)
16.000	9009	3.118	774.91	0.2884
16.500	7941	3.215	705.11	0.1946
17.000	6582	3.312	602.36	0.0356
17.500	5655	3.409	532.99	-0.0691
18.000	4933	3.505	478.44	-0.1509
18.500	4431	3.602	441.99	-0.2016
19.000	3979	3.698	407.85	-0.2504
19.500	3732	3.795	393.06	-0.2622
20.000	3474	3.891	375.65	-0.2805
20.500	3432	3.987	381.19	-0.2504
21.000	3210	4.083	365.63	-0.2660
21.500	3171	4.179	370.59	0.2362
22.000	3297	4.275	395.57	-0.1588
22.500	3310	4.371	407.22	-0.1097
23.000	3261	4.467	411.04	-0.0778
23.500	3293	4.563	425.29	-0.0187
24.000	3477	4.659	460.31	0.0962
24.500	3411	4.754	462.06	0.1287
25.000	3216	4.850	445.23	0.1122
25.500	3175	4.945	449.48	0.1523
26.000	3189	5.040	461.66	0.2163
26.500	2852	5.136	421.00	0.1293
27.000	2766	5.231	416.92	0.1461
27.500	2691	5.326	414.07	0.1668
28.000	2409	5.421	377.47	0.0820
28.500	2249	5.515	359.07	0.0507
29.000	2138	5.610	347.88	0.0407
29.500	2012	5.705	333.41	0.0186
30.000	1924	5.799	324.76	0.0147
30.500	1811	5.894	311.09	-0.0078
31.000	1708	5.988	298.51	-0.0283

Table III-9 (Continued)

Run: GM50A5
Normalization factor $\bar{A}$: 35.76
Background: 0.040 cts/sec
Counting for 10000 counts

2Θ(°)	Seconds	S(1/Å)	Intensity	i(S)
58.000	1960.0	10.863	124.99	0.0599
62.000	2363.9	11.540	113.48	0.0481
66.000	2750.2	12.204	105.92	0.0608
70.000	3240.9	12.852	96.67	0.0284
74.000	3606.0	13.485	92.51	0.0509
78.000	4090.4	14.101	85.81	0.0191
82.000	4433.7	14.700	82.29	0.0283
86.000	4717.0	15.281	79.34	0.0387
90.000	4897.8	15.844	77.32	0.0598
94.000	5166.0	16.387	73.10	0.0306
98.000	5247.3	16.911	70.82	0.0359
102.000	5364.7	17.413	67.26	0.0071

Table III-9 (Continued)

Run: GM50A6
Normalization factor $\bar{A}$: 77.59
Background: 0.040 cts/sec
Counting for 10000 counts

2Θ(°)	Seconds	S(1/Å)	Intensity	i(S)
42.000	1696.2	8.030	201.44	0.0481
44.000	1957.2	8.394	185.50	0.0373
46.000	2232.5	8.755	172.47	0.0337
48.000	2491.8	9.114	163.57	0.0505
50.000	2711.8	9.469	158.85	0.0942
52.000	3078.2	9.822	147.56	0.0746
54.000	3469.7	10.172	137.77	0.0567
56.000	3902.8	10.519	128.65	0.0340
58.000	4298.8	10.863	122.48	0.0325
60.000	4683.5	11.203	117.67	0.0393
62.000	5030.9	11.540	114.44	0.0598
64.000	5541.5	11.874	108.25	0.0385
66.000	5826.0	12.204	107.14	0.0770

Appendix IV

Analytical Approximation to i (S) Data

The following nine tables cover all nine experimental series. The equation

$$i(S) = C_0 + C_1 (S_1 - S) + C_2 (S_1 - S)^2 + C_3 (S_1 - S)^3$$

was fitted to the experimental data for a series of panels over the experimental range of S. The value S_1 is the initial value of S for the panel fitted. The coefficients C_0, C_1, C_2, and C_3 are tabulated for each panel. The RMS deviation of the experimental points from the analytical function is also listed for each panel. Since the function for the first panel was based on a graphical extrapolation rather than experimental data, no RMS deviation is given.

MM00A: Table IV-1

MM30A: Table IV-2

MM50B: Table IV-3

MG00A: Table IV-4

MG30A: Table IV-5

MG50A: Table IV-6

GM00A: Table IV-7

GM30A: Table IV-8

GM50A: Table IV-9

Table IV-1

Series: MM00A
Fit of i(S) by $C_0 + C_1(S_1 - S) + C_2(S_1 - S)^2 + C_3(S_1 - S)^3$

Panel Limits $S_1 - S_2$	Polynomial Coefficients C_0	C_1	C_2	C_3	RMS Dev.
0.00-1.50	-1.000	0.125	0.000	0.024	---
1.50-1.95	-0.73150	1.5507	-8.2014	13.723	0.026
1.95-2.15	-0.44398	1.8872	6.4117	8.4306	0.045
2.15-2.35	0.25737	6.1714	1.9379	-62.967	0.043
2.35-2.50	1.0654	-0.030429	-17.165	46.788	0.033
2.50-2.70	0.83258	-1.9663	8.0726	-23.724	0.036
2.70-2.95	0.57244	-1.7433	-2.0374	7.3906	0.016
2.95-3.20	0.12476	-1.2906	2.5112	-3.0047	0.010
3.20-3.50	-0.087901	-0.72145	1.1851	-0.50717	0.015
3.50-3.95	-0.21137	-0.10715	0.31425	0.81297	0.013
3.95-4.40	-0.12187	0.63315	1.1413	-1.7171	0.013
4.40-4.80	0.23769	0.51347	-1.6898	0.79181	0.010
4.80-5.20	0.22338	-0.38634	-0.39911	0.59305	0.013
5.20-5.75	0.042941	-0.46828	0.62347	-0.17856	0.012
5.75-6.30	-0.055721	0.076470	0.72951	-0.71991	0.013
6.30-7.00	0.087237	0.19271	-0.18337	-0.073224	0.016
7.00-7.80	0.10717	-0.16546	-0.075516	0.13590	0.016
7.80-8.60	-0.0039481	-0.0072709	0.23514	-0.15499	0.008
8.60-9.50	0.061372	0.031956	-0.13364	0.054801	0.010
9.50-11.00	0.021830	-0.095400	0.096613	-0.026071	0.008
11.00-12.50	0.0081187	0.016647	-0.027169	0.0088373	0.008
12.50-15.00	0.0017855	0.0072000	-0.0048712	0.0017301	0.006
15.00-17.50	0.016373	0.018879	-0.0044177	-0.0023014	0.005

Table IV-2

Series: MM30A
Fit of $i(S)$ by $C_0+C_1(S_1-S)+C_2(S_1-S)^2+C_3(S_1-S)^3$

Panel Limits S_1—S_2	Polynomial Coefficients C_0	C_1	C_2	C_3	RMS Dev.
0.00-1.50	-1.000	0.211	0.000	0.011	---
1.50-1.95	-0.64637	0.78112	-3.7306	7.4566	0.015
1.95-2.15	-0.37084	2.2793	7.4506	0.95943	0.022
2.15-2.35	0.39072	5.8161	3.4379	-59.125	0.026
2.35-2.50	1.2185	0.38598	-26.486	75.294	0.027
2.50-2.70	0.93453	-1.7296	4.7043	-17.571	0.018
2.70-2.95	0.63621	-2.1166	0.55586	2.9810	0.018
2.95-3.20	0.18839	-1.2634	2.0997	-3.2584	0.018
3.20-3.50	-0.047138	-0.76356	0.48670	0.91637	0.021
3.50-3.95	-0.20766	-0.24265	1.4725	-0.83940	0.012
3.95-4.40	-0.095161	0.67163	0.43180	-0.89923	0.013
4.40-4.80	0.21257	0.51403	-0.50121	-1.1485	0.018
4.80-5.20	0.26448	-0.42793	-0.51373	0.66409	0.026
5.20-5.75	0.053617	-0.42876	0.58299	-0.22136	0.020
5.75-6.30	-0.042675	0.045527	0.54301	-0.43072	0.018
6.30-7.00	0.074965	0.23284	-0.32600	0.056037	0.012
7.00-7.80	0.097437	-0.19563	-0.12460	0.21216	0.010
7.80-8.60	-0.030182	0.034759	0.19498	-0.13808	0.008
8.60-9.50	0.051718	0.048897	-0.20585	0.092079	0.008
9.50-11.00	-0.0038877	-0.069927	0.10434	-0.037595	0.010
11.00-12.50	-0.0008877	-0.028323	0.015531	-0.0035691	0.014
12.50-15.00	-0.020473	-0.0045730	-0.0024675	0.0010753	0.013
15.00-17.50	-0.030526	0.011306	-0.0021846	0.0010185	0.012

Table IV-3

Series: MM50B

Fit of $i(S)$ by $C_0+C_1(S_1-S)+C_2(S_1-S)^2+C_3(S_1-S)^3$

Panel Limits S_1-S_2	Polynomial Coefficients C_0	C_1	C_2	C_3	RMS Dev.
0.00-1.00	-1.000	0.000	0.000	0.000	---
1.00-1.95	-1.0000	2.3016	-4.4599	2.8315	0.031
1.95-2.15	-0.41085	1.8074	6.4145	8.3419	0.029
2.15-2.35	0.27395	5.5441	4.3218	-63.453	0.053
2.35-2.50	1.0480	-0.062490	-21.324	64.004	0.028
2.50-2.70	0.77486	-1.6277	6.4965	-20.747	0.043
2.70-2.95	0.54320	-1.9447	0.21450	3.2327	0.042
2.95-3.20	0.12094	-1.0967	0.63796	-0.20397	0.020
3.20-3.50	-0.11656	-0.77521	1.4730	-0.83864	0.018
3.50-3.95	-0.23919	-0.12365	0.57781	0.30841	0.015
3.95-4.40	-0.14973	0.66061	1.0326	-1.6321	0.007
4.40-4.80	0.20791	0.45980	-1.2592	0.57248	0.021
4.80-5.20	0.22700	-0.16462	-1.0159	1.2182	0.023
5.20-5.75	0.076569	-0.31564	0.22709	0.065558	0.020
5.75-6.30	-0.017430	0.088035	0.25073	-0.14417	0.015
6.30-7.00	0.082849	0.20574	-0.042887	-0.15862	0.011
7.00-7.80	0.15144	-0.10951	-0.26642	0.25906	0.014
7.80-8.60	0.025970	-0.032873	0.25774	-0.14767	0.010
8.60-9.50	0.089014	0.053331	-0.15262	0.060552	0.011
9.50-11.00	0.057528	-0.057617	0.061256	-0.018919	0.010
11.00-12.50	0.045076	-0.015482	-0.018069	0.0089074	0.008
12.50-15.00	0.011260	-0.012435	0.011105	-0.0030617	0.014
15.00-17.50	0.0017387	-0.012552	-0.0074349	0.0048709	0.008

Table IV-4

Series: MG00A
Fit of i(S) by $C_0+C_1(S_1-S)+C_2(S_1-S)^2+C_3(S_1-S)^3$

Panel Limits S_1-S_2	Polynomial Coefficients C_0	C_1	C_2	C_3	RMS Dev.
0.00-1.50	-1.000	0.125	0.000	0.024	---
1.50-1.95	-0.75662	0.91448	-3.6936	5.8141	0.008
1.95-2.15	-0.56325	1.7643	7.2569	0.63435	0.033
2.15-2.35	0.084955	5.0594	4.4305	-55.956	0.035
2.35-2.50	0.82641	0.73305	-9.2763	11.302	0.026
2.50-2.70	0.76579	-1.4375	0.22657	0.33799	0.013
2.70-2.95	0.49006	-1.2457	-2.9665	8.7567	0.029
2.95-3.20	0.13004	-0.93284	2.2258	-4.6281	0.030
3.20-3.50	-0.036369	-0.77982	0.55636	0.61806	0.017
3.50-3.95	-0.20355	-0.20007	0.91748	-0.047250	0.015
3.95-4.40	-0.11210	0.55609	0.85296	-1.1503	0.014
4.40-4.80	0.20605	0.53201	-1.0682	0.0021708	0.016
4.80-5.20	0.24807	-0.25392	-0.89751	1.1679	0.019
5.20-5.75	0.077640	-0.37043	0.22043	0.095151	0.022
5.75-6.30	-0.043584	0.0053978	0.48948	-0.37054	0.016
6.30-7.00	0.045804	0.15961	-0.14265	-0.019588	0.010
7.00-7.80	0.080915	-0.10912	-0.21451	0.23831	0.012
7.80-8.60	-0.021655	0.030840	0.16228	-0.097594	0.010
8.60-9.50	0.056906	0.066704	-0.21418	0.090748	0.011
9.50-11.00	0.0096118	-0.085617	0.10035	-0.025998	0.009
11.00-12.50	0.019228	0.046961	-0.048056	0.012846	0.008
12.50-15.00	0.024898	-0.016528	0.010109	-0.0011776	0.010
15.00-17.50	0.028357	0.0006120	-0.020293	0.0062046	0.012

Table IV-5

Series: MG30A
Fit of i(S) by $C_0+C_1 (S_1 -S)+C_2 (S_1 -S)^2+C_3 (S_1 -S)^3$

Panel Limits S_1-S_2	C_0	Polynomial Coefficients C_1	C_2	C_3	RMS Dev.
0.00-1.25	-1.000	0.000	0.000	0.000	---
1.25-1.95	-1.0000	2.6457	-6.9327	6.3373	0.031
1.95-2.15	-0.37135	2.5156	6.1746	2.2527	0.051
2.15-2.35	0.39678	5.0971	-1.3476	-48.566	0.057
2.35-2.50	0.97378	-0.64465	-16.769	56.143	0.024
2.50-2.70	0.68925	-1.5182	-0.45496	4.2188	0.036
2.70-2.95	0.40116	-1.5099	-0.025972	1.9681	0.032
2.95-3.20	0.052817	-1.0627	0.60423	1.1434	0.013
3.20-3.50	-0.15722	-0.52766	0.81083	-0.054510	0.014
3.50-3.95	-0.24402	-0.058400	0.70369	0.055941	0.016
3.95-4.40	-0.12270	0.65678	0.53553	-1.0105	0.009
4.40-4.80	0.18922	0.48772	-1.0729	-0.12041	0.006
4.80-5.20	0.20493	-0.39740	-0.62247	1.0648	0.014
5.20-5.75	0.014519	-0.35289	0.78013	-0.59898	0.009
5.75-6.30	-0.043233	-0.035123	0.22188	0.10807	0.021
6.30-7.00	0.022546	0.44523	-0.73627	0.29057	0.019
7.00-7.80	0.073100	-0.12861	-0.12029	0.15441	0.009
7.80-8.60	-0.027719	-0.0029885	0.17327	-0.099691	0.012
8.60-9.50	0.029744	0.032035	-0.099208	0.037162	0.016
9.50-11.00	0.0053076	-0.077326	0.11152	-0.035629	0.010
11.00-12.50	0.019991	-0.0034878	-0.026526	0.011774	0.009
12.50-15.00	-0.0051881	0.017710	-0.0063480	0.0001769	0.009
15.00-17.50	0.0021765	0.0008464	0.0048556	-0.0022170	0.006

Table IV-6

Series: MG50A
Fit of i(S) by $C_0+C_1 (S_1 -S)+C_2 (S_1 -S)^2+C_3 (S_1 -S)^3$

Panel Limits S_1-S_2	Polynomial Coefficients C_0	C_1	C_2	C_3	RMS Dev.
0.00-1.00	-1.000	0.000	0.000	0.000	---
1.00-1.95	-1.0000	1.4712	-2.7017	1.7320	0.017
1.95-2.15	-0.55561	1.5128	5.6147	7.3358	0.025
2.15-2.35	0.030225	4.7829	7.6988	-61.439	0.031
2.35-2.50	0.80325	0.68390	-17.801	45.336	0.018
2.50-2.70	0.65832	-1.2746	0.77619	-2.4428	0.018
2.70-2.95	0.41490	-1.3621	-0.48898	1.5105	0.016
2.95-3.20	0.067402	-1.1499	0.81894	1.1981	0.017
3.20-3.50	-0.15016	-0.59006	1.0041	-0.50400	0.018
3.50-3.95	-0.25042	-0.16397	0.59241	0.26894	0.016
3.95-4.40	-0.17974	0.51098	1.0544	-1.5926	0.016
4.40-4.80	0.11860	0.50891	-1.0128	-0.29624	0.019
4.80-5.20	0.14116	-0.41390	0.26817	-0.16855	0.016
5.20-5.75	0.0077206	-0.33989	0.27848	0.043903	0.010
5.75-6.30	-0.087672	0.013930	0.42276	-0.28089	0.011
6.30-7.00	0.0011423	0.29097	-0.42786	0.16155	0.018
7.00-7.80	0.050581	-0.14934	-0.052724	0.10390	0.017
7.80-8.60	-0.049435	0.028889	0.14825	-0.10444	0.008
8.60-9.50	0.015087	0.024359	-0.12981	0.059261	0.008
9.50-11.00	-0.024934	-0.055307	0.081105	-0.027288	0.009
11.00-12.50	-0.017504	0.0039850	-0.043212	0.016391	0.009
12.50-15.00	-0.053433	0.0003533	0.0066091	-0.0010903	0.010
15.00-17.50	-0.028278	0.0093100	-0.013611	0.0057648	0.005

Table IV-7

Series: GM00A
Fit of i(S) by $C_0+C_1 (S_1 -S)+C_2 (S_1 -S)^2+C_3 (S_1 -S)^3$

Panel Limits S_1—S_2	Polynomial Coefficients C_0	C_1	C_2	C_3	RMS Dev.
0.00-1.50	-1.000	0.000	0.000	0.027	----
1.50-1.95	-0.90887	0.14408	0.47749	-0.51397	0.017
1.95-2.15	-0.79418	0.40448	1.7815	5.0631	0.016
2.15-2.35	-0.60152	1.7806	5.8461	-12.643	0.011
2.35-2.50	-0.11269	2.7873	0.046444	-20.829	0.015
2.50-2.70	0.23616	0.90800	-8.3681	12.758	0.014
2.70-2.95	0.18509	-0.74188	-0.24794	2.5303	0.013
2.95-3.20	0.023664	-0.31306	0.33566	-3.4500	0.011
3.20-3.50	-0.087528	-0.86209	-0.47324	1.8507	0.014
3.50-3.95	-0.33878	-0.51951	1.0164	-0.37922	0.008
3.95-4.40	-0.40129	0.18736	0.81192	-0.63487	0.007
4.40-4.80	-0.21042	0.50406	-0.12571	-0.22928	0.008
4.80-5.20	-0.043581	0.27103	-0.94496	0.61235	0.015
5.20-5.75	-0.047172	-0.10205	-0.44809	0.52913	0.014
5.75-6.30	-0.15081	-0.097432	0.19173	0.10200	0.012
6.30-7.00	-0.12943	0.20667	0.091681	-0.15176	0.014
7.00-7.80	0.0081050	0.12148	-0.38676	0.24055	0.010
7.80-8.60	-0.019076	-0.022608	0.16019	-0.087145	0.012
8.60-9.50	0.020739	0.065213	0.011593	-0.027626	0.012
9.50-11.00	0.068681	-0.017615	-0.010278	0.0099428	0.008
11.00-12.50	0.052690	0.014694	-0.020170	0.0052930	0.012
12.50-15.00	0.047212	0.0048362	-0.0096479	0.0012124	0.010
15.00-17.50	0.017947	-0.033516	-0.0014723	0.0048029	0.007

Table IV-8

Series: GM30A
Fit of $i(S)$ by $C_0+C_1(S_1-S)+C_2(S_1-S)^2+C_3(S_1-S)^3$

Panel Limits S_1-S_2	C_0	Polynomial Coefficients C_1	C_2	C_3	RMS Dev.
0.00-1.25	-1.000	0.000	0.000	0.000	----
1.25-1.95	-1.0000	0.44913	0.11888	-0.10047	0.014
1.95-2.15	-0.66182	0.41775	1.1512	4.5306	0.021
2.15-2.35	-0.49598	1.6660	4.5292	8.7062	0.016
2.35-2.50	0.088040	4.5215	4.0625	-51.161	0.010
2.50-2.70	0.68500	1.6339	-18.517	38.577	0.027
2.70-2.95	0.57972	-0.75975	-0.28656	3.4156	0.025
2.95-3.20	0.42524	-0.13142	0.89788	-8.4708	0.017
3.20-3.50	0.31614	-1.5353	-1.0525	4.1440	0.029
3.50-3.95	-0.12728	-0.79996	1.6796	-1.0157	0.016
3.95-4.40	-0.23971	0.097792	0.57617	0.092962	0.010
4.40-4.80	-0.070555	0.71073	0.36862	-1.1969	0.010
4.80-5.20	0.19611	0.27498	-1.3127	1.1858	0.025
5.20-5.75	0.17197	-0.082949	-0.49155	0.34864	0.018
5.75-6.30	0.035659	-0.27613	0.14621	0.22951	0.009
6.30-7.00	-0.033796	0.13756	0.14195	-0.14350	0.011
7.00-7.80	0.082832	0.11944	-0.23154	0.094587	0.008
7.80-8.60	0.078624	-0.073962	-0.036282	0.073383	0.007
8.60-9.50	0.033806	0.017414	0.11114	-0.073893	0.008
9.50-11.00	0.085633	-0.0034633	-0.086533	0.039456	0.004
11.00-12.50	0.018902	0.0093680	0.025756	-0.013010	0.019
12.50-15.00	0.046997	-0.033319	0.0057098	-0.0006059	0.015
15.00-17.50	-0.010082	-0.0055249	0.0060164	-0.0008774	0.015

Table IV-9

Series: GM50A
Fit of i(S) by $C_0+C_1(S_1-S)+C_2(S_1-S)^2+C_3(S_1-S)^3$

Panel Limits S_1—S_2	Polynomial Coefficients C_0	C_1	C_2	C_3	RMS Dev.
0.00-1.25	-1.000	0.000	0.000	0.000	----
1.25-1.95	-1.0000	0.44053	-0.094417	0.071489	0.018
1.95-2.15	-0.71337	0.50645	1.2801	2.6910	0.016
2.15-2.35	-0.53935	1.4729	3.8484	11.809	0.015
2.35-2.50	0.0036270	3.9137	4.4627	-47.271	0.016
2.50-2.70	0.53155	1.6389	-18.258	37.255	0.016
2.70-2.95	0.42706	-0.87001	3.3856	-5.6755	0.016
2.95-3.20	0.33248	-0.14350	-1.1265	-1.6116	0.018
3.20-3.50	0.20101	-1.0740	-1.0804	2.9068	0.019
3.50-3.95	-0.13993	-0.80264	1.5647	-0.92638	0.008
3.95-4.40	-0.26869	0.072842	0.84263	-0.47614	0.014
4.40-4.80	-0.10867	0.66662	0.35324	-1.3333	0.021
4.80-5.20	0.12916	0.21003	-0.18123	-0.36176	0.026
5.20-5.75	0.16103	-0.26377	-0.077427	0.13009	0.022
5.75-6.30	0.014179	-0.20315	0.0002951	0.30449	0.013
6.30-7.00	-0.046806	0.20257	0.021712	-0.092946	0.012
7.00-7.80	0.073755	0.076360	-0.24327	0.14038	0.012
7.80-8.60	0.051030	-0.053708	0.011907	0.017891	0.011
8.60-9.50	0.024844	0.032242	0.086169	-0.060066	0.010
9.50-11.00	0.079870	0.015434	-0.083212	0.034532	0.009
11.00-12.50	0.032339	0.013513	0.0019109	0.0021865	0.014
12.50-15.00	0.049530	-0.0056804	-0.011762	0.0043380	0.011
15.00-17.50	0.029600	0.019123	0.0018377	-0.0056892	0.008

Appendix V

Radial Distribution Data

The following nine tables cover all nine experimental series. The initial radial distribution values begin at r=0.25 Å. All subsequent values are given for 0.05 Å increments in r up to a final value of 15.00 Å. The values of $4\pi r^2 \Sigma \overline{\rho}_i(r)$ are given in units of atom/Å. The function g (r) is dimensionless by definition.

MM00A: Table V-1

MM30A: Table V-2

MM50B: Table V-3

MG00A: Table V-4

MG30A: Table V-5

MG50A: Table V-6

GM00A: Table V-7

GM30A: Table V-8

GM50A: Table V-9

Table V-1 Series: MM00A

r(Å)	$4\pi r^2\Sigma\overline{\rho_2}(r)$	g(r)	r(Å)	$4\pi r^2\Sigma\overline{\rho_2}(r)$	g(r)
0.250	-91.1151	-2851.8043	2.750	5.6750	1.4679
0.300	-43.3502	-242.2326	2.800	7.1690	1.7888
0.350	-22.9830	-367.0119	2.850	8.4894	2.0445
0.400	-13.0850	-159.9788	2.900	9.5935	2.2315
0.450	-7.8132	-75.4770	2.950	10.4718	2.3539
0.500	-4.8907	-38.2686	3.000	11.0959	2.4117
0.550	-3.3188	-21.4615	3.050	11.4043	2.3982
0.600	-2.5312	-13.7544	3.100	11.3376	2.3078
0.650	-2.1093	-9.7659	3.150	10.8948	2.1479
0.700	-1.7338	-6.9217	3.200	10.1656	1.9420
0.750	-1.2405	-4.3139	3.250	9.3090	1.7240
0.800	-0.6499	-1.9864	3.300	8.4891	1.5249
0.850	-0.1207	-0.3268	3.350	7.8065	1.3607
0.900	0.1718	0.4149	3.400	7.2706	1.2303
0.950	0.1623	0.3519	3.450	6.8277	1.1221
1.000	-0.0523	-0.1024	3.500	6.4234	1.0257
1.050	-0.2687	-0.4767	3.550	6.0527	0.9395
1.100	-0.3054	-0.4938	3.600	5.7660	0.8703
1.150	-0.1192	-0.1762	3.650	5.6278	0.8263
1.200	0.1692	0.2298	3.700	5.6613	0.8089
1.250	0.3576	0.4477	3.750	5.8201	0.8096
1.300	0.3014	0.3489	3.800	6.0094	0.8141
1.350	0.0155	0.0167	3.850	6.1417	0.8105
1.400	-0.3290	-0.3284	3.900	6.1893	0.7960
1.450	-0.5127	-0.4770	3.950	6.1965	0.7769
1.500	-0.4099	-0.3564	4.000	6.2443	0.7634
1.550	-0.0731	-0.0595	4.050	6.3923	0.7624
1.600	0.2975	0.2273	4.100	6.6389	0.7726
1.650	0.4785	0.3438	4.150	6.9257	0.7866
1.700	0.3623	0.2452	4.200	7.1817	0.7964
1.750	0.0203	0.0130	4.250	7.3742	0.7986
1.800	-0.3460	-0.2089	4.300	7.5300	0.7966
1.850	-0.5329	-0.3046	4.350	7.7121	0.7973
1.900	-0.4558	-0.2470	4.400	7.9701	0.8053
1.950	-0.1878	-0.0966	4.450	8.3005	0.8200
2.000	0.1043	0.0510	4.500	8.6451	0.8351
2.050	0.2768	0.1289	4.550	8.9308	0.8439
2.100	0.2996	0.1329	4.600	9.1212	0.8432
2.150	0.2602	0.1101	4.650	9.2446	0.8364
2.200	0.2863	0.1157	4.700	9.3782	0.8305
2.250	0.4443	0.1717	4.750	9.6001	0.8323
2.300	0.6882	0.2545	4.800	9.9405	0.8440
2.350	0.8951	0.3171	4.850	10.3676	0.8622
2.400	0.9628	0.3270	4.900	10.8143	0.8811
2.450	0.9025	0.2941	4.950	11.2283	0.8964
2.500	0.8612	0.2695	5.000	11.6088	0.9084
2.550	1.0568	0.3179	5.050	12.0054	0.9209
2.600	1.6645	0.4817	5.100	12.4807	0.9387
2.650	2.7253	0.7592	5.150	13.0642	0.9636
2.700	4.1289	1.1079	5.200	13.7289	0.9932

Table V-1 (Continued) Series: MM00A

r(Å)	$4\pi r^2\Sigma\overline{\rho}(r)$	g(r)	r(Å)	$4\pi r^2\Sigma\overline{\rho}(r)$	g(r)
5.250	14.4068	1.0225	7.750	29.9022	0.9739
5.300	15.0316	1.0468	7.800	30.4345	0.9786
5.350	15.5779	1.0647	7.850	30.9448	0.9823
5.400	16.0711	1.0781	7.900	31.4461	0.9856
5.450	16.5619	1.0908	7.950	31.9721	0.9896
5.500	17.0864	1.1049	8.000	32.5512	0.9949
5.550	17.6388	1.1202	8.050	33.1836	1.0017
5.600	18.1775	1.1339	8.100	33.8389	1.0089
5.650	18.6564	1.1432	8.150	34.4746	1.0153
5.700	19.0589	1.1475	8.200	35.0637	1.0201
5.750	19.4089	1.1484	8.250	35.6102	1.0235
5.800	19.7509	1.1485	8.300	36.1424	1.0263
5.850	20.1145	1.1498	8.350	36.6900	1.0294
5.900	20.4893	1.1514	8.400	37.2607	1.0330
5.950	20.8286	1.1509	8.450	37.8335	1.0365
6.000	21.0805	1.1455	8.500	38.3748	1.0390
6.050	21.2229	1.1342	8.550	38.8624	1.0399
6.100	21.2791	1.1187	8.600	39.3030	1.0395
6.150	21.3016	1.1017	8.650	39.7277	1.0387
6.200	21.3376	1.0859	8.700	40.1699	1.0382
6.250	21.3986	1.0716	8.750	40.6419	1.0384
6.300	21.4580	1.0576	8.800	41.1249	1.0388
6.350	21.4761	1.0419	8.850	41.5822	1.0386
6.400	21.4347	1.0237	8.900	41.9847	1.0369
6.450	21.3570	1.0042	8.950	42.3310	1.0338
6.500	21.2973	0.9861	9.000	42.6487	1.0300
6.550	21.3092	0.9716	9.050	42.9751	1.0264
6.600	21.4127	0.9616	9.100	43.3325	1.0236
6.650	21.5854	0.9548	9.150	43.7142	1.0214
6.700	21.7817	0.9492	9.200	44.0917	1.0190
6.750	21.9667	0.9431	9.250	44.4371	1.0159
6.800	22.1404	0.9366	9.300	44.7440	1.0120
6.850	22.3350	0.9311	9.350	45.0324	1.0077
6.900	22.5895	0.9281	9.400	45.3340	1.0036
6.950	22.9186	0.9282	9.450	45.6691	1.0004
7.000	23.3008	0.9302	9.500	46.0316	0.9977
7.050	23.6926	0.9325	9.550	46.3946	0.9951
7.100	24.0596	0.9336	9.600	46.7308	0.9919
7.150	24.4018	0.9337	9.650	47.0345	0.9880
7.200	24.7536	0.9341	9.700	47.3294	0.9840
7.250	25.1589	0.9363	9.750	47.6548	0.9806
7.300	25.6384	0.9411	9.800	48.0413	0.9785
7.350	26.1722	0.9477	9.850	48.4918	0.9777
7.400	26.7097	0.9541	9.900	48.9813	0.9776
7.450	27.2012	0.9587	9.950	49.4754	0.9776
7.500	27.6292	0.9608	10.000	49.9543	0.9772
7.550	28.0177	0.9615	10.050	50.4253	0.9766
7.600	28.4152	0.9624	10.100	50.9159	0.9764
7.650	28.8621	0.9648	10.150	51.4517	0.9770
7.700	29.3662	0.9689	10.200	52.0361	0.9784

Table V-1 (Continued)

Series: MM00A

r(Å)	$4\pi r^2 \sum \bar{\rho}_i(r)$	g(r)
10.250	52.6454	0.9802
10.300	53.2436	0.9818
10.350	53.8051	0.9825
10.400	54.3315	0.9826
10.450	54.8434	0.9825
10.500	55.3882	0.9828
10.550	55.9681	0.9837
10.600	56.5019	0.9851
10.650	57.2078	0.9867
10.700	57.8276	0.9880
10.750	58.4421	0.9893
10.800	59.0712	0.9907
10.850	59.7386	0.9927
10.900	60.4532	0.9953
10.950	61.1997	0.9985
11.000	61.9474	1.0015
11.050	62.6686	1.0040
11.100	63.3565	1.0059
11.150	64.0272	1.0075
11.200	64.7061	1.0091
11.250	65.4082	1.0110
11.300	66.1254	1.0130
11.350	66.8314	1.0148
11.400	67.4994	1.0160
11.450	68.1201	1.0164
11.500	68.7082	1.0163
11.550	69.2916	1.0161
11.600	69.8918	1.0161
11.650	70.5094	1.0163
11.700	71.1249	1.0164
11.750	71.7135	1.0161
11.800	72.2636	1.0152
11.850	72.7851	1.0139
11.900	73.3019	1.0126
11.950	73.8345	1.0114
12.000	74.3850	1.0105
12.050	74.9357	1.0095
12.100	75.4628	1.0083
12.150	75.9551	1.0065
12.200	76.4236	1.0044
12.250	76.8964	1.0024
12.300	77.4000	1.0008
12.350	77.9425	0.9997
12.400	78.5083	0.9988
12.450	79.0696	0.9979
12.500	79.6059	0.9966
12.550	80.1185	0.9951
12.600	80.6286	0.9935
12.650	81.1631	0.9922
12.700	81.7356	0.9913
12.750	82.3384	0.9908
12.800	82.9487	0.9904
12.850	83.5468	0.9898
12.900	84.1305	0.9890
12.950	84.7182	0.9882
13.000	85.3361	0.9878
13.050	86.0013	0.9879
13.100	86.7103	0.9884
13.150	87.4431	0.9892
13.200	88.1775	0.9900
13.250	88.9047	0.9906
13.300	89.6337	0.9912
13.350	90.3833	0.9921
13.400	91.1655	0.9932
13.450	91.9756	0.9946
13.500	92.7938	0.9960
13.550	93.5988	0.9972
13.600	94.3832	0.9982
13.650	95.1585	0.9991
13.700	95.9476	1.0000
13.750	96.7675	1.0012
13.800	97.6173	1.0027
13.850	98.4767	1.0043
13.900	99.3192	1.0056
13.950	100.1285	1.0065
14.000	100.9074	1.0071
14.050	101.6736	1.0075
14.100	102.4449	1.0080
14.150	103.2255	1.0085
14.200	104.0028	1.0090
14.250	104.7566	1.0092
14.300	105.4744	1.0090
14.350	106.1615	1.0085
14.400	106.8380	1.0079
14.450	107.5249	1.0074
14.500	108.2301	1.0070
14.550	108.9429	1.0067
14.600	109.6423	1.0062
14.650	110.3124	1.0054
14.700	110.9542	1.0044
14.750	111.5851	1.0033
14.800	112.2270	1.0023
14.850	112.8909	1.0014
14.900	113.5694	1.0007
14.950	114.2431	0.9999
15.000	114.8954	0.9989

Table V-2 Series: MM30A

r(Å)	$4\pi r^2 \sum \bar{a}_2(r)$	g(r)	r(Å)	$4\pi r^2 \sum \bar{a}_2(r)$	g(r)
0.250	-38.2955	-1198.6063	2.750	5.3091	1.3733
0.300	-17.0786	-371.2091	2.800	6.8177	1.7011
0.350	-8.2385	-131.5591	2.850	8.3732	2.0165
0.400	-4.2539	-52.0084	2.900	9.7891	2.2770
0.450	-2.4548	-23.7140	2.950	10.8919	2.4483
0.500	-1.6360	-12.8016	3.000	11.5706	2.5149
0.550	-1.1671	-7.5472	3.050	11.7989	2.4811
0.600	-0.7353	-3.9953	3.100	11.6226	2.3659
0.650	-0.2707	-1.2534	3.150	11.1252	2.1933
0.700	0.1425	0.5689	3.200	10.3964	1.9861
0.750	0.3795	1.3199	3.250	9.5190	1.7629
0.800	0.3856	1.1787	3.300	8.5755	1.5404
0.850	0.2223	0.6019	3.350	7.6592	1.3351
0.900	0.0346	0.0837	3.400	6.8713	1.1628
0.950	-0.0357	-0.0775	3.450	6.2997	1.0354
1.000	0.0654	0.1279	3.500	5.9868	0.9560
1.050	0.2787	0.4945	3.550	5.9103	0.9174
1.100	0.4747	0.7674	3.600	5.9903	0.9042
1.150	0.5384	0.7964	3.650	6.1234	0.8991
1.200	0.4392	0.5967	3.700	6.2265	0.8897
1.250	0.2434	0.3047	3.750	6.2658	0.8716
1.300	0.0666	0.0771	3.800	6.2582	0.8478
1.350	-0.0003	-0.0003	3.850	6.2459	0.8243
1.400	0.0558	0.0557	3.900	6.2636	0.8056
1.450	0.1713	0.1594	3.950	6.3195	0.7923
1.500	0.2533	0.2202	4.000	6.3987	0.7823
1.550	0.2394	0.1949	4.050	6.4832	0.7732
1.600	0.1317	0.1006	4.100	6.5714	0.7647
1.650	-0.0158	-0.0113	4.150	6.6826	0.7590
1.700	-0.1402	-0.0949	4.200	6.8436	0.7589
1.750	-0.2117	-0.1352	4.250	7.0672	0.7654
1.800	-0.2462	-0.1486	4.300	7.3406	0.7766
1.850	-0.2818	-0.1610	4.350	7.6306	0.7888
1.900	-0.3414	-0.1850	4.400	7.9022	0.7985
1.950	-0.4083	-0.2101	4.450	8.1394	0.8040
2.000	-0.4340	-0.2123	4.500	8.3513	0.8068
2.050	-0.3706	-0.1725	4.550	8.5631	0.8091
2.100	-0.2053	-0.0911	4.600	8.7966	0.8132
2.150	0.0275	0.0116	4.650	9.0569	0.8194
2.200	0.2656	0.1073	4.700	9.3327	0.8265
2.250	0.4547	0.1757	4.750	9.6096	0.8332
2.300	0.5779	0.2137	4.800	9.8864	0.8394
2.350	0.6616	0.2343	4.850	10.1809	0.8467
2.400	0.7572	0.2571	4.900	10.5219	0.8573
2.450	0.9166	0.2987	4.950	10.9323	0.8728
2.500	1.1789	0.3690	5.000	11.4158	0.8933
2.550	1.5759	0.4741	5.050	11.9561	0.9171
2.600	2.1460	0.6210	5.100	12.5283	0.9422
2.650	2.9376	0.8183	5.150	13.1148	0.9673
2.700	3.9920	1.0712	5.200	13.7125	0.9920

Table V-2 (Continued)

Series: MM30A

r(Å)	$4\pi r^2 \sum \rho_i(r)$	g(r)	r(Å)	$4\pi r^2 \sum \rho_i(r)$	g(r)
5.250	14.3278	1.0169	7.750	29.5728	0.9632
5.300	14.9630	1.0420	7.800	30.1888	0.9707
5.350	15.6060	1.0666	7.850	30.8434	0.9791
5.400	16.2311	1.0889	7.900	31.5254	0.9881
5.450	16.8119	1.1072	7.950	32.2150	0.9971
5.500	17.3369	1.1211	8.000	32.8936	1.0054
5.550	17.8160	1.1314	8.050	33.5535	1.0129
5.600	18.2730	1.1398	8.100	34.1976	1.0196
5.650	18.7279	1.1476	8.150	34.8318	1.0258
5.700	19.1803	1.1548	8.200	35.4549	1.0315
5.750	19.6072	1.1601	8.250	36.0546	1.0362
5.800	19.9755	1.1616	8.300	36.6124	1.0396
5.850	20.2622	1.1582	8.350	37.1163	1.0414
5.900	20.4686	1.1503	8.400	37.5697	1.0416
5.950	20.6197	1.1394	8.450	37.9926	1.0409
6.000	20.7488	1.1275	8.500	38.4117	1.0400
6.050	20.8791	1.1159	8.550	38.8456	1.0395
6.100	21.0127	1.1047	8.600	39.2959	1.0393
6.150	21.1359	1.0932	8.650	39.7484	1.0392
6.200	21.2338	1.0806	8.700	40.1840	1.0385
6.250	21.3053	1.0669	8.750	40.5923	1.0371
6.300	21.3659	1.0530	8.800	40.9776	1.0351
6.350	21.4379	1.0400	8.850	41.3551	1.0329
6.400	21.5351	1.0285	8.900	41.7396	1.0308
6.450	21.6529	1.0181	8.950	42.1346	1.0290
6.500	21.7722	1.0081	9.000	42.5306	1.0271
6.550	21.8733	0.9973	9.050	42.9124	1.0249
6.600	21.9524	0.9858	9.100	43.2703	1.0222
6.650	22.0264	0.9743	9.150	43.6073	1.0189
6.700	22.1255	0.9642	9.200	43.9376	1.0155
6.750	22.2760	0.9564	9.250	44.2767	1.0123
6.800	22.4855	0.9513	9.300	44.6312	1.0094
6.850	22.7403	0.9480	9.350	44.9951	1.0068
6.900	23.0149	0.9456	9.400	45.3547	1.0041
6.950	23.2873	0.9431	9.450	45.6986	1.0010
7.000	23.5500	0.9402	9.500	46.0263	0.9976
7.050	23.8097	0.9371	9.550	46.3485	0.9941
7.100	24.0784	0.9344	9.600	46.6798	0.9908
7.150	24.3629	0.9322	9.650	47.0298	0.9879
7.200	24.6608	0.9306	9.700	47.3979	0.9854
7.250	24.9662	0.9291	9.750	47.7760	0.9831
7.300	25.2781	0.9279	9.800	48.1565	0.9809
7.350	25.6067	0.9272	9.850	48.5403	0.9787
7.400	25.9695	0.9277	9.900	48.9374	0.9767
7.450	26.3820	0.9298	9.950	49.3614	0.9753
7.500	26.8477	0.9337	10.000	49.8216	0.9746
7.550	27.3560	0.9388	10.050	50.3175	0.9745
7.600	27.8893	0.9445	10.100	50.8405	0.9749
7.650	28.4348	0.9505	10.150	51.3808	0.9756
7.700	28.9923	0.9566	10.200	51.9339	0.9765

Table V-2 (Continued)

Series: MM30A

r(Å)	$4\pi r^2 \Sigma \bar{A}_2(r)$	g(r)
10.250	52.5017	0.9775
10.300	53.0802	0.9789
10.350	53.6928	0.9805
10.400	54.3069	0.9822
10.450	54.9173	0.9838
10.500	55.5150	0.9850
10.550	56.1023	0.9860
10.600	56.6933	0.9870
10.650	57.3073	0.9884
10.700	57.9579	0.9903
10.750	58.6453	0.9927
10.800	59.3565	0.9955
10.850	60.0736	0.9982
10.900	60.7832	1.0008
10.950	61.4822	1.0031
11.000	62.1749	1.0052
11.050	62.8656	1.0072
11.100	63.5516	1.0090
11.150	64.2228	1.0105
11.200	64.8679	1.0116
11.250	65.4835	1.0121
11.300	66.0786	1.0123
11.350	66.6716	1.0124
11.400	67.2802	1.0127
11.450	67.9116	1.0133
11.500	68.5586	1.0141
11.550	69.2046	1.0148
11.600	69.8333	1.0152
11.650	70.4378	1.0152
11.700	71.0223	1.0149
11.750	71.5970	1.0144
11.800	72.1692	1.0139
11.850	72.7378	1.0133
11.900	73.2948	1.0125
11.950	73.8320	1.0114
12.000	74.3477	1.0100
12.050	74.8489	1.0084
12.100	75.3475	1.0067
12.150	75.8527	1.0051
12.200	76.3662	1.0037
12.250	76.8826	1.0022
12.300	77.3952	1.0007
12.350	77.9023	0.9991
12.400	78.4096	0.9976
12.450	78.9271	0.9961
12.500	79.4623	0.9948
12.550	80.0155	0.9938
12.600	80.5799	0.9929
12.650	81.1473	0.9920
12.700	81.7138	0.9911
12.750	82.2835	0.9902
12.800	82.8651	0.9894
12.850	83.4663	0.9888
12.900	84.0885	0.9885
12.950	84.7268	0.9883
13.000	85.3751	0.9882
13.050	86.0317	0.9882
13.100	86.7027	0.9883
13.150	87.3982	0.9887
13.200	88.1258	0.9894
13.250	88.8845	0.9904
13.300	89.6644	0.9916
13.350	90.4523	0.9928
13.400	91.2393	0.9940
13.450	92.0264	0.9951
13.500	92.8219	0.9963
13.550	93.6346	0.9976
13.600	94.4662	0.9991
13.650	95.3082	1.0006
13.700	96.1458	1.0021
13.750	96.9665	1.0033
13.800	97.7662	1.0042
13.850	98.5509	1.0050
13.900	99.3306	1.0057
13.950	100.1123	1.0063
14.000	100.8946	1.0070
14.050	101.6694	1.0075
14.100	102.4280	1.0078
14.150	103.1678	1.0080
14.200	103.8947	1.0079
14.250	104.6185	1.0078
14.300	105.3465	1.0078
14.350	106.0780	1.0077
14.400	106.8046	1.0076
14.450	107.5161	1.0073
14.500	108.2074	1.0068
14.550	108.8820	1.0061
14.600	109.5501	1.0053
14.650	110.2221	1.0046
14.700	110.9029	1.0040
14.750	111.5898	1.0033
14.800	112.2760	1.0027
14.850	112.9563	1.0020
14.900	113.6307	1.0012
14.950	114.3038	1.0004
15.000	114.9809	0.9997

Table V-3 Series: MM50B

r(Å)	$4\pi r^2 \Sigma \beta_2(r)$	g(r)	r(Å)	$4\pi r^2 \Sigma \beta_2(r)$	g(r)
0.250	0.5709	17.8696	2.750	5.5593	1.4380
0.300	0.4959	10.7777	2.800	7.0076	1.7485
0.350	0.2552	4.0755	2.850	8.4481	2.0346
0.400	-0.0633	-0.7744	2.900	9.6672	2.2486
0.450	-0.3517	-3.3976	2.950	10.4887	2.3577
0.500	-0.4925	-3.8540	3.000	10.8439	2.3570
0.550	-0.4413	-2.8535	3.050	10.7845	2.2678
0.600	-0.2449	-1.3310	3.100	10.4347	2.1241
0.650	-0.0200	-0.0924	3.150	9.9199	1.9557
0.700	0.1192	0.4759	3.200	9.3164	1.7797
0.750	0.1254	0.4362	3.250	8.6512	1.6022
0.800	0.0460	0.1407	3.300	7.9414	1.4265
0.850	-0.0164	-0.0443	3.350	7.2358	1.2613
0.900	0.0224	0.0542	3.400	6.6241	1.1209
0.950	0.1671	0.3622	3.450	6.2020	1.0193
1.000	0.3370	0.6593	3.500	6.0179	0.9610
1.050	0.4229	0.7504	3.550	6.0399	0.9375
1.100	0.3658	0.5914	3.600	6.1677	0.9310
1.150	0.2058	0.3045	3.650	6.2864	0.9230
1.200	0.0610	0.0829	3.700	6.3259	0.9039
1.250	0.0490	0.0614	3.750	6.2893	0.8749
1.300	0.2018	0.2335	3.800	6.2339	0.8445
1.350	0.4330	0.4647	3.850	6.2205	0.8209
1.400	0.5852	0.5841	3.900	6.2677	0.8061
1.450	0.5299	0.4930	3.950	6.3437	0.7954
1.500	0.2558	0.2224	4.000	6.3971	0.7821
1.550	-0.1141	-0.0929	4.050	6.4043	0.7638
1.600	-0.3915	-0.2992	4.100	6.3968	0.7444
1.650	-0.4382	-0.3148	4.150	6.4475	0.7323
1.700	-0.2523	-0.1708	4.200	6.6253	0.7347
1.750	0.0286	0.0183	4.250	6.9492	0.7526
1.800	0.2131	0.1286	4.300	7.3732	0.7801
1.850	0.1749	0.1000	4.350	7.8135	0.8078
1.900	-0.0682	-0.0370	4.400	8.1980	0.8283
1.950	-0.3677	-0.1892	4.450	8.5050	0.8402
2.000	-0.5374	-0.2628	4.500	8.7662	0.8468
2.050	-0.4688	-0.2182	4.550	9.0342	0.8536
2.100	-0.1943	-0.0862	4.600	9.3391	0.8634
2.150	0.1391	0.0589	4.650	9.6663	0.8745
2.200	0.3655	0.1477	4.700	9.9699	0.8829
2.250	0.4022	0.1554	4.750	10.2122	0.8854
2.300	0.2954	0.1092	4.800	10.3986	0.8829
2.350	0.1849	0.0655	4.850	10.5831	0.8801
2.400	0.2187	0.0743	4.900	10.8390	0.8831
2.450	0.4759	0.1551	4.950	11.2155	0.8954
2.500	0.9460	0.2961	5.000	11.7087	0.9162
2.550	1.5719	0.4729	5.050	12.2680	0.9410
2.600	2.3153	0.6700	5.100	12.8312	0.9650
2.650	3.1955	0.8901	5.150	13.3644	0.9857
2.700	4.2677	1.1452	5.200	13.8786	1.0040

Table V-3 (Continued)

Series: MM50B

r(Å)	$4\pi r^2 \sum A_i(r)$	g(r)
5.250	14.4137	1.0230
5.300	15.0015	1.0447
5.350	15.6371	1.0687
5.400	16.2772	1.0919
5.450	16.8676	1.1109
5.500	17.3786	1.1238
5.550	17.8233	1.1319
5.600	18.2458	1.1381
5.650	18.6869	1.1451
5.700	19.1533	1.1532
5.750	19.6107	1.1603
5.800	20.0068	1.1634
5.850	20.3065	1.1607
5.900	20.5158	1.1529
5.950	20.6767	1.1425
6.000	20.8380	1.1323
6.050	21.0229	1.1235
6.100	21.2154	1.1153
6.150	21.3762	1.1056
6.200	21.4736	1.0928
6.250	21.5091	1.0771
6.300	21.5183	1.0606
6.350	21.5468	1.0453
6.400	21.6197	1.0325
6.450	21.7255	1.0216
6.500	21.8271	1.0106
6.550	21.8917	0.9982
6.600	21.9175	0.9843
6.650	21.9396	0.9705
6.700	22.0087	0.9591
6.750	22.1595	0.9514
6.800	22.3894	0.9472
6.850	22.6626	0.9448
6.900	22.9360	0.9424
6.950	23.1886	0.9391
7.000	23.4344	0.9355
7.050	23.7093	0.9331
7.100	24.0437	0.9330
7.150	24.4393	0.9352
7.200	24.8676	0.9384
7.250	25.2901	0.9412
7.300	25.6848	0.9428
7.350	26.0611	0.9437
7.400	26.4508	0.9449
7.450	26.8834	0.9475
7.500	27.3633	0.9516
7.550	27.8652	0.9563
7.600	28.3514	0.9602
7.650	28.7989	0.9626
7.700	29.2169	0.9640
7.750	29.6414	0.9654
7.800	30.1121	0.9682
7.850	30.6465	0.9729
7.900	31.2294	0.9789
7.950	31.8247	0.9850
8.000	32.4007	0.9903
8.050	32.9499	0.9947
8.100	33.4912	0.9986
8.150	34.0517	1.0028
8.200	34.6437	1.0079
8.250	35.2530	1.0132
8.300	35.8471	1.0179
8.350	36.3977	1.0212
8.400	36.9011	1.0230
8.450	37.3808	1.0241
8.500	37.8715	1.0254
8.550	38.3948	1.0274
8.600	38.9438	1.0300
8.650	39.4880	1.0324
8.700	39.9940	1.0336
8.750	40.4486	1.0335
8.800	40.8662	1.0323
8.850	41.2777	1.0310
8.900	41.7069	1.0300
8.950	42.1537	1.0294
9.000	42.5935	1.0286
9.050	42.9953	1.0269
9.100	43.3444	1.0239
9.150	43.6531	1.0200
9.200	43.9534	1.0158
9.250	44.2752	1.0122
9.300	44.6272	1.0094
9.350	44.9929	1.0068
9.400	45.3442	1.0039
9.450	45.6634	1.0003
9.500	45.9570	0.9961
9.550	46.2518	0.9920
9.600	46.5767	0.9886
9.650	46.9431	0.9861
9.700	47.3384	0.9842
9.750	47.7368	0.9823
9.800	48.1200	0.9801
9.850	48.4924	0.9777
9.900	48.8804	0.9756
9.950	49.3159	0.9744
10.000	49.8155	0.9745
10.050	50.3702	0.9756
10.100	50.9523	0.9771
10.150	51.5346	0.9785
10.200	52.1073	0.9797

Table V-3 (Continued)

Series: MM50B

r(Å)	$4\pi r^2 \sum P_n(r)$	g(r)
10.250	52.6814	0.9809
10.300	53.2770	0.9824
10.350	53.9044	0.9844
10.400	54.5537	0.9867
10.450	55.1994	0.9888
10.500	55.8180	0.9904
10.550	56.4047	0.9913
10.600	56.9785	0.9920
10.650	57.5708	0.9929
10.700	58.2045	0.9945
10.750	58.8806	0.9967
10.800	59.5778	0.9992
10.850	60.2681	1.0015
10.900	60.9356	1.0033
10.950	61.5852	1.0047
11.000	62.2361	1.0062
11.050	62.9053	1.0078
11.100	63.5931	1.0097
11.150	64.2817	1.0115
11.200	64.9476	1.0128
11.250	65.5794	1.0136
11.300	66.1873	1.0140
11.350	66.7971	1.0143
11.400	67.4332	1.0150
11.450	68.1016	1.0161
11.500	68.7650	1.0174
11.550	69.4540	1.0185
11.600	70.0856	1.0189
11.650	70.6765	1.0187
11.700	71.2428	1.0181
11.750	71.8062	1.0174
11.800	72.3764	1.0168
11.850	72.9443	1.0162
11.900	73.4885	1.0152
11.950	73.9914	1.0136
12.000	74.4535	1.0114
12.050	74.8945	1.0090
12.100	75.3418	1.0066
12.150	75.8131	1.0046
12.200	76.3073	1.0029
12.250	76.8081	1.0013
12.300	77.2987	0.9995
12.350	77.7768	0.9975
12.400	78.2573	0.9956
12.450	78.7634	0.9940
12.500	79.3103	0.9929
12.550	79.8940	0.9923
12.600	80.4943	0.9918
12.650	81.0876	0.9913
12.700	81.6638	0.9904
12.750	82.2320	0.9895
12.800	82.8137	0.9888
12.850	83.4274	0.9884
12.900	84.0759	0.9883
12.950	84.7445	0.9885
13.000	85.4132	0.9887
13.050	86.0706	0.9887
13.100	86.7230	0.9886
13.150	87.3894	0.9886
13.200	88.0876	0.9890
13.250	88.8215	0.9897
13.300	89.5778	0.9906
13.350	90.3362	0.9915
13.400	91.0837	0.9923
13.450	91.8249	0.9929
13.500	92.5786	0.9937
13.550	93.3642	0.9947
13.600	94.1882	0.9962
13.650	95.0379	0.9978
13.700	95.8898	0.9994
13.750	96.7244	1.0008
13.800	97.5379	1.0019
13.850	98.3431	1.0029
13.900	99.1578	1.0039
13.950	99.9903	1.0051
14.000	100.8320	1.0064
14.050	101.6624	1.0074
14.100	102.4623	1.0082
14.150	103.2270	1.0085
14.200	103.9684	1.0086
14.250	104.7060	1.0087
14.300	105.4527	1.0088
14.350	106.2051	1.0089
14.400	106.9466	1.0089
14.450	107.6592	1.0086
14.500	108.3374	1.0080
14.550	108.9924	1.0071
14.600	109.6451	1.0062
14.650	110.3124	1.0054
14.700	110.9961	1.0048
14.750	111.6829	1.0042
14.800	112.3550	1.0034
14.850	113.0035	1.0024
14.900	113.6352	1.0013
14.950	114.2685	1.0001
15.000	114.9202	0.9991

Table V-4

Series: MG00A

r(Å)	$4\pi r^2 \sum \rho_i(r)$	g(r)
0.250	-79.6020	-2472.0844
0.300	-37.9283	-817.9759
0.350	-20.2286	-320.5160
0.400	-11.6431	-141.2428
0.450	-7.0004	-67.0992
0.500	-4.2894	-33.3024
0.550	-2.6868	-17.2395
0.600	-1.8116	-9.7675
0.650	-1.4180	-6.5142
0.700	-1.2806	-5.0729
0.750	-1.1967	-4.1295
0.800	-1.0319	-3.1294
0.850	-0.7590	-2.0389
0.900	-0.4485	-1.0747
0.950	-0.2106	-0.4529
1.000	-0.1202	-0.2332
1.050	-0.1685	-0.2967
1.100	-0.2707	-0.4342
1.150	-0.3209	-0.4710
1.200	-0.2608	-0.3515
1.250	-0.1159	-0.1439
1.300	0.0246	0.0283
1.350	0.0715	0.0762
1.400	0.0025	0.0025
1.450	-0.1133	-0.1046
1.500	-0.1521	-0.1312
1.550	-0.0152	-0.0123
1.600	0.2985	0.2263
1.650	0.6720	0.4791
1.700	0.9224	0.6195
1.750	0.8971	0.5686
1.800	0.5634	0.3375
1.850	0.0370	0.0210
1.900	-0.4676	-0.2514
1.950	-0.7393	-0.3774
2.000	-0.6705	-0.3254
2.050	-0.3014	-0.1392
2.100	0.2116	0.0931
2.150	0.6811	0.2860
2.200	0.9798	0.3929
2.250	1.0873	0.4169
2.300	1.0768	0.3951
2.350	1.0585	0.3720
2.400	1.1201	0.3775
2.450	1.2998	0.4203
2.500	1.6015	0.4974
2.550	2.0316	0.6064
2.600	2.6258	0.7539
2.650	3.4410	0.9511
2.700	4.5157	1.2023
2.750	5.8235	1.4946
2.800	7.2523	1.7955
2.850	8.6255	2.0612
2.900	9.7568	2.2518
2.950	10.5120	2.3446
3.000	10.8443	2.3387
3.050	10.7917	2.2517
3.100	10.4423	2.1091
3.150	9.8922	1.9350
3.200	9.2194	1.7475
3.250	8.4820	1.5586
3.300	7.7323	1.3782
3.350	7.0298	1.2158
3.400	6.4382	1.0810
3.450	6.0096	0.9800
3.500	5.7643	0.9133
3.550	5.6834	0.8753
3.600	5.7183	0.8565
3.650	5.8151	0.8472
3.700	5.9304	0.8408
3.750	6.0439	0.8342
3.800	6.1500	0.8267
3.850	6.2470	0.8180
3.900	6.3301	0.8078
3.950	6.3954	0.7956
4.000	6.4502	0.7825
4.050	6.5184	0.7713
4.100	6.6351	0.7661
4.150	6.8298	0.7697
4.200	7.1091	0.7822
4.250	7.4505	0.8006
4.300	7.8129	0.8202
4.350	8.1568	0.8367
4.400	8.4635	0.8485
4.450	8.7393	0.8566
4.500	9.0045	0.8631
4.550	9.2737	0.8695
4.600	9.5441	0.8755
4.650	9.7983	0.8796
4.700	10.0213	0.8805
4.750	10.2187	0.8791
4.800	10.4227	0.8780
4.850	10.6801	0.8813
4.900	11.0286	0.8916
4.950	11.4760	0.9091
5.000	11.9959	0.9313
5.050	12.5426	0.9546
5.100	13.0761	0.9758
5.150	13.5821	0.9940
5.200	14.0741	1.0103

Table V-4 (Continued)

Series: MG00A

r(Å)	$4\pi r^2 \sum \rho_i(r)$	g(r)	r(Å)	$4\pi r^2 \sum \rho_i(r)$	g(r)
5.250	14.5794	1.0267	7.750	30.2074	0.9762
5.300	15.1168	1.0445	7.800	30.7903	0.9823
5.350	15.6825	1.0635	7.850	31.4189	0.9896
5.400	16.2520	1.0818	7.900	32.0777	0.9976
5.450	16.7944	1.0975	7.950	32.7413	1.0055
5.500	17.2910	1.1095	8.000	33.3871	1.0126
5.550	17.7426	1.1180	8.050	34.0051	1.0185
5.600	18.1643	1.1242	8.100	34.5991	1.0236
5.650	18.5712	1.1292	8.150	35.1790	1.0280
5.700	18.9656	1.1330	8.200	35.7506	1.0320
5.750	19.3347	1.1351	8.250	36.3102	1.0355
5.800	19.6602	1.1344	8.300	36.8462	1.0381
5.850	19.9317	1.1305	8.350	37.3483	1.0397
5.900	20.1542	1.1238	8.400	37.8145	1.0402
5.950	20.3458	1.1155	8.450	38.2532	1.0399
6.000	20.5259	1.1067	8.500	38.6780	1.0391
6.050	20.7043	1.0979	8.550	39.0996	1.0381
6.100	20.8765	1.0890	8.600	39.5201	1.0371
6.150	21.0301	1.0792	8.650	39.9343	1.0359
6.200	21.1545	1.0682	8.700	40.3352	1.0343
6.250	21.2491	1.0558	8.750	40.7204	1.0323
6.300	21.3230	1.0428	8.800	41.0938	1.0300
6.350	21.3881	1.0295	8.850	41.4621	1.0275
6.400	21.4517	1.0165	8.900	41.8290	1.0250
6.450	21.5142	1.0037	8.950	42.1920	1.0224
6.500	21.5740	0.9911	9.000	42.5446	1.0195
6.550	21.6345	0.9788	9.050	42.8818	1.0162
6.600	21.7086	0.9673	9.100	43.2061	1.0127
6.650	21.8144	0.9575	9.150	43.5274	1.0091
6.700	21.9665	0.9498	9.200	43.8584	1.0058
6.750	22.1679	0.9444	9.250	44.2069	1.0028
6.800	22.4086	0.9406	9.300	44.5715	1.0003
6.850	22.6733	0.9379	9.350	44.9441	0.9979
6.900	22.9523	0.9357	9.400	45.3163	0.9954
6.950	23.2479	0.9342	9.450	45.6862	0.9930
7.000	23.5718	0.9337	9.500	46.0599	0.9906
7.050	23.9351	0.9347	9.550	46.4469	0.9885
7.100	24.3372	0.9371	9.600	46.8524	0.9868
7.150	24.7620	0.9401	9.650	47.2727	0.9853
7.200	25.1858	0.9430	9.700	47.6970	0.9839
7.250	25.5902	0.9450	9.750	48.1158	0.9824
7.300	25.9733	0.9460	9.800	48.5291	0.9808
7.350	26.3513	0.9468	9.850	48.9500	0.9793
7.400	26.7481	0.9481	9.900	49.3989	0.9783
7.450	27.1814	0.9506	9.950	49.8929	0.9782
7.500	27.6524	0.9542	10.000	50.4356	0.9789
7.550	28.1481	0.9585	10.050	51.0152	0.9804
7.600	28.6516	0.9628	10.100	51.6107	0.9820
7.650	29.1554	0.9670	10.150	52.2033	0.9835
7.700	29.6678	0.9712	10.200	52.7852	0.9848

Table V-4 (Continued)

Series: MG00A

r(Å)	$4\pi r^2 \Sigma \bar{z}(r)$	g(r)
10.250	53.3606	0.9858
10.300	53.9397	0.9869
10.350	54.5293	0.9880
10.400	55.1273	0.9893
10.450	55.7244	0.9905
10.500	56.3120	0.9914
10.550	56.8889	0.9921
10.600	57.4644	0.9927
10.650	58.0527	0.9934
10.700	58.6652	0.9946
10.750	59.3037	0.9961
10.800	59.9603	0.9978
10.850	60.6224	0.9995
10.900	61.2803	1.0011
10.950	61.9313	1.0025
11.000	62.5784	1.0038
11.050	63.2253	1.0050
11.100	63.8720	1.0062
11.150	64.5136	1.0072
11.200	65.1444	1.0080
11.250	65.7625	1.0085
11.300	66.3725	1.0089
11.350	66.9830	1.0092
11.400	67.6019	1.0096
11.450	68.2310	1.0102
11.500	68.8661	1.0107
11.550	69.5000	1.0112
11.600	70.1272	1.0116
11.650	70.7469	1.0118
11.700	71.3614	1.0118
11.750	71.9713	1.0118
11.800	72.5726	1.0116
11.850	73.1571	1.0112
11.900	73.7172	1.0104
11.950	74.2520	1.0092
12.000	74.7690	1.0078
12.050	75.2817	1.0063
12.100	75.8026	1.0049
12.150	76.3363	1.0037
12.200	76.8787	1.0026
12.250	77.4211	1.0014
12.300	77.9579	1.0002
12.350	78.4914	0.9989
12.400	79.0318	0.9977
12.450	79.5904	0.9966
12.500	80.1723	0.9959
12.550	80.7727	0.9954
12.600	81.3796	0.9949
12.650	81.9820	0.9944
12.700	82.5764	0.9937
12.750	83.1699	0.9930
12.800	83.7750	0.9925
12.850	84.4021	0.9921
12.900	85.0530	0.9920
12.950	85.7207	0.9921
13.000	86.3942	0.9922
13.050	87.0664	0.9923
13.100	87.7361	0.9924
13.150	88.4172	0.9924
13.200	89.1128	0.9927
13.250	89.8294	0.9931
13.300	90.5642	0.9937
13.350	91.3101	0.9944
13.400	92.0609	0.9951
13.450	92.8148	0.9958
13.500	93.5749	0.9966
13.550	94.3454	0.9974
13.600	95.1275	0.9983
13.650	95.9173	0.9992
13.700	96.7082	1.0001
13.750	97.4952	1.0009
13.800	98.2776	1.0017
13.850	99.0593	1.0023
13.900	99.8447	1.0030
13.950	100.6349	1.0037
14.000	101.4262	1.0044
14.050	102.2117	1.0050
14.100	102.9861	1.0054
14.150	103.7483	1.0057
14.200	104.5015	1.0059
14.250	105.2495	1.0060
14.300	105.9932	1.0061
14.350	106.7291	1.0060
14.400	107.4519	1.0058
14.450	108.1592	1.0054
14.500	108.8541	1.0049
14.550	109.5448	1.0044
14.600	110.2399	1.0038
14.650	110.9428	1.0033
14.700	111.6499	1.0029
14.750	112.3530	1.0024
14.800	113.0455	1.0017
14.850	113.7277	1.0010
14.900	114.4079	1.0002
14.950	115.0983	0.9996
15.000	115.8074	0.9990

Table V-5 Series: MG30A

r(Å)	$4\pi r^2\sum\bar{\rho}_i(r)$	g(r)	r(Å)	$4\pi r^2\sum\bar{\rho}_i(r)$	g(r)
0.250	0.1311	4.0721	2.750	5.1935	1.3329
0.300	0.1121	2.4177	2.800	6.6387	1.6436
0.350	0.0964	1.5277	2.850	7.9782	1.9065
0.400	0.1065	1.2914	2.900	9.1158	2.1039
0.450	0.1229	1.1777	2.950	9.9856	2.2272
0.500	0.1228	0.9532	3.000	10.5417	2.2735
0.550	0.0834	0.5351	3.050	10.7571	2.2445
0.600	0.0088	0.0476	3.100	10.6361	2.1482
0.650	-0.0734	-0.3370	3.150	10.2276	2.0006
0.700	-0.1251	-0.4954	3.200	9.6260	1.8246
0.750	-0.1248	-0.4307	3.250	8.9522	1.6451
0.800	-0.0802	-0.2431	3.300	8.3188	1.4827
0.850	-0.0241	-0.0648	3.350	7.7986	1.3488
0.900	0.0079	0.0188	3.400	7.4120	1.2445
0.950	0.0026	0.0055	3.450	7.1384	1.1641
1.000	-0.0216	-0.0420	3.500	6.9431	1.1001
1.050	-0.0273	-0.0481	3.550	6.8015	1.0475
1.100	0.0151	0.0242	3.600	6.7092	1.0048
1.150	0.1052	0.1544	3.650	6.6724	0.9721
1.200	0.2100	0.2830	3.700	6.6923	0.9488
1.250	0.2830	0.3515	3.750	6.7545	0.9323
1.300	0.2928	0.3363	3.800	6.8321	0.9183
1.350	0.2411	0.2567	3.850	6.8999	0.9035
1.400	0.1594	0.1579	3.900	6.9483	0.8867
1.450	0.0873	0.0806	3.950	6.9866	0.8691
1.500	0.0477	0.0412	4.000	7.0341	0.8533
1.550	0.0372	0.0301	4.050	7.1062	0.8409
1.600	0.0357	0.0271	4.100	7.2052	0.8319
1.650	0.0275	0.0196	4.150	7.3234	0.8253
1.700	0.0161	0.0108	4.200	7.4542	0.8202
1.750	0.0203	0.0129	4.250	7.6018	0.8169
1.800	0.0544	0.0326	4.300	7.7812	0.8168
1.850	0.1075	0.0610	4.350	8.0074	0.8214
1.900	0.1414	0.0760	4.400	8.2813	0.8303
1.950	0.1117	0.0570	4.450	8.5837	0.8413
2.000	0.0023	0.0011	4.500	8.8838	0.8515
2.050	-0.1524	-0.0704	4.550	9.1562	0.8584
2.100	-0.2747	-0.1209	4.600	9.3971	0.8620
2.150	-0.2821	-0.1185	4.650	9.6265	0.8641
2.200	-0.1360	-0.0545	4.700	9.8750	0.8677
2.250	0.1297	0.0497	4.750	10.1627	0.8743
2.300	0.4208	0.1544	4.800	10.4852	0.8833
2.350	0.6343	0.2229	4.850	10.8154	0.8924
2.400	0.7203	0.2427	4.900	11.1224	0.8991
2.450	0.7217	0.2334	4.950	11.3940	0.9026
2.500	0.7659	0.2379	5.000	11.6486	0.9044
2.550	1.0135	0.3025	5.050	11.9285	0.9079
2.600	1.5888	0.4562	5.100	12.2779	0.9162
2.650	2.5290	0.6990	5.150	12.7193	0.9308
2.700	3.7736	1.0047	5.200	13.2434	0.9506

Table V-5 (Continued)

Series: MG30A

r(Å)	$4\pi r^2 \sum \bar{A}_i(r)$	g(r)	r(Å)	$4\pi r^2 \sum \bar{A}_i(r)$	g(r)
5.250	13.8165	0.9730	7.750	29.6857	0.9593
5.300	14.4013	0.9951	7.800	30.3092	0.9670
5.350	14.9764	1.0156	7.850	30.9231	0.9740
5.400	15.5437	1.0346	7.900	31.5234	0.9804
5.450	16.1189	1.0533	7.950	32.1166	0.9863
5.500	16.7158	1.0726	8.000	32.7108	0.9920
5.550	17.3322	1.0922	8.050	33.3059	0.9976
5.600	17.9405	1.1110	8.100	33.8921	1.0026
5.650	18.5420	1.1274	8.150	34.4560	1.0069
5.700	19.0899	1.1404	8.200	34.9903	1.0100
5.750	19.5849	1.1498	8.250	35.5004	1.0124
5.800	20.0272	1.1555	8.300	36.0027	1.0144
5.850	20.4155	1.1579	8.350	36.5159	1.0165
5.900	20.7405	1.1565	8.400	37.0513	1.0192
5.950	20.9865	1.1506	8.450	37.6088	1.0223
6.000	21.1424	1.1399	8.500	38.1799	1.0257
6.050	21.2120	1.1248	8.550	38.7550	1.0290
6.100	21.2183	1.1068	8.600	39.3297	1.0322
6.150	21.1962	1.0877	8.650	39.9044	1.0352
6.200	21.1793	1.0694	8.700	40.4793	1.0380
6.250	21.1875	1.0528	8.750	41.0484	1.0406
6.300	21.2247	1.0380	8.800	41.5978	1.0426
6.350	21.2856	1.0246	8.850	42.1103	1.0436
6.400	21.3666	1.0125	8.900	42.5742	1.0432
6.450	21.4732	1.0018	8.950	42.9893	1.0417
6.500	21.6179	0.9931	9.000	43.3670	1.0392
6.550	21.8121	0.9868	9.050	43.7241	1.0362
6.600	22.0570	0.9828	9.100	44.0741	1.0330
6.650	22.3416	0.9806	9.150	44.4230	1.0299
6.700	22.6475	0.9792	9.200	44.7703	1.0267
6.750	22.9579	0.9780	9.250	45.1146	1.0234
6.800	23.2625	0.9765	9.300	45.4586	1.0202
6.850	23.5571	0.9745	9.350	45.8088	1.0171
6.900	23.8365	0.9718	9.400	46.1709	1.0142
6.950	24.0906	0.9680	9.450	46.5444	1.0116
7.000	24.3058	0.9628	9.500	46.9203	1.0091
7.050	24.4749	0.9558	9.550	47.2868	1.0064
7.100	24.6063	0.9474	9.600	47.6367	1.0033
7.150	24.7279	0.9388	9.650	47.9735	0.9999
7.200	24.8787	0.9315	9.700	48.3114	0.9966
7.250	25.0933	0.9266	9.750	48.6664	0.9937
7.300	25.3869	0.9247	9.800	49.0471	0.9912
7.350	25.7499	0.9252	9.850	49.4491	0.9892
7.400	26.1568	0.9271	9.900	49.8579	0.9874
7.450	26.5822	0.9296	9.950	50.2599	0.9854
7.500	27.0157	0.9322	10.000	50.6520	0.9831
7.550	27.4658	0.9352	10.050	51.0461	0.9810
7.600	27.9512	0.9393	10.100	51.4631	0.9792
7.650	28.4864	0.9448	10.150	51.9215	0.9782
7.700	29.0703	0.9517	10.200	52.4269	0.9781

Table V-5 (Continued)

Series: MG30A

r(Å)	$4\pi r^2 \Sigma \bar{\rho}_i(r)$	g(r)
10.250	52.9690	0.9786
10.300	53.5288	0.9793
10.350	54.0890	0.9800
10.400	54.6436	0.9806
10.450	55.1991	0.9811
10.500	55.7681	0.9818
10.550	56.3610	0.9829
10.600	56.9795	0.9843
10.650	57.6181	0.9860
10.700	58.2693	0.9879
10.750	58.9293	0.9898
10.800	59.5991	0.9918
10.850	60.2807	0.9939
10.900	60.9723	0.9961
10.950	61.6655	0.9982
11.000	62.3482	1.0001
11.050	63.0116	1.0016
11.100	63.6552	1.0028
11.150	64.2877	1.0037
11.200	64.9222	1.0046
11.250	65.5682	1.0056
11.300	66.2269	1.0067
11.350	66.8916	1.0079
11.400	67.5529	1.0089
11.450	68.2045	1.0098
11.500	68.8462	1.0104
11.550	69.4816	1.0109
11.600	70.1135	1.0114
11.650	70.7400	1.0117
11.700	71.3556	1.0118
11.750	71.9547	1.0116
11.800	72.5362	1.0111
11.850	73.1042	1.0105
11.900	73.6647	1.0097
11.950	74.2202	1.0088
12.000	74.7674	1.0078
12.050	75.2989	1.0065
12.100	75.8098	1.0050
12.150	76.3038	1.0033
12.200	76.7938	1.0014
12.250	77.2976	0.9998
12.300	77.8286	0.9985
12.350	78.3891	0.9976
12.400	78.9700	0.9969
12.450	79.5571	0.9962
12.500	80.1400	0.9955
12.550	80.7184	0.9947
12.600	81.3006	0.9940
12.650	81.8972	0.9934
12.700	82.5128	0.9930
12.750	83.1421	0.9927
12.800	83.7736	0.9924
12.850	84.3975	0.9921
12.900	85.0124	0.9916
12.950	85.6272	0.9910
13.000	86.2564	0.9907
13.050	86.9125	0.9906
13.100	87.5991	0.9908
13.150	88.3115	0.9913
13.200	89.0406	0.9919
13.250	89.7793	0.9926
13.300	90.5262	0.9933
13.350	91.2839	0.9941
13.400	92.0550	0.9951
13.450	92.8381	0.9961
13.500	93.6281	0.9971
13.550	94.4197	0.9982
13.600	95.2111	0.9991
13.650	96.0057	1.0001
13.700	96.8096	1.0011
13.750	97.6261	1.0023
13.800	98.4520	1.0034
13.850	99.2776	1.0046
13.900	100.0915	1.0055
13.950	100.8860	1.0062
14.000	101.6603	1.0067
14.050	102.4197	1.0070
14.100	103.1709	1.0073
14.150	103.9180	1.0074
14.200	104.6607	1.0075
14.250	105.3970	1.0074
14.300	106.1265	1.0073
14.350	106.8529	1.0072
14.400	107.5816	1.0070
14.450	108.3164	1.0069
14.500	109.0556	1.0068
14.550	109.7926	1.0066
14.600	110.5198	1.0064
14.650	111.2339	1.0060
14.700	111.9385	1.0055
14.750	112.6414	1.0049
14.800	113.3494	1.0044
14.850	114.0621	1.0039
14.900	114.7711	1.0034
14.950	115.4649	1.0027
15.000	116.1364	1.0019

Table V-6 Series: MG50A

r(Å)	$4\pi r^2 \Sigma \overline{\rho_i}(r)$	g(r)	r(Å)	$4\pi r^2 \Sigma \overline{\rho_i}(r)$	g(r)
0.250	0.0873	2.7107	2.750	5.2816	1.3555
0.300	0.4064	8.7654	2.800	6.6437	1.6448
0.350	0.5592	8.8601	2.850	8.0617	1.9264
0.400	0.4414	5.3552	2.900	9.2855	2.1430
0.450	0.0856	0.8203	2.950	10.1050	2.2538
0.500	-0.3283	-2.5487	3.000	10.4391	2.2513
0.550	-0.5882	-3.7743	3.050	10.3545	2.1605
0.600	-0.5697	-3.0713	3.100	10.0064	2.0210
0.650	-0.3093	-1.4207	3.150	9.5446	1.8671
0.700	0.0299	0.1183	3.200	9.0456	1.7146
0.750	0.2612	0.9012	3.250	8.5077	1.5634
0.800	0.2877	0.8724	3.300	7.9040	1.4088
0.850	0.1451	0.3898	3.350	7.2459	1.2532
0.900	-0.0398	-0.0954	3.400	6.6103	1.1099
0.950	-0.1431	-0.3077	3.450	6.1095	0.9963
1.000	-0.1211	-0.2350	3.500	5.8284	0.9235
1.050	-0.0223	-0.0393	3.550	5.7727	0.8891
1.100	0.0661	0.1060	3.600	5.8672	0.8787
1.150	0.0919	0.1349	3.650	6.0030	0.8746
1.200	0.0741	0.0998	3.700	6.1019	0.8651
1.250	0.0760	0.0944	3.750	6.1528	0.8492
1.300	0.1416	0.1626	3.800	6.1997	0.8333
1.350	0.2462	0.2622	3.850	6.2921	0.8239
1.400	0.3050	0.3021	3.900	6.4377	0.8215
1.450	0.2368	0.2186	3.950	6.5929	0.8202
1.500	0.0376	0.0325	4.000	6.6960	0.8123
1.550	-0.1949	-0.1575	4.050	6.7194	0.7951
1.600	-0.3116	-0.2363	4.100	6.6993	0.7735
1.650	-0.2085	-0.1487	4.150	6.7209	0.7574
1.700	0.0931	0.0626	4.200	6.8667	0.7556
1.750	0.4433	0.2810	4.250	7.1636	0.7698
1.800	0.6451	0.3865	4.300	7.5649	0.7941
1.850	0.5744	0.3258	4.350	7.9803	0.8186
1.900	0.2611	0.1404	4.400	8.3327	0.8354
1.950	-0.1216	-0.0621	4.450	8.6037	0.8433
2.000	-0.3561	-0.1728	4.500	8.8365	0.8470
2.050	-0.3060	-0.1413	4.550	9.0982	0.8530
2.100	0.0100	0.0044	4.600	9.4283	0.8648
2.150	0.4398	0.1847	4.650	9.8109	0.8807
2.200	0.7978	0.3199	4.700	10.1893	0.8953
2.250	0.9761	0.3742	4.750	10.5109	0.9042
2.300	0.9986	0.3664	4.800	10.7692	0.9072
2.350	0.9878	0.3472	4.850	11.0127	0.9087
2.400	1.0761	0.3626	4.900	11.3133	0.9146
2.450	1.3257	0.4287	4.950	11.7177	0.9282
2.500	1.7117	0.5316	5.000	12.2163	0.9485
2.550	2.1730	0.6486	5.050	12.7509	0.9705
2.600	2.6880	0.7718	5.100	13.2565	0.9893
2.650	3.3139	0.9159	5.150	13.7064	1.0031
2.700	4.1557	1.1065	5.200	14.1290	1.0142

Table V-6 (Continued)

Series: MG50A

r(Å)	$4\pi r^2 \Sigma \rho_i(r)$	g(r)	r(Å)	$4\pi r^2 \Sigma \rho_i(r)$	g(r)
5.250	14.5847	1.0271	7.750	30.1845	0.9754
5.300	15.1196	1.0447	7.800	30.6788	0.9787
5.350	15.7288	1.0666	7.850	31.2411	0.9840
5.400	16.3556	1.0887	7.900	31.8472	0.9905
5.450	16.9274	1.1062	7.950	32.4500	0.9966
5.500	17.4028	1.1166	8.000	33.0106	1.0011
5.550	17.7972	1.1215	8.050	33.5242	1.0041
5.600	18.1694	1.1246	8.100	34.0215	1.0065
5.650	18.5788	1.1296	8.150	34.5455	1.0095
5.700	19.0430	1.1376	8.200	35.1201	1.0138
5.750	19.5249	1.1462	8.250	35.7327	1.0190
5.800	19.9567	1.1515	8.300	36.3420	1.0239
5.850	20.2845	1.1505	8.350	36.9059	1.0274
5.900	20.5010	1.1431	8.400	37.4088	1.0290
5.950	20.6458	1.1319	8.450	37.8698	1.0294
6.000	20.7747	1.1201	8.500	38.3271	1.0296
6.050	20.9202	1.1094	8.550	38.8096	1.0305
6.100	21.0730	1.0992	8.600	39.3170	1.0318
6.150	21.1939	1.0876	8.650	39.8212	1.0330
6.200	21.2490	1.0729	8.700	40.2876	1.0331
6.250	21.2387	1.0553	8.750	40.7006	1.0318
6.300	21.2018	1.0368	8.800	41.0736	1.0295
6.350	21.1910	1.0201	8.850	41.4380	1.0269
6.400	21.2381	1.0064	8.900	41.8192	1.0247
6.450	21.3361	0.9954	8.950	42.2175	1.0230
6.500	21.4489	0.9854	9.000	42.6085	1.0210
6.550	21.5430	0.9746	9.050	42.9627	1.0182
6.600	21.6173	0.9632	9.100	43.2694	1.0142
6.650	21.7085	0.9528	9.150	43.5488	1.0096
6.700	21.8677	0.9455	9.200	43.8405	1.0054
6.750	22.1254	0.9425	9.250	44.1792	1.0022
6.800	22.4686	0.9431	9.300	44.5719	1.0003
6.850	22.8470	0.9451	9.350	44.9943	0.9990
6.900	23.2054	0.9460	9.400	45.4087	0.9975
6.950	23.5175	0.9450	9.450	45.7900	0.9952
7.000	23.8010	0.9428	9.500	46.1427	0.9924
7.050	24.1012	0.9412	9.550	46.4966	0.9895
7.100	24.4575	0.9417	9.600	46.8847	0.9874
7.150	24.8755	0.9445	9.650	47.3195	0.9863
7.200	25.3239	0.9482	9.700	47.7848	0.9857
7.250	25.7587	0.9512	9.750	48.2479	0.9851
7.300	26.1551	0.9526	9.800	48.6840	0.9839
7.350	26.5248	0.9530	9.850	49.0948	0.9822
7.400	26.9071	0.9537	9.900	49.5078	0.9804
7.450	27.3386	0.9561	9.950	49.9572	0.9794
7.500	27.8274	0.9602	10.000	50.4601	0.9794
7.550	28.3450	0.9652	10.050	51.0052	0.9802
7.600	28.8484	0.9694	10.100	51.5612	0.9811
7.650	29.3111	0.9721	10.150	52.0997	0.9816
7.700	29.7429	0.9737	10.200	52.6155	0.9816

Table V-6 (Continued)

Series: MG50A

r(Å)	$4\pi r^2 \sum \bar{a}^2(r)$	g(r)
10.250	53.1296	0.9815
10.300	53.6735	0.9820
10.350	54.2659	0.9833
10.400	54.8988	0.9852
10.450	55.5426	0.9872
10.500	56.1683	0.9889
10.550	56.7687	0.9900
10.600	57.3654	0.9910
10.650	57.9948	0.9925
10.700	58.6839	0.9949
10.750	59.4314	0.9982
10.800	60.2072	1.0019
10.850	60.9709	1.0053
10.900	61.6956	1.0079
10.950	62.3806	1.0098
11.000	63.0461	1.0113
11.050	63.7137	1.0128
11.100	64.3883	1.0143
11.150	65.0539	1.0156
11.200	65.6862	1.0164
11.250	66.2725	1.0164
11.300	66.8229	1.0158
11.350	67.3662	1.0150
11.400	67.9307	1.0146
11.450	68.5266	1.0145
11.500	69.1396	1.0147
11.550	69.7429	1.0147
11.600	70.3165	1.0143
11.650	70.8617	1.0134
11.700	71.3989	1.0124
11.750	71.9515	1.0115
11.800	72.5270	1.0110
11.850	73.1095	1.0105
11.900	73.6607	1.0098
11.950	74.1851	1.0083
12.000	74.6563	1.0063
12.050	75.1085	1.0040
12.100	75.5760	1.0019
12.150	76.0815	1.0003
12.200	76.6233	0.9992
12.250	77.1801	0.9983
12.300	77.7287	0.9972
12.350	78.2616	0.9959
12.400	78.7922	0.9946
12.450	79.3444	0.9936
12.500	79.9338	0.9930
12.550	80.5548	0.9927
12.600	81.1837	0.9925
12.650	81.7948	0.9921
12.700	82.3784	0.9913
12.750	82.9484	0.9904
12.800	83.5327	0.9896
12.850	84.1547	0.9892
12.900	84.8177	0.9893
12.950	85.5039	0.9896
13.000	86.1888	0.9899
13.050	86.8600	0.9900
13.100	87.5275	0.9900
13.150	88.2176	0.9902
13.200	88.9553	0.9909
13.250	89.7465	0.9922
13.300	90.5735	0.9938
13.350	91.4054	0.9955
13.400	92.2181	0.9968
13.450	93.0073	0.9979
13.500	93.7882	0.9989
13.550	94.5813	0.9999
13.600	95.3957	1.0011
13.650	96.2214	1.0024
13.700	97.0360	1.0035
13.750	97.8209	1.0043
13.800	98.5745	1.0047
13.850	99.3124	1.0049
13.900	100.0562	1.0052
13.950	100.8170	1.0056
14.000	101.5874	1.0060
14.050	102.3472	1.0063
14.100	103.0786	1.0064
14.150	103.7802	1.0061
14.200	104.4690	1.0056
14.250	105.1690	1.0053
14.300	105.8949	1.0051
14.350	106.6415	1.0052
14.400	107.3875	1.0052
14.450	108.1106	1.0050
14.500	108.8032	1.0044
14.550	109.4781	1.0037
14.600	110.1591	1.0031
14.650	110.8649	1.0026
14.700	111.5955	1.0024
14.750	112.3330	1.0022
14.800	113.0539	1.0019
14.850	113.7460	1.0012
14.900	114.4162	1.0003
14.950	115.0855	0.9994
15.000	115.7739	0.9987

Table V-7

Series: CM00A

r(Å)	$4\pi r^2 \sum A_i(r)$	g(r)	r(Å)	$4\pi r^2 \sum A_i(r)$	g(r)
0.250	-105.9203	-2576.3283	2.750	8.6971	1.7483
0.300	-51.6799	-872.9330	2.800	9.3463	1.8123
0.350	-28.6948	-356.0977	2.850	9.8591	1.8452
0.400	-17.6180	-167.3938	2.900	10.0925	1.8243
0.450	-11.5615	-86.7941	2.950	9.9502	1.7382
0.500	-7.7560	-47.1630	3.000	9.4528	1.5967
0.550	-5.0795	-25.5271	3.050	8.7412	1.4285
0.600	-3.1484	-13.2952	3.100	8.0101	1.2671
0.650	-1.8776	-6.7558	3.150	7.4144	1.1359
0.700	-1.2174	-3.7769	3.200	7.0076	1.0403
0.750	-1.0192	-2.7545	3.250	6.7466	0.9710
0.800	-1.0292	-2.4446	3.300	6.5520	0.9146
0.850	-0.9827	-2.0678	3.350	6.3786	0.8640
0.900	-0.7292	-1.3685	3.400	6.2471	0.8215
0.950	-0.3024	-0.5094	3.450	6.2210	0.7946
1.000	0.1136	0.1727	3.500	6.3498	0.7880
1.050	0.3098	0.4271	3.550	6.6245	0.7991
1.100	0.1937	0.2434	3.600	6.9769	0.8184
1.150	-0.1406	-0.1616	3.650	7.3229	0.8356
1.200	-0.4602	-0.4858	3.700	7.6161	0.8457
1.250	-0.5322	-0.5178	3.750	7.8720	0.8510
1.300	-0.2674	-0.2406	3.800	8.1458	0.8576
1.350	0.2214	0.1847	3.850	8.4813	0.8698
1.400	0.6859	0.5320	3.900	8.8695	0.8865
1.450	0.8923	0.6451	3.950	9.2484	0.9011
1.500	0.7620	0.5148	4.000	9.5456	0.9070
1.550	0.4159	0.2632	4.050	9.7325	0.9020
1.600	0.0950	0.0564	4.100	9.8519	0.8910
1.650	0.0097	0.0054	4.150	9.9967	0.8824
1.700	0.2149	0.1131	4.200	10.2536	0.8837
1.750	0.5879	0.2918	4.250	10.6498	0.8963
1.800	0.9189	0.4312	4.300	11.1387	0.9158
1.850	1.0535	0.4680	4.350	11.6346	0.9347
1.900	0.9903	0.4170	4.400	12.0706	0.9478
1.950	0.8744	0.3496	4.450	12.4410	0.9551
2.000	0.8941	0.3398	4.500	12.7983	0.9608
2.050	1.1514	0.4165	4.550	13.2089	0.9699
2.100	1.5952	0.5499	4.600	13.7001	0.9843
2.150	2.0580	0.6768	4.650	14.2359	1.0009
2.200	2.3716	0.7449	4.700	14.7391	1.0143
2.250	2.4826	0.7455	4.750	15.1439	1.0204
2.300	2.4928	0.7164	4.800	15.4419	1.0189
2.350	2.5992	0.7155	4.850	15.6897	1.0140
2.400	2.9759	0.7854	4.900	15.9725	1.0113
2.450	3.6739	0.9305	4.950	16.3494	1.0144
2.500	4.6019	1.1193	5.000	16.8177	1.0227
2.550	5.5930	1.3076	5.050	17.3205	1.0325
2.600	6.5074	1.4634	5.100	17.7898	1.0398
2.650	7.3000	1.5803	5.150	18.1954	1.0429
2.700	8.0116	1.6707	5.200	18.5632	1.0436

Table V-7 (Continued)

Series: GM00A

r(Å)	$4\pi r^2 \sum \bar{\rho}_2(r)$	g(r)	r(Å)	$4\pi r^2 \sum \bar{\rho}_2(r)$	g(r)
5.250	18.4534	1.0454	7.750	39.9852	1.0120
5.300	19.4122	1.0506	7.800	40.6040	1.0146
5.350	19.9340	1.0587	7.850	41.2797	1.0184
5.400	20.4597	1.0666	7.900	41.9851	1.0227
5.450	20.9126	1.0703	7.950	42.6676	1.0263
5.500	21.2470	1.0678	8.000	43.2821	1.0281
5.550	21.4771	1.0600	8.050	43.8187	1.0279
5.600	21.6657	1.0503	8.100	44.3063	1.0266
5.650	21.8829	1.0421	8.150	44.7907	1.0251
5.700	22.1638	1.0370	8.200	45.3035	1.0243
5.750	22.4920	1.0342	8.250	45.8421	1.0239
5.800	22.8207	1.0313	8.300	46.3760	1.0234
5.850	23.1110	1.0266	8.350	46.8713	1.0220
5.900	23.3623	1.0203	8.400	47.3167	1.0194
5.950	23.6114	1.0139	8.450	47.7317	1.0162
6.000	23.9034	1.0094	8.500	48.1524	1.0132
6.050	24.2568	1.0075	8.550	48.6056	1.0108
6.100	24.6482	1.0070	8.600	49.0908	1.0090
6.150	25.0277	1.0059	8.650	49.5822	1.0074
6.200	25.3533	1.0027	8.700	50.0495	1.0052
6.250	25.6191	0.9970	8.750	50.4810	1.0023
6.300	25.8578	0.9904	8.800	50.8923	0.9991
6.350	26.1160	0.9846	8.850	51.3153	0.9960
6.400	26.4215	0.9806	8.900	51.7745	0.9937
6.450	26.7662	0.9781	8.950	52.2700	0.9920
6.500	27.1167	0.9757	9.000	52.7790	0.9906
6.550	27.4448	0.9725	9.050	53.2747	0.9888
6.600	27.7533	0.9686	9.100	53.7492	0.9867
6.650	28.0781	0.9652	9.150	54.2223	0.9846
6.700	28.4637	0.9639	9.200	54.7299	0.9830
6.750	28.9299	0.9653	9.250	55.2995	0.9825
6.800	29.4537	0.9683	9.300	55.9299	0.9831
6.850	29.9805	0.9713	9.350	56.5914	0.9841
6.900	30.4589	0.9726	9.400	57.2446	0.9849
6.950	30.8746	0.9717	9.450	57.8676	0.9851
7.000	31.2600	0.9698	9.500	58.4705	0.9849
7.050	31.6736	0.9688	9.550	59.0881	0.9849
7.100	32.1615	0.9699	9.600	59.7551	0.9857
7.150	32.7288	0.9732	9.650	60.4821	0.9874
7.200	33.3390	0.9777	9.700	61.2479	0.9896
7.250	33.9416	0.9817	9.750	62.0145	0.9917
7.300	34.5069	0.9844	9.800	62.7533	0.9933
7.350	35.0455	0.9862	9.850	63.4642	0.9944
7.400	35.5970	0.9882	9.900	64.1743	0.9954
7.450	36.1995	0.9915	9.950	64.9168	0.9968
7.500	36.8596	0.9962	10.000	65.7062	0.9989
7.550	37.5467	1.0013	10.050	66.5264	1.0013
7.600	38.2142	1.0058	10.100	67.3406	1.0035
7.650	38.8322	1.0087	10.150	68.1161	1.0051
7.700	39.4091	1.0105	10.200	68.8458	1.0060

Table V-7 (Continued)

Series: GM00A

r(Å)	$4\pi r^2 \sum \rho_i(r)$	g(r)
10.250	69.5520	1.0064
10.300	70.2699	1.0069
10.350	71.0220	1.0079
10.400	71.8023	1.0092
10.450	72.5803	1.0104
10.500	73.3222	1.0110
10.550	74.0142	1.0109
10.600	74.6710	1.0103
10.650	75.3242	1.0096
10.700	75.9998	1.0091
10.750	76.6996	1.0090
10.800	77.4002	1.0088
10.850	78.0705	1.0082
10.900	78.6937	1.0069
10.950	79.2796	1.0052
11.000	79.8585	1.0033
11.050	80.4614	1.0018
11.100	81.1016	1.0007
11.150	81.7694	0.9999
11.200	82.4437	0.9991
11.250	83.1099	0.9983
11.300	83.7723	0.9973
11.350	84.4499	0.9966
11.400	85.1611	0.9962
11.450	85.9085	0.9962
11.500	86.6750	0.9963
11.550	87.4360	0.9964
11.600	88.1775	0.9962
11.650	88.9075	0.9958
11.700	89.6511	0.9956
11.750	90.4331	0.9958
11.800	91.2590	0.9964
11.850	92.1090	0.9972
11.900	92.9498	0.9978
11.950	93.7557	0.9981
12.000	94.5250	0.9979
12.050	95.2802	0.9975
12.100	96.0524	0.9973
12.150	96.8596	0.9975
12.200	97.6961	0.9978
12.250	98.5381	0.9982
12.300	99.3630	0.9984
12.350	100.1669	0.9984
12.400	100.9683	0.9983
12.450	101.7958	0.9984
12.500	102.6670	0.9989
12.550	103.5753	0.9997
12.600	104.4929	1.0006
12.650	105.3885	1.0012
12.700	106.2474	1.0014
12.750	107.0803	1.0014
12.800	107.9141	1.0013
12.850	108.7723	1.0014
12.900	109.6586	1.0018
12.950	110.5544	1.0022
13.000	111.4332	1.0024
13.050	112.2795	1.0023
13.100	113.1006	1.0019
13.150	113.9215	1.0015
13.200	114.7678	1.0013
13.250	115.6482	1.0014
13.300	116.5487	1.0016
13.350	117.4428	1.0018
13.400	118.3097	1.0016
13.450	119.1482	1.0013
13.500	119.9761	1.0008
13.550	120.8175	1.0004
13.600	121.6860	1.0002
13.650	122.5771	1.0001
13.700	123.4739	1.0001
13.750	124.3616	1.0000
13.800	125.2394	0.9997
13.850	126.1212	0.9995
13.900	127.0245	0.9994
13.950	127.9560	0.9996
14.000	128.9050	0.9998
14.050	129.8502	1.0000
14.100	130.7737	1.0000
14.150	131.6747	0.9998
14.200	132.5698	0.9995
14.250	133.4814	0.9993
14.300	134.4219	0.9993
14.350	135.3843	0.9995
14.400	136.3473	0.9996
14.450	137.2908	0.9996
14.500	138.2108	0.9993
14.550	139.1231	0.9990
14.600	140.0533	0.9988
14.650	141.0192	0.9989
14.700	142.0183	0.9991
14.750	143.0294	0.9994
14.800	144.0272	0.9996
14.850	144.9996	0.9996
14.900	145.9556	0.9994
14.950	146.9185	0.9993
15.000	147.9096	0.9993

Table V-8 Series: GM30A

r(Å)	$4\pi r^2\Sigma\bar{\rho}_2(r)$	g(r)	r(Å)	$4\pi r^2\Sigma\bar{\rho}_2(r)$	g(r)
0.250	0.4208	10.2342	2.750	11.0373	2.2187
0.300	0.2571	4.3421	2.800	11.1085	2.1540
0.350	-0.0180	-0.2228	2.850	10.8420	2.0292
0.400	-0.3262	-3.0997	2.900	10.3255	1.8664
0.450	-0.5516	-4.1408	2.950	9.6608	1.6876
0.500	-0.6036	-3.6707	3.000	8.9492	1.5116
0.550	-0.4618	-2.3207	3.050	8.2757	1.3524
0.600	-0.1962	-0.8283	3.100	7.6972	1.2176
0.650	0.0629	0.2265	3.150	7.2346	1.1084
0.700	0.1893	0.5874	3.200	6.8771	1.0210
0.750	0.1288	0.3480	3.250	6.5961	0.9493
0.800	-0.0712	-0.1691	3.300	6.3663	0.8887
0.850	-0.2856	-0.6009	3.350	6.1807	0.8372
0.900	-0.3818	-0.7165	3.400	6.0537	0.7961
0.950	-0.2963	-0.4990	3.450	6.0090	0.7675
1.000	-0.0732	-0.1112	3.500	6.0616	0.7522
1.050	0.1576	0.2173	3.550	6.2045	0.7484
1.100	0.2536	0.3186	3.600	6.4096	0.7518
1.150	0.1417	0.1629	3.650	6.6427	0.7580
1.200	-0.1369	-0.1445	3.700	6.8826	0.7643
1.250	-0.4449	-0.4329	3.750	7.1323	0.7710
1.300	-0.6211	-0.5587	3.800	7.4158	0.7807
1.350	-0.5645	-0.4708	3.850	7.7602	0.7959
1.400	-0.2867	-0.2224	3.900	8.1757	0.8171
1.450	0.0956	0.0691	3.950	8.6455	0.8424
1.500	0.4210	0.2844	4.000	9.1306	0.8675
1.550	0.5614	0.3552	4.050	9.5883	0.8887
1.600	0.4774	0.2835	4.100	9.9910	0.9035
1.650	0.2261	0.1262	4.150	10.3378	0.9125
1.700	-0.0758	-0.0399	4.200	10.6503	0.9178
1.750	-0.3078	-0.1528	4.250	10.9600	0.9224
1.800	-0.3914	-0.1836	4.300	11.2933	0.9285
1.850	-0.3066	-0.1362	4.350	11.6636	0.9370
1.900	-0.0811	-0.0341	4.400	12.0717	0.9479
1.950	0.2335	0.0934	4.450	12.5127	0.9606
2.000	0.5817	0.2211	4.500	12.9811	0.9745
2.050	0.9153	0.3311	4.550	13.4710	0.9892
2.100	1.1981	0.4130	4.600	13.9737	1.0039
2.150	1.4132	0.4648	4.650	14.4743	1.0176
2.200	1.5749	0.4947	4.700	14.9548	1.0292
2.250	1.7388	0.5221	4.750	15.3997	1.0376
2.300	1.9987	0.5744	4.800	15.8044	1.0428
2.350	2.4643	0.6784	4.850	16.1774	1.0455
2.400	3.2222	0.8504	4.900	16.5368	1.0470
2.450	4.2974	1.0884	4.950	16.9004	1.0485
2.500	5.6321	1.3699	5.000	17.2779	1.0506
2.550	7.0940	1.6585	5.050	17.6677	1.0532
2.600	8.5096	1.9137	5.100	18.0611	1.0556
2.650	9.7106	2.1021	5.150	18.4497	1.0575
2.700	10.5730	2.2048	5.200	18.8319	1.0587

Table V-8 (Continued) Series: GM30A

r(Å)	$4\pi r^2 \sum \rho_i(r)$	g(r)	r(Å)	$4\pi r^2 \sum \rho_i(r)$	g(r)
5.250	19.2136	1.0597	7.750	40.1858	1.0171
5.300	19.6030	1.0609	7.800	40.9638	1.0236
5.350	20.0047	1.0625	7.850	41.7421	1.0298
5.400	20.4154	1.0643	7.900	42.5109	1.0355
5.450	20.8250	1.0658	7.950	43.2580	1.0405
5.500	21.2207	1.0664	8.000	43.9716	1.0445
5.550	21.5907	1.0656	8.050	44.6432	1.0473
5.600	21.9260	1.0629	8.100	45.2685	1.0489
5.650	22.2200	1.0582	8.150	45.8449	1.0492
5.700	22.4682	1.0513	8.200	46.3707	1.0484
5.750	22.6699	1.0424	8.250	46.8445	1.0463
5.800	22.8331	1.0318	8.300	47.2675	1.0431
5.850	22.9763	1.0206	8.350	47.6469	1.0389
5.900	23.1267	1.0100	8.400	47.9966	1.0341
5.950	23.3113	1.0010	8.450	48.3337	1.0291
6.000	23.5463	0.9943	8.500	48.6722	1.0241
6.050	23.8287	0.9897	8.550	49.0164	1.0193
6.100	24.1378	0.9861	8.600	49.3597	1.0146
6.150	24.4454	0.9825	8.650	49.6893	1.0096
6.200	24.7315	0.9781	8.700	49.9949	1.0041
6.250	24.9952	0.9727	8.750	50.2775	0.9983
6.300	25.2562	0.9674	8.800	50.5516	0.9924
6.350	25.5453	0.9631	8.850	50.8406	0.9868
6.400	25.8889	0.9609	8.900	51.1672	0.9820
6.450	26.2970	0.9609	8.950	51.5444	0.9782
6.500	26.7591	0.9628	9.000	51.9716	0.9754
6.550	27.2510	0.9656	9.050	52.4390	0.9733
6.600	27.7467	0.9683	9.100	52.9343	0.9718
6.650	28.2283	0.9704	9.150	53.4510	0.9705
6.700	28.6897	0.9716	9.200	53.9904	0.9697
6.750	29.1333	0.9720	9.250	54.5592	0.9694
6.800	29.5643	0.9720	9.300	55.1642	0.9696
6.850	29.9865	0.9715	9.350	55.8071	0.9704
6.900	30.4021	0.9708	9.400	56.4844	0.9718
6.950	30.8148	0.9698	9.450	57.1894	0.9735
7.000	31.2316	0.9689	9.500	57.9164	0.9756
7.050	31.6623	0.9684	9.550	58.6621	0.9778
7.100	32.1152	0.9685	9.600	59.4251	0.9802
7.150	32.5935	0.9692	9.650	60.2044	0.9828
7.200	33.0940	0.9705	9.700	60.9970	0.9855
7.250	33.6107	0.9721	9.750	61.7994	0.9883
7.300	34.1401	0.9739	9.800	62.6093	0.9910
7.350	34.6849	0.9760	9.850	63.4275	0.9938
7.400	35.2538	0.9787	9.900	64.2575	0.9967
7.450	35.8575	0.9821	9.950	65.1022	0.9997
7.500	36.5026	0.9865	10.000	65.9604	1.0027
7.550	37.1887	0.9918	10.050	66.8251	1.0058
7.600	37.9088	0.9977	10.100	67.6851	1.0087
7.650	38.6534	1.0041	10.150	68.5291	1.0112
7.700	39.4142	1.0106	10.200	69.3505	1.0133

Table V-8 (Continued)

Series: GM30A

r(Å)	$4\pi r^2 \Sigma \rho_i(r)$	g(r)
10.250	70.1490	1.0150
10.300	70.9299	1.0164
10.350	71.7002	1.0175
10.400	72.4646	1.0185
10.450	73.2242	1.0194
10.500	73.9761	1.0200
10.550	74.7156	1.0205
10.600	75.4365	1.0206
10.650	76.1317	1.0204
10.700	76.7928	1.0197
10.750	77.4121	1.0183
10.800	77.9855	1.0164
10.850	78.5160	1.0139
10.900	79.0155	1.0110
10.950	79.5030	1.0080
11.000	79.9979	1.0051
11.050	80.5139	1.0024
11.100	81.0546	1.0001
11.150	81.6143	0.9980
11.200	82.1844	0.9960
11.250	82.7600	0.9941
11.300	83.3445	0.9923
11.350	83.9483	0.9907
11.400	84.5836	0.9894
11.450	85.2578	0.9886
11.500	85.9697	0.9882
11.550	86.7109	0.9881
11.600	87.4711	0.9882
11.650	88.2434	0.9884
11.700	89.0272	0.9887
11.750	89.8264	0.9891
11.800	90.6454	0.9897
11.850	91.4849	0.9904
11.900	92.3411	0.9913
11.950	93.2071	0.9922
12.000	94.0766	0.9932
12.050	94.9463	0.9940
12.100	95.8157	0.9949
12.150	96.6857	0.9957
12.200	97.5569	0.9964
12.250	98.4293	0.9971
12.300	99.3033	0.9978
12.350	100.1813	0.9985
12.400	101.0678	0.9992
12.450	101.9673	1.0001
12.500	102.8814	1.0010
12.550	103.8070	1.0019
12.600	104.7363	1.0029
12.650	105.6604	1.0038
12.700	106.5720	1.0045
12.750	107.4685	1.0050
12.800	108.3515	1.0054
12.850	109.2249	1.0056
12.900	110.0921	1.0057
12.950	110.9551	1.0058
13.000	111.8143	1.0056
13.050	112.6699	1.0057
13.100	113.5227	1.0056
13.150	114.3732	1.0055
13.200	115.2207	1.0053
13.250	116.0627	1.0050
13.300	116.8960	1.0046
13.350	117.7197	1.0041
13.400	118.5370	1.0036
13.450	119.3551	1.0030
13.500	120.1819	1.0025
13.550	121.0224	1.0021
13.600	121.8750	1.0017
13.650	122.7322	1.0014
13.700	123.5849	1.0010
13.750	124.4277	1.0005
13.800	125.2624	0.9999
13.850	126.0983	0.9993
13.900	126.9465	0.9988
13.950	127.8147	0.9985
14.000	128.7032	0.9982
14.050	129.6046	0.9981
14.100	130.5090	0.9979
14.150	131.4089	0.9977
14.200	132.3031	0.9975
14.250	133.1969	0.9972
14.300	134.0983	0.9969
14.350	135.0142	0.9967
14.400	135.9476	0.9967
14.450	136.8976	0.9967
14.500	137.8614	0.9968
14.550	138.8356	0.9970
14.600	139.8177	0.9971
14.650	140.8052	0.9973
14.700	141.7952	0.9975
14.750	142.7845	0.9977
14.800	143.7715	0.9978
14.850	144.7577	0.9979
14.900	145.7483	0.9980
14.950	146.7504	0.9982
15.000	147.7699	0.9984

Table V-9

Series: GM50A

r(Å)	$4\pi r^2 \sum \bar{A}_2(r)$	g(r)
0.250	0.0326	0.7922
0.300	-0.3649	-6.1635
0.350	-0.6157	-7.6408
0.400	-0.6029	-5.7287
0.450	-0.3776	-2.8346
0.500	-0.1292	-0.7854
0.550	-0.0453	-0.2274
0.600	-0.1796	-0.7583
0.650	-0.4122	-1.4832
0.700	-0.5392	-1.6728
0.750	-0.4244	-1.1471
0.800	-0.1081	-0.2569
0.850	0.2115	0.4451
0.900	0.3140	0.5893
0.950	0.1149	0.1936
1.000	-0.2632	-0.4002
1.050	-0.5651	-0.7792
1.100	-0.5731	-0.7200
1.150	-0.2598	-0.2987
1.200	0.1863	0.1966
1.250	0.4841	0.4710
1.300	0.4512	0.4059
1.350	0.1328	0.1108
1.400	-0.2231	-0.1731
1.450	-0.3334	-0.2411
1.500	-0.0777	-0.0525
1.550	0.4076	0.2579
1.600	0.8077	0.4796
1.650	0.8345	0.4660
1.700	0.4248	0.2235
1.750	-0.2015	-0.1000
1.800	-0.6648	-0.3119
1.850	-0.6549	-0.2909
1.900	-0.1206	-0.0508
1.950	0.7014	0.2804
2.000	1.4330	0.5446
2.050	1.7835	0.6452
2.100	1.7150	0.5912
2.150	1.4464	0.4757
2.200	1.3047	0.4098
2.250	1.5272	0.4586
2.300	2.1432	0.6159
2.350	2.9996	0.8257
2.400	3.8991	1.0291
2.450	4.7436	1.2014
2.500	5.5825	1.3579
2.550	6.5395	1.5288
2.600	7.6758	1.7262
2.650	8.8958	1.9257
2.700	9.9635	2.0777
2.750	10.6237	2.1356
2.800	10.7466	2.0838
2.850	10.3985	1.9462
2.900	9.7947	1.7705
2.950	9.1699	1.6019
3.000	8.6534	1.4617
3.050	8.2283	1.3447
3.100	7.7943	1.2330
3.150	7.2783	1.1151
3.200	6.7118	0.9964
3.250	6.2202	0.8952
3.300	5.9369	0.8288
3.350	5.9071	0.8002
3.400	6.0539	0.7961
3.450	6.2313	0.7959
3.500	6.3259	0.7850
3.550	6.3341	0.7641
3.600	6.3613	0.7462
3.650	6.5426	0.7466
3.700	6.9431	0.7710
3.750	7.5067	0.8115
3.800	8.0902	0.8517
3.850	8.5560	0.8775
3.900	8.8586	0.8854
3.950	9.0647	0.8832
4.000	9.2958	0.8832
4.050	9.6356	0.8930
4.100	10.0692	0.9106
4.150	10.4978	0.9266
4.200	10.8161	0.9321
4.250	10.9963	0.9255
4.300	11.1176	0.9141
4.350	11.3192	0.9094
4.400	11.7084	0.9194
4.450	12.2886	0.9434
4.500	12.9561	0.9726
4.550	13.5687	0.9964
4.600	14.0368	1.0085
4.650	14.3765	1.0108
4.700	14.6882	1.0108
4.750	15.0800	1.0161
4.800	15.5888	1.0286
4.850	16.1560	1.0441
4.900	16.6710	1.0555
4.950	17.0512	1.0579
5.000	17.3008	1.0520
5.050	17.5078	1.0436
5.100	17.7832	1.0394
5.150	18.1863	1.0424
5.200	18.6888	1.0507

Table V-9 (Continued)

Series: GM50A

r(Å)	$4\pi r^2 \sum \bar{\rho}_i(r)$	g(r)	r(Å)	$4\pi r^2 \sum \bar{\rho}_i(r)$	g(r)
5.250	19.2008	1.0590	7.750	40.3724	1.0218
5.300	19.6384	1.0628	7.800	41.1105	1.0272
5.350	19.9826	1.0613	7.850	41.7533	1.0300
5.400	20.2880	1.0577	7.900	42.3213	1.0309
5.450	20.6367	1.0562	7.950	42.8737	1.0312
5.500	21.0718	1.0590	8.000	43.4625	1.0324
5.550	21.5592	1.0640	8.050	44.0942	1.0344
5.600	22.0068	1.0668	8.100	44.7260	1.0363
5.650	22.3261	1.0632	8.150	45.2981	1.0367
5.700	22.4942	1.0525	8.200	45.7791	1.0350
5.750	22.5715	1.0378	8.250	46.1907	1.0317
5.800	22.6628	1.0241	8.300	46.5938	1.0282
5.850	22.8508	1.0151	8.350	47.0465	1.0258
5.900	23.1460	1.0108	8.400	47.5636	1.0248
5.950	23.4891	1.0086	8.450	48.1068	1.0242
6.000	23.8001	1.0050	8.500	48.6118	1.0228
6.050	24.0386	0.9984	8.550	49.0333	1.0197
6.100	24.2318	0.9900	8.600	49.3759	1.0149
6.150	24.4515	0.9828	8.650	49.6893	1.0096
6.200	24.7591	0.9792	8.700	50.0318	1.0049
6.250	25.1587	0.9791	8.750	50.4304	1.0013
6.300	25.5936	0.9803	8.800	50.8633	0.9985
6.350	25.9881	0.9798	8.850	51.2802	0.9953
6.400	26.3035	0.9762	8.900	51.6429	0.9911
6.450	26.5683	0.9708	8.950	51.9567	0.9860
6.500	26.8585	0.9664	9.000	52.2713	0.9810
6.550	27.2435	0.9653	9.050	52.6402	0.9772
6.600	27.7348	0.9679	9.100	53.1197	0.9752
6.650	28.2748	0.9720	9.150	53.6690	0.9745
6.700	28.7747	0.9745	9.200	54.2441	0.9743
6.750	29.1744	0.9734	9.250	54.7977	0.9736
6.800	29.4832	0.9693	9.300	55.3227	0.9724
6.850	29.7727	0.9646	9.350	55.8585	0.9713
6.900	30.1281	0.9620	9.400	56.4639	0.9714
6.950	30.5909	0.9628	9.450	57.1744	0.9733
7.000	31.1348	0.9659	9.500	57.9761	0.9766
7.050	31.6886	0.9692	9.550	58.8129	0.9803
7.100	32.1905	0.9708	9.600	59.6234	0.9835
7.150	32.6331	0.9704	9.650	60.3804	0.9857
7.200	33.0688	0.9697	9.700	61.1062	0.9873
7.250	33.5717	0.9710	9.750	61.8533	0.9891
7.300	34.1843	0.9752	9.800	62.6638	0.9919
7.350	34.8867	0.9817	9.850	63.5380	0.9956
7.400	35.6109	0.9886	9.900	64.4327	0.9994
7.450	36.2883	0.9939	9.950	65.2900	1.0025
7.500	36.8969	0.9972	10.000	66.0769	1.0045
7.550	37.4754	0.9994	10.050	66.8053	1.0055
7.600	38.0922	1.0026	10.100	67.5214	1.0062
7.650	38.7955	1.0078	10.150	68.2706	1.0074
7.700	39.5762	1.0147	10.200	69.0652	1.0092

Table V-9 (Continued)

Series: GM50A

r(Å)	$4\pi r^2 \sum \rho_i(r)$	g(r)	r(Å)	$4\pi r^2 \sum \rho_i(r)$	g(r)
10.250	69.8768	1.0111	12.750	107.4384	1.0047
10.300	70.6596	1.0125	12.800	108.3688	1.0055
10.350	71.3859	1.0131	12.850	109.2483	1.0058
10.400	72.0684	1.0129	12.900	110.0738	1.0056
10.450	72.7528	1.0128	12.950	110.8755	1.0051
10.500	73.4853	1.0133	13.000	111.6961	1.0047
10.550	74.2786	1.0145	13.050	112.5607	1.0048
10.600	75.1002	1.0161	13.100	113.4610	1.0051
10.650	75.8922	1.0172	13.150	114.3626	1.0054
10.700	76.6082	1.0172	13.200	115.2309	1.0054
10.750	77.2419	1.0161	13.250	116.0575	1.0049
10.800	77.8287	1.0144	13.300	116.8601	1.0044
10.850	78.4178	1.0126	13.350	117.6960	1.0039
10.900	79.0387	1.0113	13.400	118.5734	1.0039
10.950	79.6820	1.0103	13.450	119.4916	1.0041
11.000	80.3110	1.0090	13.500	120.4147	1.0044
11.050	80.8924	1.0071	13.550	121.3014	1.0044
11.100	81.4240	1.0046	13.600	122.1325	1.0038
11.150	81.9395	1.0019	13.650	122.9224	1.0029
11.200	82.4862	0.9996	13.700	123.7070	1.0020
11.250	83.0925	0.9981	13.750	124.5180	1.0012
11.300	83.7485	0.9971	13.800	125.3600	1.0007
11.350	84.4142	0.9962	13.850	126.2099	1.0002
11.400	85.0494	0.9949	13.900	127.0359	0.9995
11.450	85.6441	0.9931	13.950	127.8236	0.9985
11.500	86.2270	0.9912	14.000	128.5890	0.9974
11.550	86.8469	0.9897	14.050	129.3698	0.9963
11.600	87.5392	0.9890	14.100	130.2003	0.9956
11.650	88.3021	0.9891	14.150	131.0883	0.9953
11.700	89.0990	0.9895	14.200	132.0108	0.9953
11.750	89.8854	0.9897	14.250	132.9322	0.9952
11.800	90.6405	0.9896	14.300	133.8306	0.9949
11.850	91.3817	0.9893	14.350	134.7147	0.9945
11.900	92.1508	0.9893	14.400	135.6189	0.9943
11.950	92.9832	0.9899	14.450	136.5787	0.9944
12.000	93.8805	0.9911	14.500	137.6050	0.9949
12.050	94.8085	0.9926	14.550	138.6755	0.9958
12.100	95.7198	0.9939	14.600	139.7480	0.9966
12.150	96.5862	0.9946	14.650	140.7880	0.9972
12.200	97.4177	0.9950	14.700	141.7902	0.9975
12.250	98.2546	0.9954	14.750	142.7794	0.9977
12.300	99.1381	0.9962	14.800	143.7909	0.9980
12.350	100.0807	0.9975	14.850	144.8440	0.9985
12.400	101.0577	0.9991	14.900	145.9286	0.9992
12.450	102.0239	1.0006	14.950	147.0130	0.9999
12.500	102.9450	1.0016	15.000	148.0671	1.0004
12.550	103.8203	1.0021			
12.600	104.6809	1.0024			
12.650	105.5654	1.0029			
12.700	106.4905	1.0037			

Propositions

Proposition I

It is proposed that a model based on elementary kinetic gas theory can be used for quantitative predictions and estimations of radionuclide fractionation and scavenging in the cloud and base surge of surface and underwater nuclear detonations.

Background

The approach to the problem was to consider the interaction of single atoms or molecules with the surface of water droplets. The problem was broken into two parts. The first part considers only the interaction of a non-gaseous molecule with a water droplet and ultimately defines a rate constant for the scavenging mechanism of the molecule by a water droplet. The second part deals with the scavenging and exchange of a gaseous molecule with a water droplet. The result is given in the form of two rate constants. One defines the scavenging rate or uptake of the gas by the water droplet. The other defines the rate of loss of the gas from a droplet.

If a portion of a nuclide chain containing a gas is considered, such as $I^{140} \longrightarrow Xe^{140} \longrightarrow Cs^{140}$, a reaction diagram can be written

$$\begin{array}{ccccc} S_1 & \longrightarrow & G & \longrightarrow & S_2 \\ \downarrow & & \downarrow\uparrow & & \downarrow \\ S_1' & \longrightarrow & G' & \longrightarrow & S_2' \end{array}$$

where S_1, G, and S_2 are nuclide molecules in the gas phase and S_1', G', and S_2' are nuclide molecules in the liquid phase (i.e. in the water droplets). The

horizontal arrows indicate radioactive decay, while the vertical arrows indicate scavenging and exchange of the different nuclide molecules in the two phases. Only the uptake or scavenging of S_1 and S_2 is taken into account since the loss of dissolved ions or solid particles from water droplets to the atmosphere would be negligible.

The rate equations for the above reaction diagram are

$$\frac{dS_1}{dt} = -(\lambda^*_{S_1} + \lambda_s) S_1$$

$$\frac{dS_1'}{dt} = \lambda_s S_1 - \lambda^*_{S_1} S_1'$$

$$\frac{dG}{dt} = \lambda^*_{S_1} S_1 + \lambda_{c'} G' - (\lambda^*_c + \lambda_c) G$$

$$\frac{dG'}{dt} = \lambda^*_{S_1} S_1' + \lambda_c G - (\lambda^*_c + \lambda_{c'}) G'$$

$$\frac{dS_2}{dt} = \lambda^*_c G - \lambda_s S_2$$

$$\frac{dS_2'}{dt} = \lambda^*_c G' + \lambda_s S_2$$

where λ^* is the radioactive decay constant, λ_s is the scavenging rate constant of the non-gaseous molecules, and λ_c and $\lambda_{c'}$ are the rate constants for the exchange of the gaseous molecules from the gas to the liquid and the liquid to the gas phase respectively.

Determination of λ_s: (The initial derivation assumes there is no agglomeration of the individual non-gaseous molecules.)

From kinetic theory

$$\frac{d\tilde{S}}{dt} = \frac{1}{4} S \bar{v}$$

where S = number of molecules per unit volume[1]

$\bar{v}$ = average velocity

$\frac{d\tilde{S}}{dt}$ = number of molecules striking a unit area per unit time.

Therefore the rate of scavenging of S per unit area is

$$\frac{dS}{dt} = -\gamma \frac{d\tilde{S}}{dt} = -\frac{1}{4} S \bar{v} \gamma$$

where γ is an efficiency factor to account for any rebound of the impinging molecules. Experiments carried out at USNRDL by Evans using radon and its decay products gave indirect evidence that the value of γ is quite close to unity.

If there are $\bar{N}$ water droplets of radius r per unit volume, the rate of scavenging per unit volume is

$$\frac{dS}{dt} = -\bar{N} \pi r^2 \bar{v} \gamma S$$

which is defined as

$$\frac{dS}{dt} = -\lambda_s S$$

[1] The unit volume used here and throughout the rest of the proposition is a unit volume of space which contains both the ambient atmosphere and the aerosol. S_1, S_2, G, etc. are given in terms of this unit volume and not in terms of a unit volume of the ambient atmosphere. Respectively, S_1', $\overline{S_2'}$, G', etc. are given in terms of the above unit volume and not in terms of a unit volume of the water aerosol. (Definition is good only if total droplet volume is not more than one to two percent of the unit volume.)

Therefore

$$\lambda_s = \bar{N} \pi r^2 \bar{v} \gamma$$

and from

$$\bar{v} = \left[\frac{8kT}{\pi m}\right]^{1/2},$$

$$\lambda_s = \bar{N} r^2 \gamma \left[\frac{8\pi k T}{m}\right]^{1/2}$$

where k = Boltzmann's constant

T = temperature

m = mass of scavenged molecule or particle

γ = efficiency factor, ~ 1.

If the droplet size in the population is not monodisperse, λ_s will take the form

$$\lambda_s = \left[\bar{N}_1 r_1^2 + \bar{N}_2 r_2^2 + \cdots \bar{N}_n r_n^2\right] \gamma \left[\frac{8\pi k T}{m}\right]^{1/2}$$

In the case that the molecules are not singularly dispersed but exist as a monodisperse agglomerate, λ_s must be divided by the number of molecules per particle so that the dimensions of S, dS/dt, and λ_s are compatible and consistent. Obviously the agglomerate must still be small enough so that kinetic theory is still valid in order for the above derivation to be applicable.

Determination of λ_c and $\lambda_{c'}$:

The derivation of λ_c and $\lambda_{c'}$ is quite similar to that of λ_s and does in fact use the same considerations from kinetic theory with the additional use of Henry's Law.

For the determination of λ_c and $\lambda_{c'}$ only the reaction $G \rightleftarrows G'$ need be considered. For this reaction the rate expressions are

$$\frac{dG}{dt} = -\lambda_c G + \lambda_{c'} G'$$

$$\frac{dG'}{dt} = -\lambda_{c'} G' + \lambda_c G$$

But if the aerosol with an initial concentration of G' of zero is considered, the initial rate of dG/dt can be written

$$\frac{dG}{dt} = -\lambda_c G$$

This expression can be rewritten in the form

$$\frac{dG}{dt} = -\bar{N}\pi r^2 \bar{v} \mathcal{B} G$$

where G = number of gas molecules per unit volume

$\mathcal{B}$ = efficiency factor.

In this case $\mathcal{B}$, the efficiency factor, has the form

$$\mathcal{B} = e^{-E/RT}$$

where E is the activation energy. Therefore λ_c can be written

$$\lambda_c = \bar{N}\pi r^2 \bar{v} e^{-E/RT}$$

or for the case of the polydisperse droplet population

$$\lambda_c = \left[\bar{N}_1 r_1^2 + \bar{N}_2 r_2^2 + \cdots \bar{N}_n r_n^2 \right] \pi \bar{v} e^{-E/RT}$$

The expression for $\lambda_{c'}$ is evaluated by the use of the equilibrium condition where the rate expressions dG/dt and dG'/dt are zero, and consequently $\lambda_c G$ must equal $\lambda_{c'} G'$.

By Henry's Law

$$P_{G'} = K X_{G'}$$

where K = Henry's constant

$X_{G'}$ = mole fraction of G dissolved in the droplets.

The mole fraction $X_{G'}$ written in terms of G' is

$$X_{G'} = \frac{\frac{3 G'}{4\pi r^3 N}}{\frac{L_o}{\tilde{V}} + \frac{3 G'}{4\pi r^3 N}}$$

where G' = number of molecules of G per unit volume, but dissolved in the droplets

L_o = Avogadro's number

$\tilde{V}$ = molar volume of water.

Since

$$\frac{L_o}{\tilde{V}} >> \frac{3 G'}{4\pi r^3 N} \quad ,$$

$X_{G'}$ can be approximated by

$$X_{G'} \approx \frac{3 \tilde{V} G'}{4\pi r^3 N L_o}$$

From kinetic theory

$$P_G = G k T$$

Therefore

$$G k T = K X_{G'} = \frac{3 K \tilde{V} G'}{4\pi r^3 N L_o}$$

and

$$G = \frac{3 K \tilde{V} G'}{4\pi r^3 N L_o k T}$$

From the original equilibrium condition of

$$\lambda_c G = \lambda_{c'} G'$$

the function $\lambda_{c'}$ can be written

$$\lambda_{c'} = \frac{3 K \nabla}{4\pi r^3 N L_o k T} \lambda_c$$

and for the case of the polydisperse droplet population

$$\lambda_{c'} = \left[\frac{1}{N_1 r_1^3} + \frac{1}{N_2 r_2^3} + \cdots \frac{1}{N_n r_n^3} \right] \frac{3 K \nabla}{4\pi L_o k T} \lambda_c$$

The final model will allow the determination of nuclide distribution in the cloud and base surge as a function of time, droplet size, droplet density, and temperature. Once the nuclide distribution is known, the radiation field from the fission product mixture can be determined. This latter application is of prime tactical importance to the Navy in that it can be used to predict a safe stand-off distance in the use of nuclear weapons.

References for Proposition I

(1) R. Caputi, Theoretical Model for Molecular and Particulate Interaction with Water Aerosol, U. S. Naval Radiological Defense Laboratory Technical Report, USNRDL-TR-463, September 1960.

The references of the above report are:

(1) E. C. Evans III and T. Shirasawa, WT-1621, May 1960 (CONFIDENTIAL FRD).

(2) W. R. Schell and R. W. Caputi, U. S. Naval Radiological Defense Laboratory Technical Memorandum, USNRDL-TM-115, October 1959 (CONFIDENTIAL).

(3) E. C. Freiling, Fractionation II; ....U. S. Naval Radiological Defense Laboratory, technical report in preparation.

(4) E. H. Kennard, Kinetic Theory of Gases, McGraw-Hill, New York (1938).

(5) F. Goodridge, Trans. Faraday Soc., 49, 1324 (1953).

(6) I. S. and E. S. Sokolnikoff, Higher Mathematics for Engineers and Physicists, McGraw-Hill, New York (1941).

(7) N. E. Dorsey, Properties of Ordinary Water-Substances, A. C. S. Monograph Series, Reinhold Publishing Corporation, New York (1940).

(8) K. O. May, Elementary Analysis, John Wiley and Sons, Inc., New York (1950).

Proposition II

An experimental technique is proposed that will give a semi-quantitative determination of the liquid/solid-liquid interface of a three-component phase diagram.

Background

The usual method used to determine a three-component phase diagram is first to determine thre three two-component phase diagrams which make up the three sides of the three-component system and then to determine a number of points on the liquid/solid-liquid interface of the three-component system. This technique was used on an actual three-component system made up of p-nitrophenol, benzamide, and nicotinic acid amide.

In determining the two-component phase diagram an initial semi-quantitative determination was made using the technique described in reference (1). Briefly, this technique consists of contacting the two pure components on a microscope slide so that there will be a zone at the contact line such that the full range of mole fraction mixtures will be represented. Schematically the system would look like Figure 1.

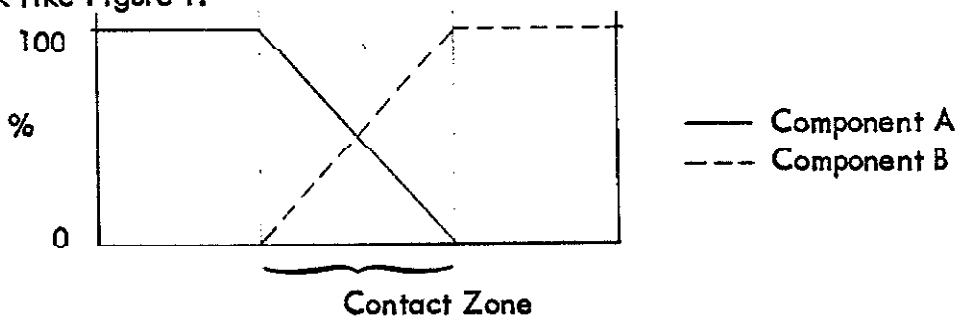

Figure 1.

The melting points of the zone are then observed to determine the presence of eutectics and compounds.

Once the above analysis was completed, a series of known mixtures of the two components was made to determine more specifically the compound and eutectic composition and the general shape of the two-component phase diagram.

Finally a series of mixtures containing all three components was made to determine the interior liquid/solid-liquid interface of the combined two-component systems.

It was on the basis of these measurements that both the original and secondary analysis of the total system was made. Because of the limited time and therefore limited number of measurements, certain areas of the diagram were uncertain or ambiguous. More recently new measurements were taken. In particular, the technique proposed was developed and used.

Essentially the technique is identical to the one described above, that of contact samples. The one significant difference is that one of the pure components was replaced with a mixture of known composition. The idea was to determine qualitatively the profile of the line connecting the pure component and the mixture, such as the profile of AD or CE in Figure 2 (a) and as shown in Figure 2 (e) and 2 (f).

Figure 2

b_1, b_2, b_3, b_4 : binary eutectic points.

t_1, t_2 : ternary eutectic points.

$b_1t_1, b_2t_1, b_3t_2, b_4t_2, t_1t_2$: eutectic curves.

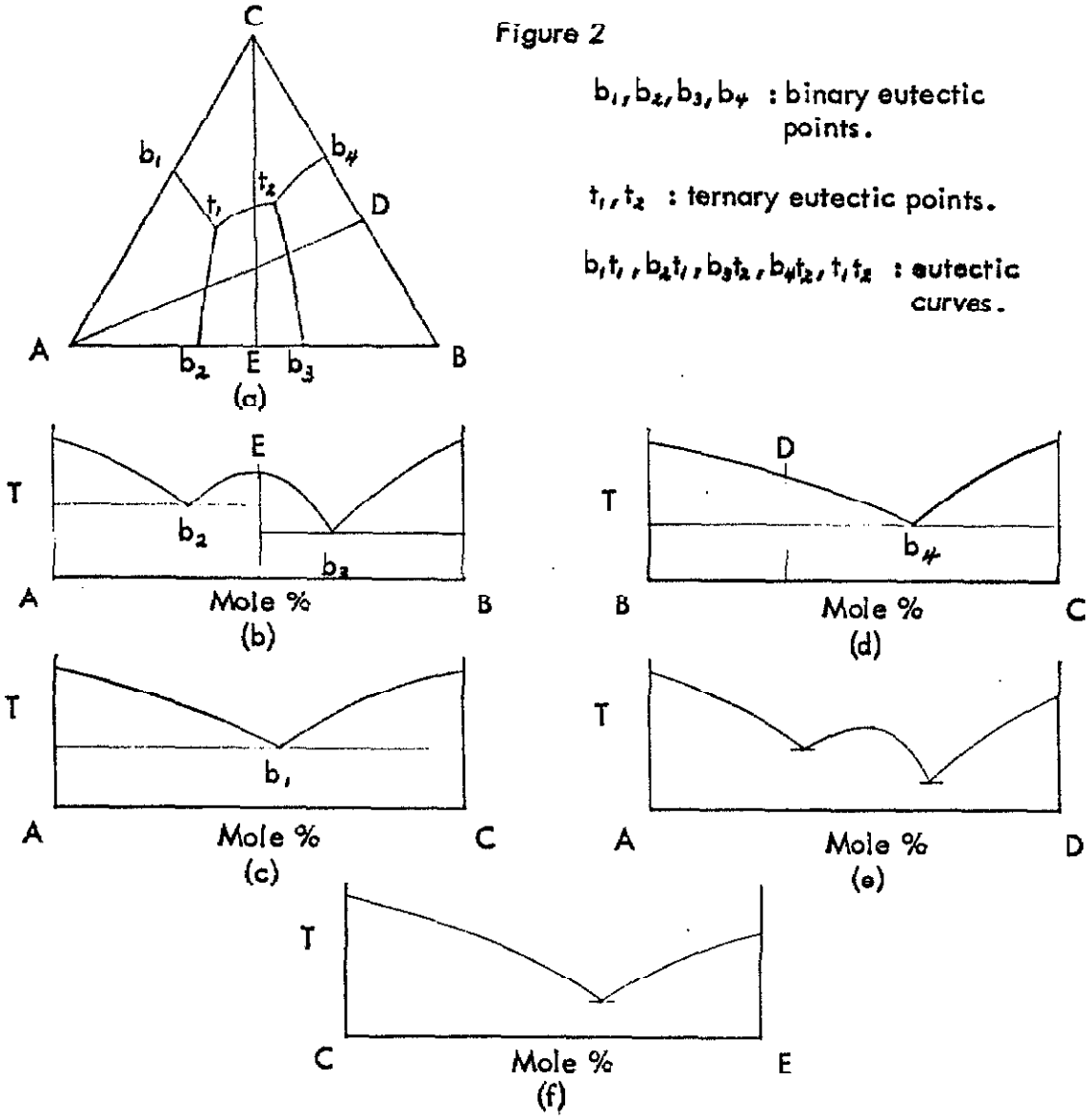

In both theory (2) and experiment the profile of CE and AD can be established qualitatively by the proposed technique. Although it is not possible to determine accurately the melting point where the eutectic curves cross the composition lines AD or CE using this contact method, the existence of the eutectic eutectic curves can very definitely be determined. It is also possible to determine exactly the melting points of maximums such as F of Figure 2 (e).

A total of 26 contact samples were run; 11 p-nitrophenol/nicotinic acid amide mixtures contacted with benzamide, 8 benzamide/nicotinic acid amide mixtures contacted with p-nitrophenol, and 7 p-nitrophenol/benzamide mixtures contacted with nicotinic acid amide. In every case the samples agreed with the previous interface interpretation done independently of the proposed technique. In three instances this technique removed the ambiguity where two or three equally reasonable interpretations were possible for a limited region of the interface.

The real value of this technique is that it greatly reduced the time needed to determine the liquid/solid-liquid interface of a three-component phase diagram, and it gives an immediate semi-quantitative picture of the interface showing any ternary compounds which may be present.

References for Proposition II

(1) L. Kofler and A. Kofler, Thermo-Mikro-Methoden, Weinheim, Bergstrasse, Verlag Chemie (1954).

(2) A. Findlay, The Phase Rule and Its Applications, Ninth Edition, Dover Publications, Inc., New York (1951).

Proposition III

It is proposed that a scintillation detector for x-rays be built making use of the photoelectric absorption and subsequent fluorescence in a thin metallic absorber in order to increase the energy resolution of a standard scintillation detector.

Background

A number of techniques have been developed to insure that the observed scattered radiation in a diffraction experiment is more or less monochromatic. The method which gives the sharpest energy discrimination is that of the crystal monochromator. Unfortunately the exceptional resolution of this method is coupled with a very low signal.

A second system which gives a relatively much stronger signal, but with decreasing resolution, is the matched filter technique developed by Ross (1). This method can be described briefly by the use of Figure 1 given below.

Figure 1.

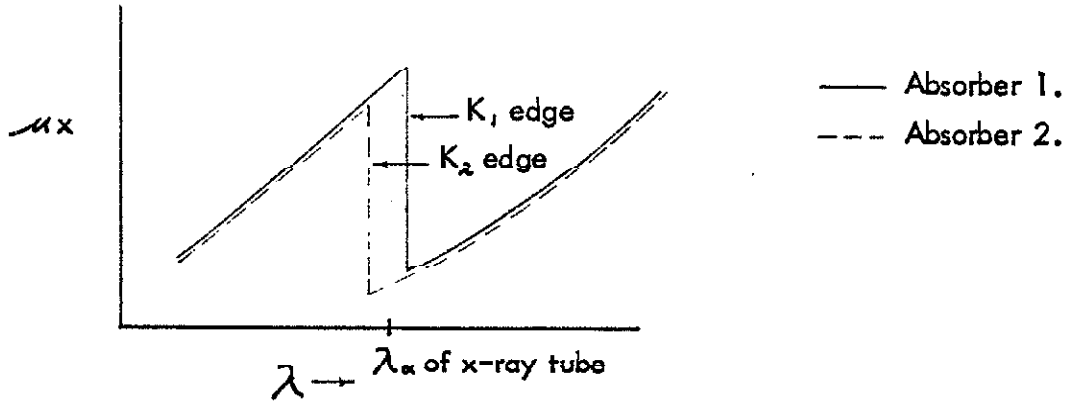

The absorbers 1 and 2 are matched such that μx (abs. coeff. x thickness) for any wavelength other than the wavelengths in the shaded portion is the same for both absorbers. The absorbers are also chosen so that the absorption edge K_1 is just beyond the K_α line of the tube used and K_2 is just short of K_α line. Normally absorber 2 is the beta filter. The complete diffraction experiment is then carried out twice, first with absorber 1 and then with absorber 2. The arithmetical difference of the experimental intensities is then just the intensity due to the range of wavelengths in the shaded portion of Figure 1.

The third technique uses a pulse height analyzer to limit the observed photon energy spectra by electronic means. Although this last technique has the poorest discrimination, it also has the shortest total count time.

The detector proposed is shown schematically in Figure 2.

Figure 2.

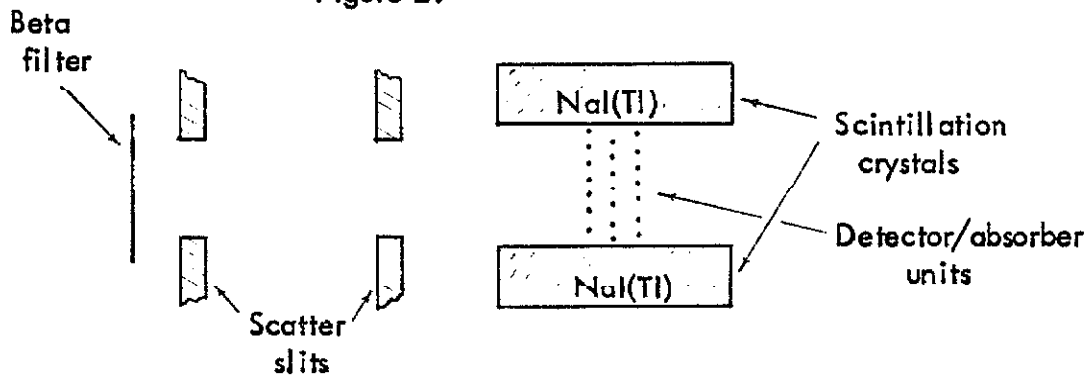

The metal used for the detector/absorber units would be the same as absorber 1 used in the matched Ross filters. If the photoelectric or fluorescent absorption discrimination for wavelengths just before and just after the K absorption edge is maximized, the optimum detector/absorber thickness is of the order of 5×10^{-4} cm for cobalt and nickel and 10^{-3} cm for metals such as rhodium,

ruthenium, niobium, and zirconium. Using the absorption coefficients of reference (2) and the above mentioned thicknesses, the effective absorption before and after the K absorption edge is of the order of 80% and 20% respectively. According to Evans (3) the photoelectric absorption process is essentially the entire primary absorption in the range of the standard x-ray energies used for x-ray diffraction work. The resulting fluorescent radiation, scattering uniformly, would then be detected by the scintillation crystals.

Ideally, the detector/absorber should be placed between the scintillation crystals in a parallel array of wires effectively blocking the entire sensitive area but presenting a thickness no greater than a single wire for any part of this entire area. The advantage of using a gridwork of wires rather than a strip of foil is that the self-absorption of the subsequent fluorescent radiation is minimized. Practically it would be easier to vacuum evaporate the metal in narrow parallel strips to the correct thickness on thin sheets of Mylar (T. M. DuPont). These sheets could then be mounted between the two scintillation crystals.

Although the energy resolution of this detector would not be quite as good as that of the matched Ross filters, it has the very marked advantage of reducing the experimental running time considerably over that of the Ross filter technique. In a number of experimental systems this reduction could mean the difference between the experiment being feasible or not.

References for Proposition III

(1) P. A. Ross, Rev. Sci. Instr., 16, 433 (1928). (J. Opt. Soc. Amer.)

(2) A. Taylor, X-Ray Metallography, p. 936, John Wiley and Sons, Inc., New York (1961).

(3) R. D. Evans, The Atomic Nucleus, p. 711, McGraw-Hill, New York (1955).

Proposition IV

It is proposed that a detailed and systematic theoretical computer study be carried out to derive the exact experimental intensity functions expected from monatomic two element liquid mixtures.

Background

The primary theoretical difficulty that all investigators experience in determining the liquid structure of mixtures is the mathematical impossibility of inverting the exact intensity expression. One useful approximation has been developed by Warren, Krutter, and Morningstar (1) to get around this difficulty. By assuming that all atomic scattering factors of the elements involved have the identical angular dependence and differ only by a constant, it is possible to simplify the intensity expression and carry out the Fourier inversion. This approximation works very well for elements quite close together in the periodic table. As the difference becomes greater, the detail and accuracy of the information about the system in question becomes more qualitative and limited. In most of the studies of liquid mixtures and alloys described in review articles by Kruh (2) and Furukawa (3), the above mentioned approximation is the only technique used to determine the liquid structure.

Because of the increased interest in liquid state studies and in more complex liquid systems, it is mandatory that the limitations imposed by the approximation of Warren et al. be eliminated. The technique which the author

proposes is that of systematically developing and synthesizing an array of radial distribution functions for alloys and mixtures based on physically realistic models. The prime basis for these models would most probably be the experimentally determined radial distribution functions for the pure elements of the alloy or mixture. Once the complete radial distribution function has been defined analytically for the liquid mixture and the different component terms have been multiplied by the appropriate scattering factors, the expressions can be integrated to give the expected experimental coherent scatter. In this way a systematic array of intensity curves could be determined for a given system using a number of probable configurations ranging from microcrystals or microdroplets dispersed in a solvent to true solutions. Besides the previously mentioned advantages of eliminating the atomic scattering factor approximation, this technique has the added advantages of being able to compare experimental intensity curves directly and of showing quantitatively the uncertainties in determining the radial distribution functions for the various systems. An example of this latter point is where several radial distribution functions are developed and integrated to give essentially the same intensity curves within the experimental uncertainties. From these results it would be seen that no single function is the "obvious" one and that the experimental technique is not sufficient to determine it. The techniques and approximations normally used at the present time allow only very qualitative statements to be made concerning the uncertainties of the derived radial distribution functions for liquid mixtures.

Ultimately, a catalogue or library of intensity curves would be developed covering a variety of liquid mixtures and alloys and their probable distribution functions. A library of this sort could be used universally and directly for comparison with corrected experimental coherent intensity curves of any experiment. A similar direct comparison of radial distribution functions from two independent experimental systems is by no means as simple or exact.

References for Proposition IV

(1) B. E. Warren, H. Krutter, and O. Morningstar, J. Am. Ceram. Soc., 19, 202 (1936).

(2) R. F. Kruh, Chem. Rev., 62, 319 (1962).

(3) K. Furukawa, Rep. Prog. Phys., 25, 395 (1962).

Proposition V

It is proposed that a high flux neutron pulse technique be used to study early time phenomena of nuclear detonation in the laboratory.

Background

One of the major problems of studying a large number of nuclear detonation processes is that the usual nuclear weapon cannot be scaled down to be used in the laboratory. Ignoring the present political and governmental limitations imposed on nuclear testing, there still exists the problem of the minimum size detonation possible consistent with critical mass. If the "detonation" could be moved into the laboratory, there would be two major gains. First, the problem of controlled conditions would be greatly reduced. Field conditions leave a great deal to be desired even at their best. Instruments must be protected from the weather and the environment usually at the expense of optimum experimental design. Second, the instruments could be placed much nearer the point of "detonation" for increased resolution without loss or damage.

It is proposed that the problem of critical mass can be overcome by the use of a very high intensity, outside source of neutrons. At the present time there are nuclear reactors which produce a fast neutron flux of the order of 5×10^{14} neutrons/cm^2sec (1). Although this flux sustains a nuclear reaction, it does not cause an explosion in the reactor. The proposed technique would take advantage of two factors to enable this sustaining flux to promote "explosive"

fission in a uranium or plutonium bead in the laboratory. The first of these factors is that the fission cross sections of U^{235} or Pu^{239} are strongly dependent on the individual neutron energies. U^{235} and Pu^{239} have respective fission cross sections of 1.4 and 1.9 barns for fast neutrons and 582 and 738 barns for thermal neutrons (2). Although the flux quoted above would be reduced by one to two orders of magnitude in the thermalization process, the increased cross section would more than compensate for this reduction.

The second factor which would increase the effective fission cross section of the entire bead by an order of magnitude over that of a reactor is to make the bead of pure U^{235} or Pu^{239}. Even the reactors which use enriched uranium still contain a large percentage of U^{238}. This isotope has a fission cross section of 0.2 barns for fast neutrons and 5×10^{-4} barns for thermal neutrons (2).

Using the cross section given above for U^{235}, a density of 19 g/ml, and 1.5 grams of U^{235} (1 cm x 1 cm x 0.08 cm), it can be calculated that $\sim$90% of the external thermal neutron flux will lead to fissioning. Assuming a flux of 10^{13} neutrons/cm^2 sec, an average energy of 200 MeV/fission (3), and a specific heat for uranium of 0.028 cal/g/°C (4), the temperature of the sample after 1 second would be of the order of 2000° C. This simplified model assumes linear temperature increase with time and neglects any radiation loss which would tend to lower the temperature. The fission build-up from the three neutrons released from each fissioning atom has also been neglected. Although the fission cross section for these fast neutrons is quite a bit smaller than

for thermal neutrons, the overall effect of these neutrons is not negligible. Unfortunately no simple calculation can be made to give a quantitative estimate of their effect.

Just how efficient this internal source of neutrons would be to increase the temperature and produce a more effective "explosion" is best determined by an actual experiment. Although with further development in reactor design and neutron reflectors, an increase of ten in the intensity of neutron fluxes is by no means impossible and would change the previously calculated figure of 2000° C in 1 second to 20,000° C in 1 second.

References for Proposition V

(1) Personal communication with J. Eyraud.

(2) H. Etherington (Editor), Nuclear Engineering Handbook, pp. 2-5 to 2-7, McGraw-Hill, New York (1958).

(3) G. Friedlander and J. W. Kennedy, Nuclear and Radiochemistry, p. 73, John Wiley and Sons, Inc., New York (1955).

(4) Handbook of Chemistry and Physics, 30th Edition, Chemical Rubber Publishing Co., Cleveland (1947).